

INFORMATION TO USERS

This manuscript has been reproduced from the microfilm master. UMI films the text directly from the original or copy submitted. Thus, some thesis and dissertation copies are in typewriter face, while others may be from any type of computer printer.

The quality of this reproduction is dependent upon the quality of the copy submitted. Broken or indistinct print, colored or poor quality illustrations and photographs, print bleedthrough, substandard margins, and improper alignment can adversely affect reproduction.

In the unlikely event that the author did not send UMI a complete manuscript and there are missing pages, these will be noted. Also, if unauthorized copyright material had to be removed, a note will indicate the deletion.

Oversize materials (e.g., maps, drawings, charts) are reproduced by sectioning the original, beginning at the upper left-hand corner and continuing from left to right in equal sections with small overlaps.

Photographs included in the original manuscript have been reproduced xerographically in this copy. Higher quality 6" x 9" black and white photographic prints are available for any photographs or illustrations appearing in this copy for an additional charge. Contact UMI directly to order.

ProQuest Information and Learning
300 North Zeeb Road, Ann Arbor, MI 48106-1346 USA
800-521-0600



GREEN FLUORESCENT PROTEIN

BIOSENSORS

by

GEORGE T. HANSON

A DISSERTATION

Presented to the Department of Chemistry
and the Graduate School of the University of Oregon
in partial fulfillment of the requirements
for the degree of
Doctor of Philosophy

June 2001

UMI Number: 3018368

Copyright 2001 by
Hanson, George T.

All rights reserved.

UMI[®]

UMI Microform 3018368
Copyright 2001 by Bell & Howell Information and Learning Company.
All rights reserved. This microform edition is protected against
unauthorized copying under Title 17, United States Code.

Bell & Howell Information and Learning Company
300 North Zeeb Road
P.O. Box 1346
Ann Arbor, MI 48106-1346

"Green Fluorescent Protein Biosensors," a dissertation prepared by George T. Hanson in partial fulfillment of the requirements for the Doctor of Philosophy degree in the Department of Chemistry. This dissertation has been approved and accepted by:

F.W.Dahlquist
Dr. Frederick W. Dahlquist, Chair of Examining Committee

May 23, 2001
Date

Committee in charge: Dr. Frederick W. Dahlquist, Chair
Dr. S. James Remington, Advisor
Dr. Brian W. Matthews
Dr. Tom H. Stevens
Dr. Peter H. von Hippel

Accepted by:

Miriam Lin
Dean of the Graduate School

© 2001 George T. Hanson

An Abstract of the Dissertation of

George T. Hanson

for the degree of

Doctor of Philosophy

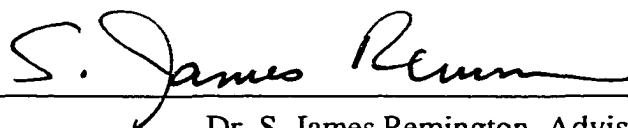
in the Department of Chemistry

to be taken

June 2001

Title: GREEN FLUORESCENT PROTEIN BIOSENSORS

Approved:



Dr. S. James Remington, Advisor

The green fluorescent protein (GFP) originally isolated from the Pacific Northwest jellyfish, *Aequorea victoria*, is unique from other light emitting proteins in that it has the remarkable ability to spontaneously generate its own highly fluorescent chromophore. This chromophore is responsible for the intense green light seen in the jellyfish and in samples of the purified protein. GFP is also distinct from synthetic fluorescent dyes in that it is genetically encoded, allowing it to be expressed in living organisms and targeted subcellularly without exposure to harsh chemicals. Since GFP is easily visualized, genetically encoded, and non-toxic, it has become an extremely popular fluorescent marker of gene expression and protein localization within living cells and

organisms. Given the advantages and popularity of GFP, we sought to determine if GFP could be made responsive to environmental pH and redox conditions and thus become a more useful tool for cell and molecular biologists.

Aided by the three-dimensional structure of GFP, site-specific mutagenesis was carried out near the chromophore region of GFP to create several types of pH-sensitive GFP variants as well as novel redox-sensitive GFP variants. These new biosensors change color or emission intensity due to changes in pH or redox potential. For example, one class of the pH-sensitive GFP variants change their fluorescence emission from green to blue in response to acidification of the surrounding environment.

GFP biosensors were also expressed in living cells and monitored by fluorescence microscopy to estimate the pH and redox potential of mitochondria, the energy producing organelle found in most cell types. In addition, the three-dimensional crystal structures of several GFP biosensors were determined to better understand how protein structure relates to environmental sensitivity.

This dissertation includes my unpublished, previously published, and co-authored materials.

CURRICULUM VITA

NAME OF AUTHOR: George Thomas Hanson

PLACE OF BIRTH: Robbinsdale, Minnesota

DATE OF BIRTH: April 22, 1975

GRADUATE AND UNDERGRADUATE SCHOOLS ATTENDED:

University of Oregon

University of Minnesota Duluth

DEGREES AWARDED:

Doctor of Philosophy in Chemistry, 2001

University of Oregon

Bachelor of Science in Biochemistry and Molecular Biology, 1997

University of Minnesota

AREAS OF SPECIAL INTEREST:

Protein Engineering

Fluorescence Spectroscopy

Macromolecular Structure and Function

PROFESSIONAL EXPERIENCE:

Research Assistant, Department of Chemistry and Institute of Molecular Biology

University of Oregon, 1998-2001

Teaching Assistant, Department of Chemistry

University of Oregon, 1997-1998

Undergraduate Research Assistant, Department of Chemistry

University of Minnesota, 1995-1997

HONORS AND AWARDS:

Dean's List, 1995-1997

All American in Track and Field, 1996

GRANTS:

National Institute of Health Training Grant, 1998-2001

PUBLICATIONS:

Esliger, M.-A., Wachter, R.M., Hanson, G.T., Kallio, K., and Remington, S.J. 1999.

Structural and spectral response of green fluorescent protein variants to changes
in pH. *Biochemistry* 38: 5296-5301.

Wachter, R.M., Esliger, M.-A., Kallio, K., Hanson, G.T., and Remington, S.J. 1998.

Structural basis of spectral shifts in the yellow-emission variants of green
fluorescent protein. *Structure* 6: 1267-1277.

ACKNOWLEDGEMENTS

To accomplish anything, a little talent, a bit of luck, and a considerable amount of help are necessary. There are several individuals to whom I am indebted to for their kindness and for their enthusiasm and wisdom of science. Rebekka will always be the first person to show me the all important “research ropes” in graduate school. Dan, will ever be remembered for breaking-up a monotonous day by introducing a new exotic plant species to the “lab jungle” or by simply ‘clucking’ like a chicken. Karen, undoubtedly will always be the nicest and neatest laboratory technician I will ever get the privilege to work alongside. Of course Jim will not only be remembered for having the most colorful and exciting research projects imaginable, but also his genuine excitement and passion for science will never be forgotten. I owe much of my research success to these individuals, along with the countless others that have been a part of the Remington and Matthews labs during my tenure.

Many other individuals have also had a great influence on my wellbeing during my years as a student. First, I thank my parents and sister for all their love and support throughout my life and academic career. I am also thankful for having a large group of

extended family and friends (especially Marla, Hannah, and everyone that makes Wednesday nights special) who bring joy into everyday life. Finally, I acknowledge and praise my wife, Bonnie, for her steadfast love, compassion, and direction. Clearly the participation of these individuals in my life, has helped to shape the person I am today.

DEDICATION

To Bonnie

TABLE OF CONTENTS

Chapter	Page
I. INTRODUCTION	1
Fluorescence Analysis	1
History of the Green Fluorescent Protein	4
GFP as a Fluorescent Probe	9
Research Focus	12
II. pH-SENSITIVE GREEN FLUORESCENT PROTEIN VARIANTS WITH VARIOUS pK_aS AND DUAL-EXCITATION WAVELENGTHS	15
Summary	15
Introduction	16
Results	20
Neutral pK _a Variant, GFP S65T/H148G	20
High pK _a Variant, YFP H148G	23
Structural Analysis of YFP H148G	26
Ratiometric GFP S65T/H148D	31
Discussion	36
GFP as an <i>In Vivo</i> pH Indicator	36
Solvent Accessibility of the Chromophore	38
Experimental Procedures	39
Mutagenesis and Protein Preparation	39
Spectroscopy and pH Titrations	41
Crystallization and Structure Determination of YFP H148G	42
Crystallization and Structure Determination of GFP S65T/H148D	43

TABLE OF CONTENTS (CONTINUED)

Chapter		Page
III. GREEN FLUORESCENT PROTEIN VARIANTS AS RATIOMETRIC DUAL EMISSION pH SENSORS.....		45
Summary		45
Introduction		47
Results.....		49
Design of Ratiometric pH-Sensitive GFPs		49
Structural Basis for Dual-Emission		51
Fluorescence of the Neutral Chromophore		64
Dynamic Range of deGFP4.....		65
Discussion		72
Experimental Procedures		77
Mutagenesis and Protein Preparation		77
Spectroscopy and pH Titrations		78
Crystallization.....		79
Data Collection and Refinement		80
Fluorescence Microscopy		81
Two-Photon Laser Scanning Microscopy		81
IV. OXIDATION REDUCTION SENSITIVE GREEN FLUORESCENT PROTEIN VARIANTS WITH RATIOMETRIC REDOX AND pH INDICATING CAPABILITIES		83
Summary		83
Introduction		85
Results.....		88
Design of Redox-Sensitive GFPs		88
Disulfide-Bond Formation and Redox Sensitivity of Engineered Cysteines.....		90
pH-Sensitivity of rosGFPs		96
Structural Basis for Dual-Wavelength Excitation		106
<i>In vivo</i> Redox Status		118

TABLE OF CONTENTS (CONTINUED)

Chapter	Page
What Factors Influence the Redox State of rosGFPs <i>In Vivo</i> ?	121
Discussion	126
Accuracy of Standard Redox Potentials	128
Experimental Procedures	132
Construction and Expression of Redox-Sensitive GFPs.....	132
SDS-PAGE.....	134
Spectroscopy and pH Titrations	134
Redox Titrations	135
Crystallization.....	136
Data Collection and Refinement	136
Mammalian Cell Transfection and Fluorescence Microscopy....	137
V. CONCLUSIONS	139
Green Fluorescent Protein Homologues	139
Structure-Based Design	141
Concluding Remarks.....	143
Future Directions	144
APPENDIX	146
Determination of Redox Potentials.....	146
pH-Dependence of Redox Potentials	149
BIBLIOGRAPHY	151

LIST OF TABLES

Table	Page
1. Data Collection and Refinement Statistics for YFP H148G and GFP S65T/H148D.....	27
2. Spectroscopic and Biochemical Properties of GFPs.....	34
3. Spectroscopic and Biochemical Properties of deGFP Variants	54
4. Data Collection and Refinement Statistics for deGFP1 at Low and High pH	56
5. Spectroscopic and Biochemical Properties of rosGFPs.....	97
6. Data Collection and Refinement Statistics for Oxidized and Reduced rosGFP2	111

LIST OF FIGURES

Figure	Page
1. Milestones in the History of GFP	6
2. Fluorescence Excitation Spectra of Two pH-Sensitive GFP Variants as a Function of pH.....	21
3. Absorbance Spectra of GFP S65T/H148G at Varying pHs	22
4. Absorbance and Fluorescence Emission Spectra of YFP H148G Versus pH.....	24
5. Absorbance and Fluorescence pH Titrations of YFP H148G	25
6. Overlay of the Backbone-Atom Trace of YFP and YFP H148G	28
7. Stereoview of the Solvent-Accessible Surface of YFP H148G	30
8. Absorbance and Fluorescence Excitation Spectra of GFP S65T/H148D	32
9. Overlay of the Chromophore Region of GFP S65T and GFP S65T/H148D	35
10. Absorbance and Fluorescence Emission Spectra of deGFP1 as a Function of pH.....	52
11. Absorbance and Fluorescence Emission Spectra of deGFP4 as a Function of pH.....	53
12. Pictures of Fluorescent deGFP1 Crystals.....	57

LIST OF FIGURES (CONTINUED)

Figure	Page
13. Overlay of Low and High pH Structures of deGFP1.....	59
14. Overlay of the Chromophore Environment at Low and High pH of deGFP1	60
15. Structural Comparison of S65T and the High pH Structure of deGFP1	61
16. Schematic Diagram Showing the Immediate Chromophore Environment of deGFP1 at Low and High pH.....	63
17. Electron Density Around the Chromophore and Cys 203 of the High pH Structure of deGFP1	66
18. Images of PS120 Cells Transfected with deGFP4 and Loaded with SNARF-1 [®]	67
19. The Normalized Ratio of pH Changes in PS120 Cells as Monitored with SNARF-1 [®] and deGFP4.....	69
20. Individual Wavelength Signals of deGFP4 as a Function of pH Changes in PS120 Cells	70
21. Two-Photon Excitation Images of PS120 Cells Expressing deGFP4.....	71
22. Two-Photon Excitation Spectra of deGFP4 as a Function of pH.....	73
23. Two-Photon Emission Spectra of deGFP4 as a Function of pH	74
24. SDS-PAGE Reveals Disulfide Linkage in rosGFP2	91
25. Absorbance and Fluorescence Excitation Spectra of rosGFP2 at Various Redox Potentials.....	92

LIST OF FIGURES (CONTINUED)

Figure	Page
26. Fluorescence Excitation Spectra of rosGFP4 as a Function of Redox Potential	94
27. Fluorescence Excitation Spectra of rosGFP6 as a Function of Redox Potential	95
28. Absorbance and Fluorescence Excitation Spectra of Oxidized rosGFP2 as a Function of pH.....	98
29. pH Titration of Oxidized and Reduced rosGFP2	99
30. Absorbance and Fluorescence Excitation Spectra of Reduced rosGFP2 as a Function of pH.....	100
31. Fluorescence Excitation Spectra of rosGFP1 at Various Redox Potentials	102
32. Fluorescence Excitation Spectra of rosGFP3 at Various Redox Potentials	103
33. Fluorescence Excitation Spectra of rosGFP5 at Various Redox Potentials	104
34. A Fluorescence Excitation Ratio Results in the Cancellation of pH Artifacts	105
35. Dual-Emission characteristics of rosGFP2	107
36. A Fluorescence Emission Ratio Results in the Cancellation of Redox Potential Changes on pH Determination.....	108
37. Ribbon Diagram of rosGFP2 Dimer	110

LIST OF FIGURES (CONTINUED)

Figure	Page
38. Dimer Interface of rosGFP2	113
39. Electron Density Surrounding the Disulfide Bridge in the Oxidized Structure of rosGFP2	114
40. Overlay of the Chromophore Environment of Oxidized and Reduced rosGFP2	116
41. A HeLa Cell Expressing rosGFP1 Localized to the Mitochondria	117
42. Response of rosGFP1 to H ₂ O ₂ and DTT Induced Redox Potential Changes in HeLa Cell Mitochondria	119
43. NADH-Dependent Reduction of rosGFP1 via Lipomide Dehydrogenase	125
44. Fluorescence Excitation Spectra of rosGFP2 at Varying Concentrations of DTT _{red} and DTT _{ox}	147
45. Redox Equilibrium Titration of rosGFP2 with Dithiothreitol.....	148

CHAPTER I

INTRODUCTION

Fluorescence Analysis

Light is a form of electromagnetic radiation and is characterized by a wavelength and a frequency. When light comes in contact with matter it can either pass through or be absorbed by the molecules that make up the material. In the latter case, energy is transferred to the molecules during the absorption process. Every molecule possesses a series of closely spaced energy levels and can move from a lower to a higher energy level by the absorption of light. This absorption of light is highly specific and only light of a particular energy (wavelength) is absorbed, dependent upon the atomic structure of the molecule. After a molecule has been promoted to an excited state, it returns to the ground state and releases the absorbed energy as luminescence. If the release of energy occurs almost immediately, faster than 10^{-6} seconds after the absorption, this type of luminescence is known as fluorescence (Guilbault 1990). Since some energy is lost in

the brief period before emission can occur, the emitted energy is of a longer wavelength (lower energy) than the energy that was absorbed.

Making use of a molecule's characteristic fluorescence has its advantages. First, fluorometric methods are highly sensitive. They can often detect concentrations of substances as low as one part in ten billion, a sensitivity more than 1,000 times greater than spectrophotometric methods (Guilbault 1990). The increased sensitivity is the result of directly measuring the emitted radiation over a zero background signal. While in spectrophotometric measurements the absorbed radiation is measured indirectly as the difference between the incident and transmitted beams. Second, fluorescence methods have excellent specificity. Although many compounds absorb energy, only about ten percent will emit luminescent radiation. Furthermore, even if two molecules absorb the same wavelength of light, they will probably not emit at the same wavelength. Finally, fluorescence methods display a large linear range of analysis. Fluorometers can often accurately detect fluorescence intensities over a range of six to seven orders of magnitude. In contrast, spectrophotometric analysis covers only two to three orders of magnitude before the linear range is exceeded and significant error is introduced.

The study of the biology of cells is greatly assisted by the use of fluorescence. By utilizing fluorescent reagents, the inner workings of cells can be studied in real time and

on living samples. Such experiments most commonly employ the use of a fluorometer, flow cytometer, or fluorescence microscope, with each piece of equipment having a specialized function. The fluorometer is the most common fluorometric device and is often used in cell biology to study populations of cells. The flow cytometer serves a similar role however it inspects and sorts each individual cell and thus gives a better resolution analysis of the population. For the highest resolution visualization of individual cells, groups of cells, or even small organisms, the fluorescence microscope is the preferred instrument. The fluorescence microscope is not only used to extract meaningful data of intracellular conditions, but also affords a detailed visual inspection of subcellular architecture. Regardless of the choice of instrumentation, these types of observations give unique insights into how a living organism functions on a cellular level.

Most fluorescence experiments are greatly facilitated by the use of small (less than 1,000 Da), synthetic molecules. These molecules come in a rainbow of colors and can be used for a myriad of applications. For example, the seminaphthorhidafluor dyes are pH indicators that undergo a fluorescence emission color change from red to orange upon acidification. However, dyes and other synthetic fluorescent probes require unnatural means of cellular incorporation. Fluorescent compounds are usually incorporated into cells by simple diffusion during an incubation period. Often the

incorporation of a fluorescent probe is complicated by compartmentalization, incomplete ester hydrolysis, and dye leakage problems (Haugland 1996). Moreover, the ability to specifically target man-made molecules to subcellular organelles and compartments is very poor to impossible. Due to these limitations, there are many intracellular processes left in the dark, unable to be seen by cell biologists.

History of the Green Fluorescent Protein

In 1962, Shimomura et al. (1962) discovered the green fluorescent protein (GFP), a protein associated with aequorin, the well known chemiluminescent protein found in the jellyfish species *Aequorea victoria*. Shortly after this report, the same group published the emission spectrum of GFP, which peaked at 508 nm (Johnson et al. 1962). In this report, they noted two things. First, the bioluminescence of the *Aequorea* jellyfish also peaked near this wavelength, and second, one of the two excitation peaks (395 nm and 475 nm) of GFP closely matched the 470 nm, blue emission of purified aequorin. Therefore, it was concluded that GFP absorbs the blue light of aequorin and converts this energy into the green light seen in the jellyfish. Nearly ten years later, Morin and Hastings (1971) found the same energy transfer process in the related coelenterates

Obelia and *Renilla*, a hydroid and a sea pansy, respectively. Figure 1 highlights the major milestones in the history of GFP.

Over the next approximately 20 years, researchers worked to characterize GFP. Morise et al. (1974) were able to purify and crystallize GFP, as well as measure its absorbance spectrum and determine its fluorescence quantum yield. They also demonstrated that aequorin could efficiently transfer its luminescence energy to GFP *in vitro*. In 1978, Prendergast and Mann (1978) obtained the first clear estimate of the molecular weight of GFP, which was 30,000 Da. At the same time, Shimomura (1979) using proteolytic fragments of denatured GFP was able to correctly predict the chromophore structure as a 4-(*p*-hydroxybenzylidene) imidazolidin-5-one attached to the peptide backbone through the 1- and 2- positions of the ring. Soon after this report, *Aequorea* and *Renilla* fluorescent proteins were shown to have the same chromophore (Ward et al. 1980). The final work of significance during this period was performed by Ward et al., who explored the pH sensitivity, aggregation tendency, and renaturation of the *Aequorea* GFP (Ward et al. 1982; Ward and Bokman 1982).

Despite all these efforts to characterize GFP, the real usefulness of GFP had still not been realized during this 30 year period. The major breakthroughs finally came in 1992 when Prasher et al. cloned the gene encoding GFP and in 1994 when Chalfie et al.

- 1962** *Aequorea victoria* GFP discovered. Emission peak: 508 nm, (Shimomura et al.).
- 1971** GFPs found in *Obelia* and *Renilla*, (Morin and Hastings).
- 1974** Purified and crystallized, (Morise et al.).
- 1978** Molecular weight determined, (Prendergast and Mann).
- 1979** Chromophore structure correctly proposed, (Shimomura).
- 1980** *Aequorea* and *Renilla* GFPs have the same chromophore, (Ward et al.)
- 1982** pH sensitivity, aggregation tendency, and renaturation investigated, (Ward et al.).
- 1992** Gene cloned from *Aequorea victoria*, (Prasher et al.).
- 1994** Expressed in other organisms, (Chalfie et al. and Inouye and Tsuji).
- 1996** Crystal structure determined, (Ormo et al.).
- 1997** Structural basis for dual excitation proposed, (Brejc et al.).
- 1997** Blue emission variant structure reported and pH sensing capabilities discussed, (Wachter et al.).
- 1998** Structure and spectra of yellow emission variant reported, (Wachter et al.).
- 1999** Structure and spectra versus pH explained, (Elsliger et al.).
- 1999** Halide and nitrate sensitivity of YFP, (Wachter and Remington).
- 2000** deGFPs and rsGFPs created (Hanson, unpublished data).

Figure 1. Milestones in the history of GFP.

(1994) and Inouye and Tsuji (1994) demonstrated that expression of the gene in organisms other than jellyfish leads to fluorescence. The ability of GFP to fluoresce in other organisms meant that it did not require any jellyfish specific enzymes, cofactors, or substrates for the production of its green light. In other words, the GFP gene sequence contains all the necessary information for the post-translational synthesis of the fluorophore. This is in contrast to most other known light emitting proteins such as firefly luciferase, which is an enzyme that needs firefly luciferin to catalyze a reaction with molecular oxygen to yield light (Lehninger et al. 1993).

The cloning of the GFP gene opened the door for mutagenesis and structure determination that had previously been shut. Random mutagenesis was performed to better understand what amino acids were responsible for the absorption and emission attributes of wild-type GFP. Ehrig et al. (1995) identified that substitution of threonine at position 203 with isoleucine (T203I) and E222G each result in mutant GFPs that have only one of the two fluorescence excitation bands seen in wild-type. Random mutagenesis has also led to mutants of GFP with enhanced properties. While wild-type GFP matures slowly at temperatures above which the jellyfish would have been exposed, modifications termed “folding mutations” were identified that improve the ability of GFP to mature and fluoresce at these elevated temperatures. Another substitution, S65T, was

identified as a mutation that leads to a six-fold brighter and a more photostable protein than wild-type GFP (Heim et al. 1995). In addition, the S65T mutation simplifies the excitation spectrum to a single peak centered at 489 nm. Lastly, replacements at position 66, one of the amino acids that forms the chromophore, with histidine or tryptophan yield fluorescent protein variants with blue or cyan emission, respectively (Heim et al. 1994).

In 1996, Ormö et al. solved the three-dimensional crystal structure of the S65T mutant of GFP, and Yang et al. independently determined the wild-type GFP structure (Ormö et al. 1996; Yang et al. 1996). The structures clearly showed that nearly all 238 amino acids that make up GFP are involved in forming an 11-stranded β -barrel motif. Traversing the center of the barrel is a slightly distorted α -helix, on which reside serine 65, tyrosine 66, and glycine 67, the amino acids that undergo oxidation and cyclization reactions to form the chromophore. The chromophore is therefore located near the exact center of the protein and is shielded from the surroundings by the barrel and the small helical stretches and loops present at the ends of the barrel. The structure also revealed a large number of polar groups buried near and in some cases interacting with the chromophore. Some of these interactions presumably help to stabilize the charge state of the chromophore (Kneen et al. 1998; Elsliger et al. 1999), and still others are proposed to aid in the chemistry of chromophore formation (Cody et al. 1993).

GFP as a Fluorescent Probe

Another remarkable quality of GFP is that it is incredibly stable and protease resistant. *In vivo* this translates into GFP having been successfully expressed in nearly all organisms tested, including many plants, mammals, yeast, bacteria, and fungi (Tsien 1998). Likewise, GFP has been successfully targeted to practically every major organelle of the cell, including the nucleus, mitochondria, endoplasmic reticulum, Golgi apparatus, secretory vesicles, peroxisomes, vacuoles, phagosomes, and plasma membrane (Tsien 1998). Therefore, the size of GFP and the various pHs, redox potentials, and ionic strengths of such organelles and organisms do not appear to impose any serious barrier to fluorescence.

Soon after the finding that GFP autocatalytically forms its own chromophore, the number of reports utilizing GFP skyrocketed, from 17 in 1994 to 3,664 by 2000, according to Medline, the online abstract service. For the first time, researchers had a self-sufficient genetically encoded fluorescent marker, which was particularly useful for the first proposed application of GFP. The experiment was to confirm the expression pattern of the *mec-7* promoter in the nematode *Caenorhabditis elegans* (Chalfie et al. 1994). GFP worked particularly well for this application, because the *Caenorhabditis elegans* cuticle hinders access of substrates required for detecting other reporter genes.

Nowadays, GFP is most often used as a genetic fusion partner to host proteins to monitor their localization within cells or their expression patterns in organisms, especially during embryogenesis and early development. This is performed by fusing the gene for GFP in frame with the gene encoding an endogenous protein of interest. When expressed, the resulting chimera hopefully maintains the normal function and localization of the host protein, but is also fluorescent. Thus a previously indiscernible protein is given a fluorescent tag, allowing it to be tracked throughout an individual cell or organism. This ability to visually follow proteins brings about a better understanding of how they function.

Along with utilizing the idle fluorescent qualities of GFP, dynamic indicators of GFP have become popular tools for studying the biology of cells. The active indicators rely on modulation of the chromophore environment and hence the fluorescence of GFP in response to environmental factors such as membrane potential, molecular proximity, calcium and halide ion fluctuation, and pH. The first genetically encoded optical sensor of membrane potential was made by fusion of GFP into the Shaker voltage-sensitive K⁺ channel (Siegel and Isacoff 1997). The GFP chimera exhibited a 5% fluorescence decrease in response to depolarization, with a time constant of 85 ms.

Fluorescence resonance energy transfer (FRET) is a phenomenon that occurs when two fluorophores are spatially close (within 100 Å) and the emission of the donor overlaps the excitation of the acceptor. Experimentally this is achieved by fusing GFPs of differing color to separate host proteins and assaying for their interaction by exciting the donor and detecting the emission from the acceptor. Besides detecting protein interactions, FRET was exploited to create the first dynamically responsive biochemical indicator based on GFP. These Ca^{2+} biosensors were developed almost simultaneously by Rosomer et al. and Miyawaki et al. by fusing GFPs of different color to calmodulin, a calcium binding protein (Rosomer et al. 1997; Miyawaki et al. 1997). Upon addition of calcium, varying degrees of FRET were detected and after calibration, *in vivo* Ca^{2+} concentrations could be determined. Baird et al. later improved on these FRET based Ca^{2+} sensors by circularly permutating and inserting calmodulin into GFP (Baird et al. 1999).

Useful biosensors have also been developed by mutagenesis of GFP. Many of the original pH-sensitive variants were serendipitously created while trying to enhance the passive fluorescent attributes of GFP. Kneen et al. employed the GFP mutant F64L/S65T to determine the pH of the cytoplasm of CHO and LLC-PK1 cell lines (Kneen et al. 1998). Llopis and coworkers used a GFP variant with an increased chromophore

ionization constant (pK_a), to measure the alkaline pH of mitochondria as well as the pH of the Golgi apparatus and cytosol of HeLa cells and rat neonatal cardiomyocytes (Llopis et al. 1998). Recently, it was discovered that an engineered variant of GFP, which contains the T203Y substitution plus mutations to improve brightness and folding at 37°C (S65G/V68L/S72A), has a pK_a which is dependent on the concentration of halide or nitrate ions (Wachter and Remington 1999; Wachter et al. 2000). Jayaraman et al. used this variant with the additional mutation, H148Q, to assay Cl^- transport through plasma membrane cystic fibrosis transmembrane conductance regulator Cl^- channels with excellent sensitivity to extracellular Cl^-/I^- exchange (Jayaraman et al. 2000). These findings suggest that GFP's usefulness may be extended even further by designing new mutants with unique spectral properties.

Research Focus

As there are many limitations with the use of small molecule fluorescent probes and there are clear advantages of a genetically encoded fluorescent marker, the further extension of GFP as a biosensor should be pursued. Therefore, my research has focused on designing improved pH-sensitive and novel oxidation-reduction (redox) sensitive GFP biosensors. Primarily this work has been accomplished through rational design of

mutations based on the three-dimensional structure of GFP. In many cases, the resulting GFP biosensors were tested *in vivo* for their ability to function as intracellular pH or redox indicators and their structures were solved in order to better understand the structural basis for the modified spectral properties.

The original pH-sensitive GFPs lacked ideal physiological pK_a values and furthermore they required extensive calibration in order to accurately account for the varying amount of GFP present within living cells due to nonuniform expression levels, distribution, or cell thickness. Additionally, photobleaching of some GFP variants has been reported, which might otherwise be misinterpreted as an acidification. Most of these drawbacks can be reduced or eliminated by a ratiometric sensor. A ratiometric sensor is one that has two excitation or emission intensities with an opposite response to an environmental factor. Accordingly, the specific goals of this portion of my project were to amend the calibration methodology, expand the pK_a range, and create near neutral pK_a variants of pH-sensitive GFPs.

Another goal of my research was to overcome the invasive, labor intensive, whole cell determinations of current methods in determining redox status in cells. Current methods require cells to be harvested before their contents are analyzed. Therefore, these methods do not allow for single cell or subcellular determinations of redox status.

Moreover, it is impossible to monitor redox changes over time in the same cell or group of cells. Current methods are also time consuming and consist of multi-step procedures that most likely do not accurately depict the *in vivo* redox environment. Engineering a redox-sensitive GFP that can detect changes in redox potentials was pursued to overcome these limitations.

CHAPTER II

pH-SENSITIVE GREEN FLUORESCENT PROTEIN VARIANTS WITH VARIOUS pK_a S AND DUAL-EXCITATION WAVELENGTHS

Portions of the work presented in this chapter were done in collaboration with Rebekka M. Wachter, Marc-André Elsliger, Karen Kallio, and S. James Remington of the Institute of Molecular Biology and Department of Physics at the University of Oregon. Portions of this chapter were published in *Structure* 6, 1267-1277 (1998) and *Biochemistry* 38, 5296-5301 (1999).

This chapter describes the design and characterization of pH-sensitive variants of the green fluorescent protein having physiological pK_a s, one of which showed ratiometric-by-excitation properties.

Summary

Mutations were designed in the popular S65T variant of the green fluorescent protein (GFP) to improve its pH-dependent spectral properties. The H148G substitution

resulted in a chromophore ionization constant (pK_a) of 7.0. Whereas the replacement H148D raised the pK_a to 7.8 and resulted in fluorescence of the neutral chromophore species as well as the anionic species. These fluorescence peaks displaying ratiometric properties in response to pH changes with a pH-independent isosbestic point should greatly facilitate *in vivo* pH monitoring. The crystal structure of this variant was solved to 2.1 Å, however the strand encompassing residue 148 was somewhat disordered indicating a high degree of flexibility in this region. The H148G mutation was also placed in the yellow emission variant (S65G/V68L/S72A/T203Y) of GFP to examine the effects of solvent accessibility to the chromophore. Structural analysis of this variant indicated that a solvent channel to the chromophore had opened up and that solvent access was not detrimental to fluorescence. In this chapter, improved pH-sensitive GFP variants with alkaline shifted pK_a s, more physiological pK_a s, and ratiometric-by-excitation properties are described.

Introduction

Measurement of pH is one of the most important and frequently used procedures in biochemistry. Almost every biological process is pH-dependent. In normal healthy cells, maintenance of intracellular pH is a regulated process that allows for optimal

activity of many cellular processes. In the secretory pathway, cleavage of prohormones and posttranslational processing of secretory proteins is pH-dependent, as is the retrieval of escaped luminal endoplasmic reticulum proteins (Schmidt and Moore 1995; Wilson et al. 1993). Across the inner mitochondrial, thylakoid, and bacterial plasma membranes, a proton gradient can be established by pumping protons against a concentration gradient, thereby creating a difference of pH. The F_1F_o ATP synthase can then use this proton-motive force to drive ATP synthesis. Nearly all cells take advantage of this mechanism of chemiosmotic coupling of electron transport to ATP synthesis to meet their energy needs.

pH also plays an important role in many other normal and abnormal physiological processes. For instance, pH signaling has been implicated in apoptosis. Changes in intramitochondrial and cytosolic pH have been found to occur early in the apoptosis process and modulate caspase activation during apoptosis (Matsuyama et al. 2000). Tumors are known to have a higher pH than non-cancerous tissue (Gillies et al. 1994). In addition, in many mitochondrial disorders, dysfunction of the oxidative phosphorylation system leads to a build-up of lactic acid caused by anaerobic respiration (Taylor et al. 1997). To better understand pH changes that take place *in vivo*, good intracellular pH indicators are needed.

The green fluorescent protein (GFP) has burst on to the cell biology stage as a highly versatile, genetically encoded fluorescent marker. Although the GFP chromophore is locked in a rigid protein shell, experimentation has shown that the GFP chromophore phenolic hydroxyl ionizes as a function of pH in certain mutant backgrounds. Ionization of the chromophore leads to two distinct absorption bands, centered near 400 nm (band A) and near 490 nm (band B). Previous spectroscopic and structural analysis have revealed that band A is likely to be the neutral form of the chromophore, while band B is thought to be the anionic chromophore species (Kneen et al. 1998; Elsliger et al. 1999). In wild-type GFP, the ratio of band A to band B is fixed at a biologically relevant pH (Ward et al. 1982), on the other hand, in most GFP mutants the ratio changes with pH (Miesenbock et al. 1997; Llopis et al. 1998; Robey et al. 1998). However, excitation of band A in most variants leads to weak or non-existent emission (Wachter et al. 1998; Elsliger et al. 1999).

GFP variants have been used to examine the pH of various intracellular organelles. Kneen et al. employed the GFP mutant F64L/S65T to determine the pH of the cytoplasm of CHO and LLC-PK1 cell lines (Kneen et al. 1998). Llopis and coworkers used a yellow emission variant of GFP (YFP), with an increased ionization constant (pK_a), to measure the alkaline pH of mitochondria as well as the pH of the Golgi

apparatus and cytosol of HeLa cells and rat neonatal cardiomyocytes (Llopis et al. 1998). However, they noted that mitochondrial pH in some cell types may be almost one pH unit above YFP's pK_a, thus saturating the probe. Therefore it was hypothesized that mutagenesis might be able to improve properties such as pK_a and/or dynamic range. In addition, mutagenesis could also help to create novel ratiometric GFPs with pH-dependent excitation or emission shifts.

To this end, rationally designed mutations were introduced at histidine 148 of GFP and YFP, and the resultant mutants were analyzed for their ability to enhance the characteristics of these early pH-sensitive GFP variants. Crystal structure analysis was performed on two of the mutants in order to correlate structural changes more closely with spectral and biochemical properties. These findings demonstrate that mutagenesis can manipulate the pK_a of the chromophore and yield mutant GFPs with ratiometric properties. Moreover, these studies revealed that solvent access to the fluorophore is not detrimental to fluorescence. In this work, improved pH-sensitive GFP variants with alkaline shifted pK_as, more physiological pK_as, and ratiometric-by-excitation properties are described.

Results

Neutral pK_a Variant, GFP S65T/H148G

In the crystal structure of the GFP S65T variant, histidine 148 is within hydrogen bonding distance to the chromophore phenolic hydroxyl and serves as a barrier between bulk solvent and the chromophore (Ormö et al. 1996; Elsliger et al. 1999). With the typical pK_a for a free histidine in solution being 6.0 and this value corresponding exactly to the chromophore pK_a of GFP S65T, it is likely that histidine 148 is instrumental in governing the chromophore ionization. To better understand both the role of histidine 148 in maintaining the chromophore pK_a and to examine the effects of solvent accessibility on the fluorescent properties, histidine 148 was mutated to a glycine in GFP S65T. The resulting mutant, GFP S65T/H148G, had a pK_a of 7.0, a full order of magnitude increase compared to GFP S65T. Therefore, histidine 148 appears to play a direct role in maintaining the chromophore charge state. Despite the large change in pK_a, the fluorescence excitation spectra of these two variants are nearly identical (Figure 2). In both cases, only the anionic chromophore species has any appreciable fluorescence. Figure 3 shows the dual absorbance behavior of GFP S65T/H148G and illustrates how

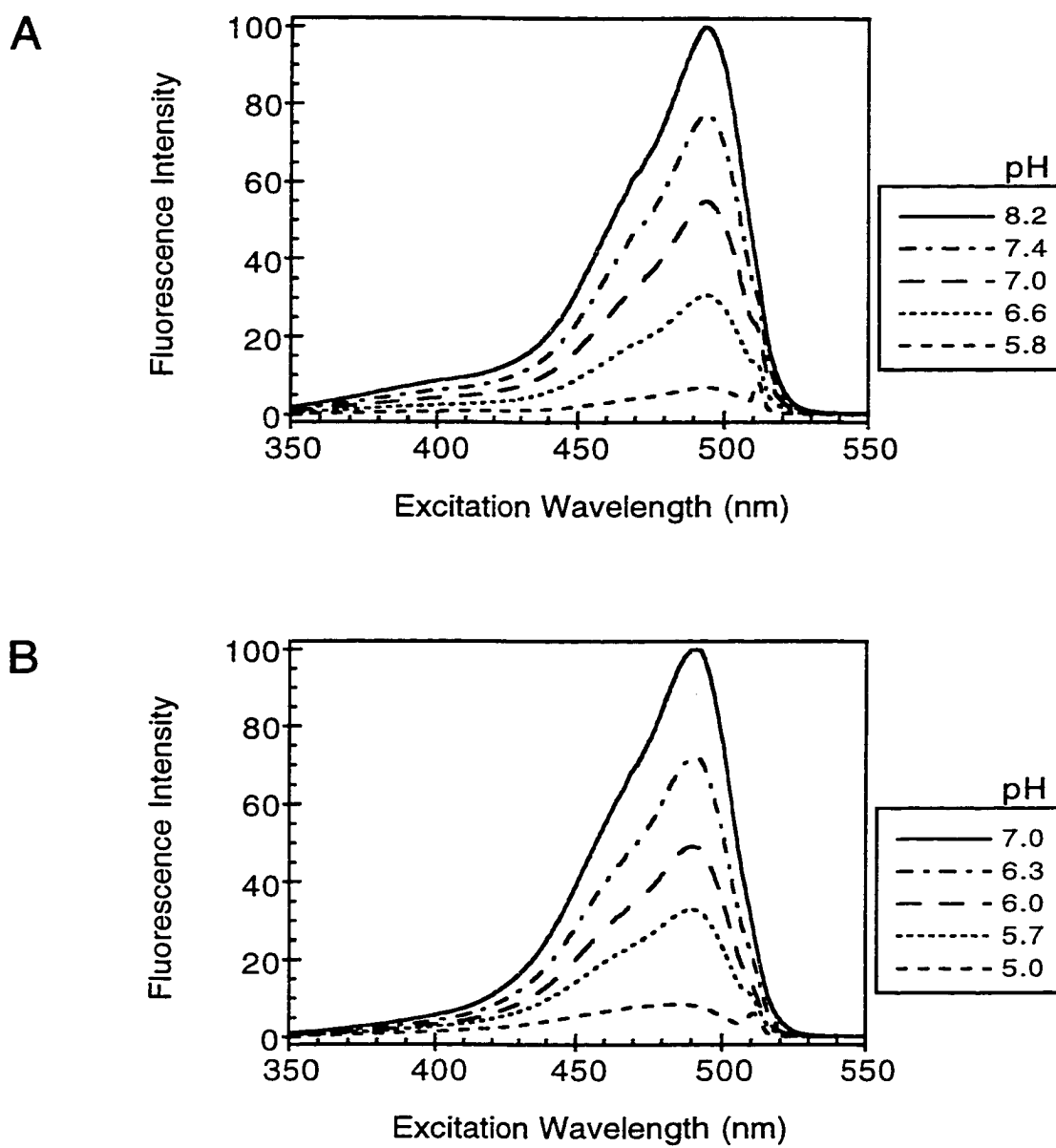


Figure 2. Fluorescence excitation spectra of two pH-sensitive GFP variants as a function of pH. Fluorescence intensity values were normalized to the maximum intensity of GFP S65T/H148G (A) at pH 8.2 and of GFP S65T (B) at pH 7.0. Emission was monitored at 510 nm.

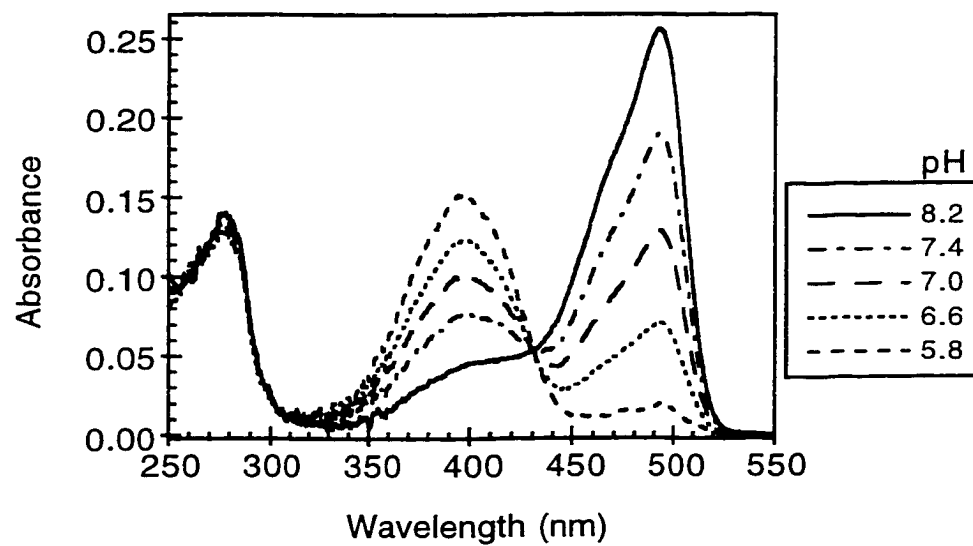


Figure 3. Absorbance spectra of GFP S65T/H148G at varying pHs. Absorbance spectra were collected from 250 to 550 nm at the indicated pHs.

the neutral chromophore species (397 nm) decreases as the anionic form (492 nm) increases when going from acidic to basic pH.

High pK_a Variant, YFP H148G

The analogous mutation had a similar effect in YFP. Like GFP S65T/H148G, YFP H148G has two absorbance maxima whose relative ratio is pH-dependent (Figure 4A). The UV-absorption peaks at 397 nm, whereas the visible absorption peaks at 514 nm. Intense fluorescence emission is observed upon excitation at the longer wavelength band (Figure 4B), while excitation of the shorter wavelength band yields only very weak emission. The chromophore pK_a of YFP H148G was determined by absorbance (Figure 5A) as being 8.0 and by fluorescence (Figure 5B) as being 7.9 at physiologic salt concentration (~140 mM), again one pH unit higher than the original YFP variant. Excitation of phenolic chromophores normally entails migration of electron density from the phenol towards the rest of the chromophore, which stabilizes the phenolate and thus makes the proton prone to leave in the excited state (Stewart 1985). This may explain the lower pK_a value obtained by fluorescence.

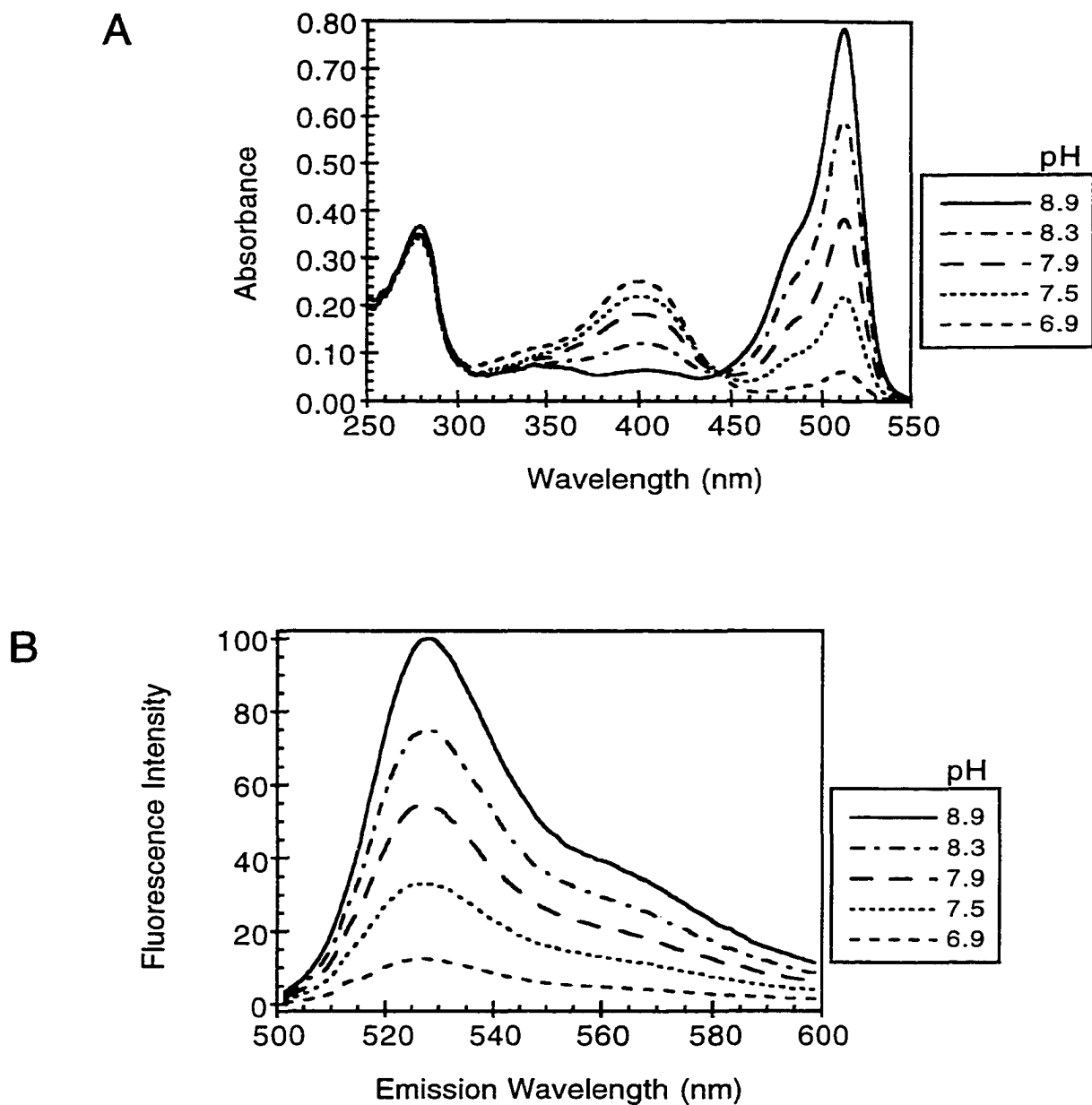


Figure 4. Absorbance and fluorescence emission spectra of YFP H148G versus pH. Absorbance was scanned at the indicated pHs (A). Fluorescence emission spectra (B) were collected on two-fold diluted absorbance samples (see experimental procedures), excited at 512 nm. Fluorescence spectra were normalized to the maximum intensity of the pH 8.9 sample.

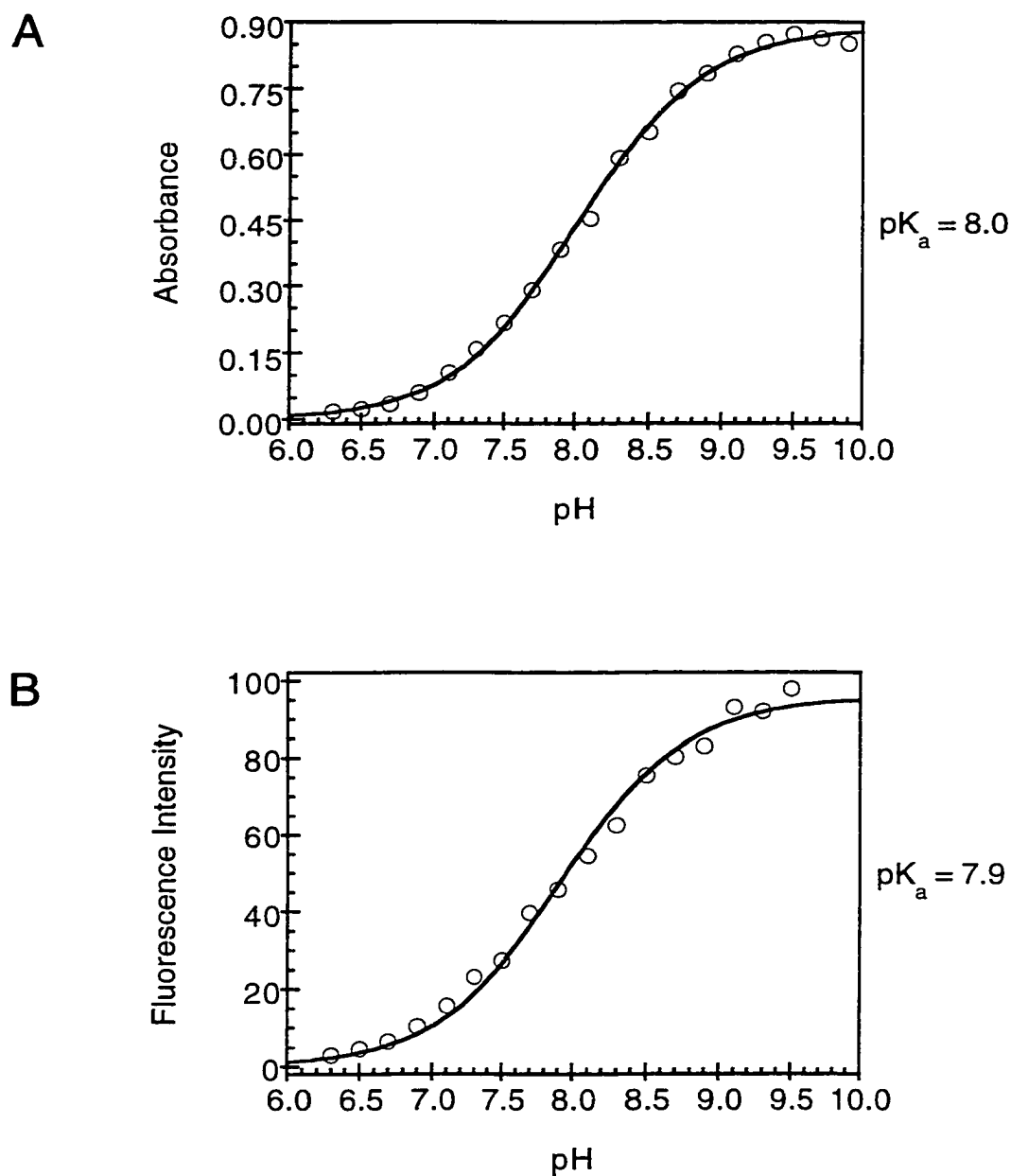


Figure 5. Absorbance and fluorescence pH titrations of YFP H148G. Absorbance values at 512 nm are plotted as a function of pH (A) and fit to a titration curve with a single pK_a . Normalized fluorescence intensity at 528 nm is plotted versus pH (B) and fit to a titration curve.

Structural Analysis of YFP H148G

To examine the solvent accessibility to the chromophore and any structural effects caused by the H148G mutation, the crystal structure of YFP H148G was solved to 2.6 Å resolution (Table 1). In the presence of polyethylene glycol and acetate at pH 4.6, the mutant protein crystallized as a monomer in spacegroup P₂,2₁2₁, isomorphous to GFP S65T (Ormo et al. 1996). When compared with the structure of YFP (Wachter et al. 1998), the α -carbons (C_α) of YFP H148G overlay closely (rms deviation of 0.35 Å) in all areas except around the C_α of residue 148, where a movement of 1.1 Å is observed (Figure 6). This movement has not been observed in other low pH structures crystallizing in the same spacegroup (Wachter et al 1997; Elsliger et al. 1999). Additionally, neither residue 148, nor the adjacent residues are involved in crystal contacts, further indicating that the observed movement is due to the H148G substitution and not due to the crystallization conditions.

In nearly all previous GFP structures examined to date, the β -barrel is somewhat perturbed around the phenolic end of the chromophore. The β -strand nearest the chromophore in that region bulges out around histidine 148, so that the ideal anti-parallel arrangement of hydrogen bonds is broken between residues 146 to 150 and 165 to 168.

Table 1. Data Collection and Refinement Statistics for YFP H148G and GFP S65T/H148D.

<i>Data Collection</i>	YFP H148G	GFP S65T/H148D
Crystal		
Total observations	29,904	78,165
Unique reflections	7,373	13,829
Cell dimensions (a, b, c; Å)	52.0, 62.7, 69.9	51.65, 63.14, 70.30
Resolution (Å)	20-2.60	19.8-2.10
Highest resolution shell (Å)	2.80-2.60	2.15-2.10
Completeness ¹ (%)	99 (97)	98.6 (96.9)
R _{merge} ^{1,2}	0.065	0.059 (0.374)
<i>Refinement</i>		
Spacegroup	P2 ₁ 2 ₁ 2 ₁	P2 ₁ 2 ₁ 2 ₁
Number of protein atoms	1,747	1,761
Number of solvent atoms	30	65
R _{factor} ³	0.159	0.177
Average B-factors (Å ²)	25.2	41.1
Protein atoms	25.0	40.8
Solvent	34.5	49.6
rms deviations		
Bond lengths (Å)	0.012	0.008
Bond angles (°)	2.07	1.883
B-factor correlations (Å ²)	3.82	3.697

¹Values in parentheses indicate statistics for the highest resolution shell.

²R_{merge} = $\sum|I - \langle I \rangle| / \sum|I|$, where I is the observed intensity, and $\langle I \rangle$ is the average of intensity obtained from multiple observations of symmetry related reflections.

³R_{factor} = $\sum||F_o - F_c|| / \sum|F_o|$, where F_o and F_c are the observed and calculated structure factors, respectively.

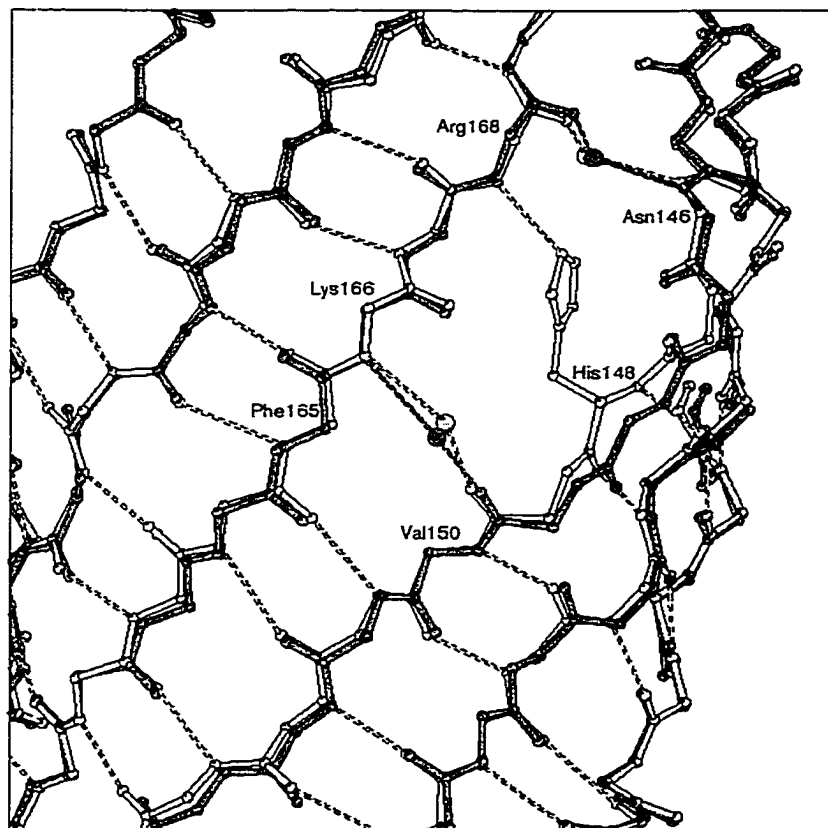


Figure 6. Overlay of the backbone-atom trace of YFP and YFP H148G. Part of the β -barrel and the β -strand bulge around His 148 are shown. The strand movement at position 148 of YFP H148G (green) away from the position seen in YFP (yellow) is also visible. The dashed lines represent potential hydrogen bonds.

These strands are instead laced together with the imidazole ring of histidine 148 and several bound water molecules. It was anticipated that the H148G replacement would either allow the bulge to close or open up a solvent channel to the chromophore.

The crystal structure clearly showed a solvent channel to the chromophore has formed upon elimination of the imidazole ring by the H148G substitution (Figure 7). The H148G mutation led to only minor structural rearrangements of protein atoms. The side chain of isoleucine 167 has moved 1.1 Å toward the position normally occupied by the imidazole side chain. Surprisingly, the β -strand encompassing residue 148 did not move toward this position, forming a hydrogen bonded sheet to the neighboring strand of residues 165 to 168, but instead the C_α of residue 148 has actually moved in the opposite direction by 1.1 Å, opening an even larger gap between the backbone atoms of residues 148 and 168 (Figure 6). In the absence of the imidazole ring, direct access to the phenolic end of the chromophore is greatly improved. Calculation of the solvent-accessible surface area of the chromophore using a 1.4 Å radius sphere, shows that 22% of the chromophore surface is solvent-accessible. Eight percent of the chromophore, entirely at the phenolic end, is exposed to exterior solvent and 14% is accessible to interior solvent as a result of contact with internal cavities. Despite the solvent exposed chromophore, H148G substituted GFP variants continue to be highly fluorescent.



Figure 7. Stereoview of the solvent-accessible surface of YFP H148G. The surface (cyan) was calculated using a 1.4 Å probe after deleting the chromophore (magenta) and all water molecules (red). The outer surface of the protein is on the left edge of the figure. On the right side of the figure, internal cavities appear as appendages to the chromophore cavity.

Ratiometric GFP S65T/H148D

To create a high pK_a variant that overcomes the halide sensitivity problem imposed by the background mutations present in YFP (see discussion), histidine 148 was substituted for aspartic acid in GFP S65T. The rationale behind this designed change was to introduce a potential negative charge near the chromophore, which in turn could raise the chromophore pK_a by destabilizing the anionic species. The new variant, GFP S65T/H148D, exhibited pH-dependent absorbance spectra with peaks at 415 nm and 487 nm (Figure 8A). The pK_a was 7.8, a shift of nearly two orders of magnitude in the equilibrium constant for ionization, presumably due to the proximity of the negatively charged residue to the phenolic end of the chromophore.

Excitation of the neutral chromophore (band A) in wild-type GFP leads to bright green fluorescence. However, most GFP variants exhibit very little fluorescence upon excitation at this shorter absorbance wavelength. Unexpectedly, GFP S65T/H148D displays significant green fluorescence in response to excitation of band A (Figure 8B). This green fluorescence upon illumination at 415 nm is clearly not just the result of band overlap with band B, as is observed for GFP S65T (Figure 2B). A clean isosbestic point is visible in the excitation spectra as a function of pH. Emission intensities of band A and B excitation, have opposite response to pH changes, therefore GFP S65T/H148D is a

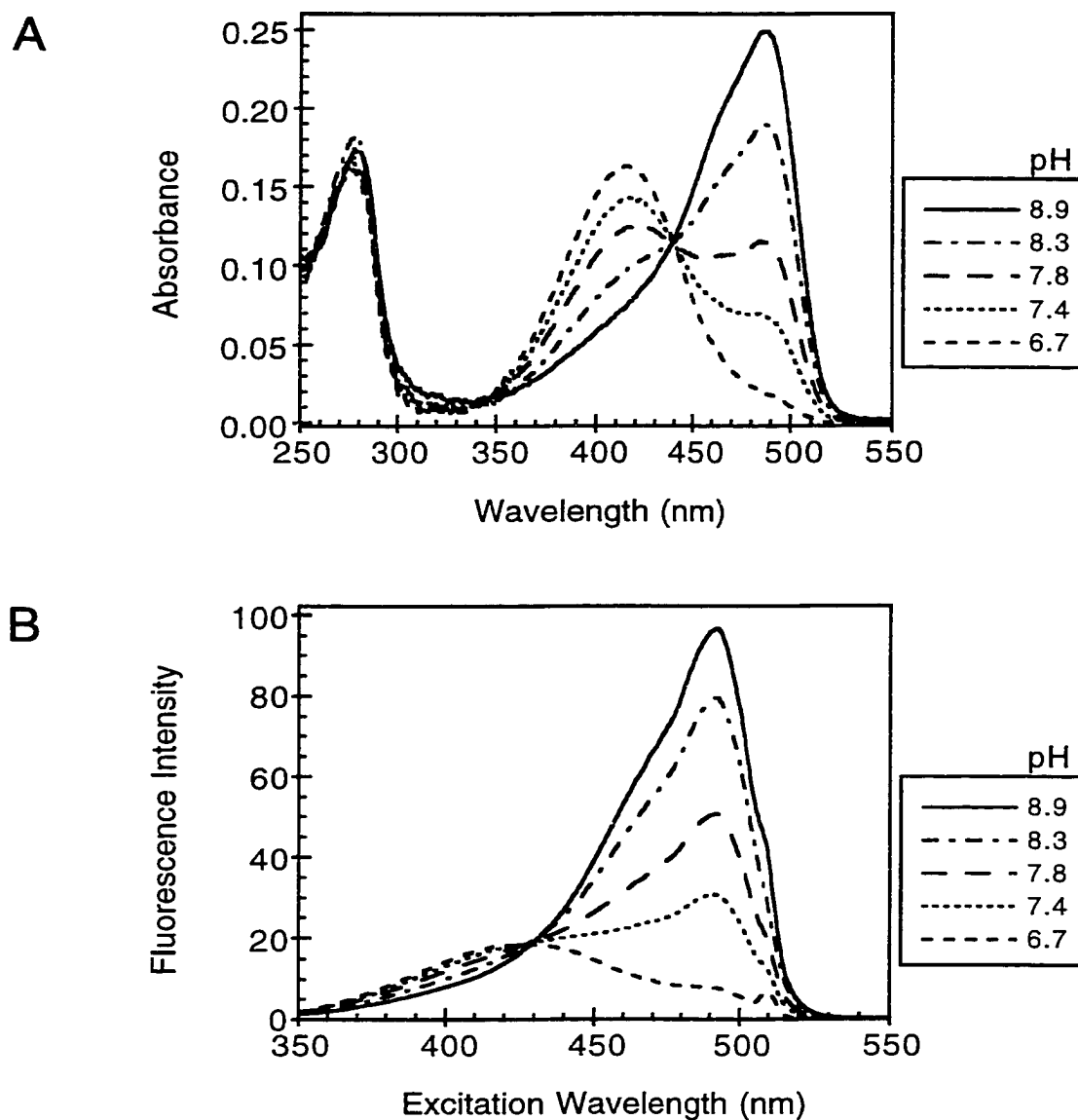


Figure 8. Absorbance and fluorescence excitation spectra of GFP S65T/H148D. Absorbance (A) was scanned at the indicated pHs. Samples were diluted two-fold (see experimental procedures) and the fluorescence excitation (B) was collected by monitoring emission at 510 nm. Fluorescence spectra were normalized to the maximum intensity of the pH 9.1 sample (not shown), which was given a value of 100 at 490 nm.

ratiometric-by-excitation pH sensor. As the pH is changed from acid to base, emission from band A excitation decreases, and at the same time, emission from band B excitation increases. The maximum fluorescence intensity of the shorter excitation peak at pH 6.9 and lower, is approximately 20% of the maximum emission intensity of the longer wavelength peak obtained at pH 9.1. This translates into a 26-fold change in the dynamic range for a ratio of excitation peak intensities. Table 2 compares some of the biochemical and spectroscopic characteristics of the GFP S65T/H148G, YFP H148G, and GFP S65T/H148D to wild type GFP, GFP S65T, and YFP.

To better relate structural aspects of the introduced substitution to the observed spectroscopic properties of the mutant, the crystal structure of GFP S65T/H148D was solved. This structure revealed only modest differences when compared to GFP S65T in the area surrounding the phenolic end of the chromophore (Figure 9). The most striking differences were the high degree of flexibility surrounding residue 148 and the lack of potential hydrogen bonds to the chromophore. The B-factors for residues 145-149 were found to be 2.7 times higher than those for GFP S65T (Orm   et al. 1996) in this region. In fact, the side chain of the aspartic acid 148 substitution was too disordered to model past the C_{  } atom. The disorder in this region coupled to the fact that the pH of the crystallization condition (~8.0) was close to the pK_a (7.8), suggests that a pH-dependent

Table 2. Spectroscopic and Biochemical Properties of GFPs.

	Absorbance band		Emission band ¹		pK _a ²	
	A	B	A	B	absorbance	fluorescence
WT GFP	395	475	460/508	504	NA	NA
S65T	394	489	NA	511	5.95	6.04
S65T/H148G	397	492	NA	512	7.04	6.97
S65T/H148D	415	487	510	510	7.95	7.75
YFP	392	514	NA	528	7.00	6.95
YFP H148G	397	512	NA	528	8.02	7.93

¹Emission band(s) A and B are peaks in the emission spectrum and result from excitation at the wavelength of absorbance band A and B, respectively.

²pK_a values were determined by both absorbance and by fluorescence.

All absorbance and emission values are given in units of nanometers.

NA: not applicable

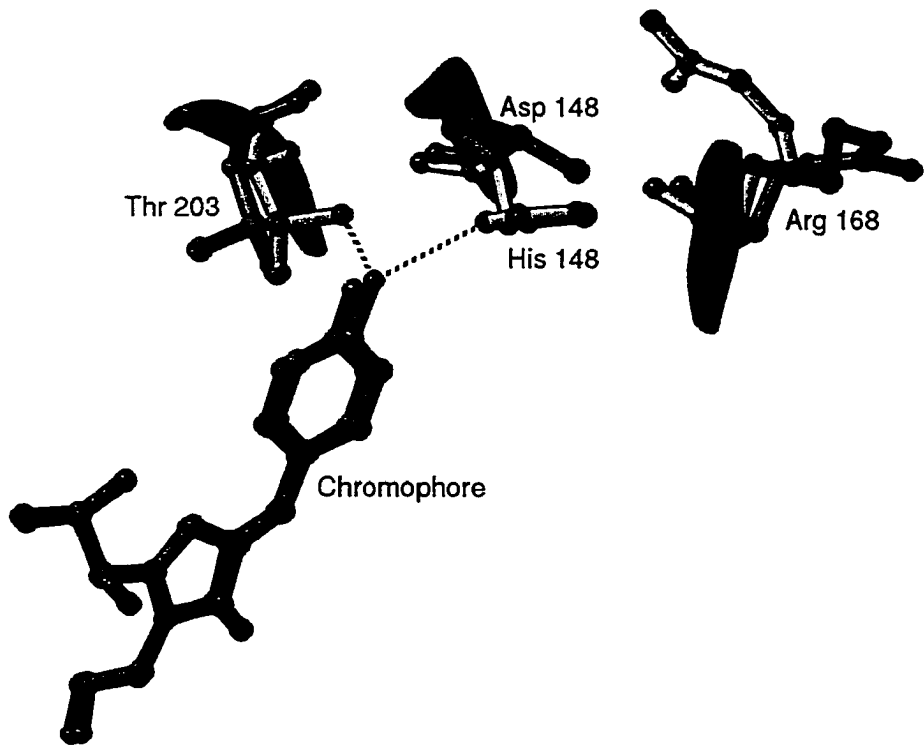


Figure 9. Overlay of the chromophore region of GFP S65T and GFP S65T/H148D. Dashed lines indicate possible hydrogen bonds from His 148 and Thr 203 to the chromophore phenolate in GFP S65T (Orm   et al. 1996). The side chains of GFP S65T/H148D are shown in red. Only the C_{  } atom of Asp 148 is shown as the remainder of the side chain was too disordered to model. Conformational switching of Thr 203 destroys the potential hydrogen bond to the chromophore and Arg 168 adopts a new position further away from Asp 148.

rearrangement of this area may occur. The almost two-orders-of-magnitude shift in pK_a introduced by the single H148D mutation, may be due in part to the lack of anionic chromophore stabilizing residues. In this variant, threonine 203 rotates away from the location seen in GFP S65T and is no longer in position to interact with the chromophore. In addition, the introduction of a potentially negatively charged residue near the chromophore further destabilizes the anionic species.

Discussion

GFP as an *In Vivo* pH Indicator

To better understand pH changes that take place *in vivo*, a good intracellular “pH meter” is needed. pH-sensitive small molecule indicators have been available for some time now, however these dyes stain the whole cell, precluding experiments on individual organelles. In this work, improved pH-sensitive GFP variants with alkaline shifted pK_as, more physiological pK_as, and ratiometric-by-excitation properties were described. These new GFPs are not only targettable to subcellular compartments, but given the range of pK_as, they should be ideal for studying a wide range of environments from the relatively acidic environments found in the Golgi apparatus and the vacuole to the more alkaline compartments like the mitochondrial matrix.

Given the dual-excitation properties of the GFP S65T/H148D mutation, this mutant has tremendous promise as an intracellular pH indicator. In fact this variant has been used by De Giorgi et al. (submitted) to investigate the mechanism of cytochrome c release from mitochondria during apoptosis. By targeting GFP S65T/H148D to the mitochondrial matrix they were able to demonstrate that directed repetitive gatings of the mitochondrial permeability transition pore in the live cell signal apoptosis by directing Bax translocation to the mitochondria. Subsequently, Bax-dependent outer membrane permeabilization leads to cytochrome c release and caspase activation. GFP S65T/H148D has also been used by Fasano et al. to discover that changes in root cap pH are required for the gravity response of the *Arabidopsis* root (Fasano et al. 2001). Since the fluorescence excitation of GFP S65T/H148D is ratiometric, quantitative imaging is greatly facilitated because ratios cancel out the contribution of inner filter effects and variations in expression levels, cell or tissue thickness, and excitation intensity (Whitaker et al. 1991).

In near-neutral pH environments, the most useful GFP variant for monitoring pH changes may be GFP S65T/H148G. Despite the fact that this variant exhibits only one pH-dependent excitation and emission wavelength, it is not plagued by the halide sensitivity that afflicts YFP variants. It has been shown that both the absorption and

emission of yellow variants of GFP have pK_as that are dependent upon the concentration of halide or nitrate ions (Wachter and Remington 1999; Wachter et al. 2000). Consequently, YFP and YFP H148G are not the most ideal choice of pH indicators despite their pK_as of 7.0 and 8.0, respectively. Nontheless, YFP has been used to study *in vivo* pH (Kneen et al. 1998), and the halide sensitivity of the H148Q variant of YFP has been exploited to study Cl⁻ transport through plasma membrane cystic fibrosis transmembrane cystic fibrosis conductance regulator Cl⁻ channels (Jayaraman et al. 2000). Furthermore, YFP variants may find increased utility with the addition of the Q69M mutation, which yields a mutant unaffected by chloride, with twice the photostability of previous YFPs, and with better expression at 37°C and in organelles (Griesbeck et al. submitted).

Solvent Accessibility of the Chromophore

GFP H148G and YFP H148G were both found to be highly fluorescent, with the light-emitting properties of the fluorophore seemingly unaffected by the introduction of a solvent channel to the chromophore, indicating that significant quenching does not occur. Since in spite of an opening in the β-barrel, the protein fold is still intact in YFP H148G and almost certainly in GFP H148G, the H148G substitution may be useful for allowing

access of small molecules and ions to the chromophore. This mutation in conjunction with as yet to be determined substitutions may lead to engineering of analyte binding sites near the chromophore of GFP. Such binding sites may be designed to detect ions such as Ca^{2+} , Mg^{2+} , Zn^{2+} , or other ions of interest. As a result, the H148G mutation may hold a key to future biosensor design based on GFP.

Experimental Procedures

Mutagenesis and Protein Preparation

Mutagenesis was carried out on a histidine-tagged version of the S65T and YFP/10C (S65G/V68L/S72A/T203Y) variants of GFP in the plasmid pRSET_B. Mutations were introduced via the QuikChange™ Site-Directed Mutagenesis Kit (Stratagene, La Jolla, CA), following the manufacturer's protocol. All mutations were verified by DNA sequencing of the entire GFP coding sequence. Mutant protein was recombinantly expressed in *Escherichia coli*, strain JM109(DE3). Transformed bacteria were grown in four liters of S-LBH media at 37°C, stirred at 450 rpm, with 5 liters per minute air flow, and in the presence of 0.27 mM ampicillin. After the culture reached a density of approximately OD₅₉₅ equal to 1.0, then protein expression was induced by addition of isopropyl-β-D thiogalactopyranoside (IPTG) to a final concentration of 1

mM. Concomitantly, the temperature of the culture was reduced to 25°C and allowed to grow for an addition three hours. Cells were then harvested by centrifugation at 4°C in a Beckman KA-9.1000 rotor at 11,800 x g for 5 minutes. The bacterial cell pellet was resuspended in 100 mL of 50 mM HEPES (pH 7.9), 300 mM NaCl, 10% glycerol, 3 mM β-mercaptoethanol, and 0.1 mM phenylmethylsulfonyl fluoride (PMSF). The resuspended cells were then sonicated for a total of five minutes. The cell lysate was clarified twice by centrifugation in a Beckman JA-20 rotor at 4°C for 20 minutes. Next, the supernatant was loaded onto a pre-equilibrated nickel-nitriloacetic acid (Ni-NTA) metal-affinity column (Qiagen, Hilden, Germany). The equilibration and subsequent washing of the column was performed using washing buffer (50 mM HEPES, pH 7.9 and 300 mM NaCl,). Proteins were eluted from the column by a step gradient of washing buffer plus 20 mM imidazole to remove mostly unwanted proteins and then with washing buffer plus 100 mM imidazole to elute the GFP variant of interest. To remove the amino-terminal histidine tag and as a further purification step the eluted protein was incubated with $1/50$ (w/w) γ-chymotrypsin at 22°C for 22 hours. The protein was then dialyzed against washing buffer and concentrated to approximately 15 mg mL⁻¹ by filtration (Centricon 10; Amicon Inc., Beverly, MA). The final purification step was to desalt the protein by buffer exchange on a PD-10 Sephadex column (Amersham Pharmacia,

Piscataway, NJ) into 20 mM HEPES (pH 7.9). Characteristic yields of mutant GFP protein were in the range of 25 to 120 milligrams and with a purity greater than 95%. All protein concentrations were found using the A_{280} and the theoretical ϵ_{280} ($19,890 \text{ M}^{-1} \text{ cm}^{-1}$) determined for GFP S65T using the method developed by the Gill and von Hippel (1989), which were in good agreement with protein concentrations determined using the BCA assay kit (Bio-Rad, Hercules, CA) with bovine serum albumin as the standard.

Spectroscopy and pH Titrations

pH titrations were performed using approximately $200 \mu\text{g mL}^{-1}$ mutant GFP in 75 mM buffer and 140 mM NaCl. According to the desired pH, an appropriate buffer was chosen from MES, HEPES, or CHES and the final pH was adjusted by HCl or NaOH addition. The absorbance was then scanned between 250 and 550 nm on a Shimadzu 2101 spectrophotometer. Fluorescence measurements were performed on a Hitachi F4500 fluorescence spectrophotometer at a protein concentration of approximately $100 \mu\text{g mL}^{-1}$ in the same buffers used for absorbance measurements. For emission scans, the excitation wavelength was set to the absorbance maximum of band B for each mutant. Apparent chromophore pK_a values were determined by plotting the absorbance of band B or the emission intensity when excited at band B as a function of pH and fitting the data

to a titration curve (Kaleidagraph, Abelbeck Software).

Crystallization and Structure Determination of YFP H148G

The mutant protein, S65G/V68L/S72A/H148G/T203Y, was concentrated to approximately 12 mg mL⁻¹ in 20 mM HEPES buffer at pH 7.9. Rod-shaped crystals grew in 3 to 4 days measuring 1.8 x 0.08 x 0.04 mm. Crystals were grown at 4°C from hanging drops containing 4 µL protein and 4 µL mother liquor. The mother liquor consisted of 50 mM sodium acetate (pH 4.6), 50 mM ammonium acetate, and 16% polyethylene glycol 4000.

X-ray diffraction data were collected on a single crystal at room temperature using a Xuong-Hamlin area detector (Hamlin 1985). Data were collected in space group P2₁2₁2₁, and were reduced using the supplied software (Howard et al. 1985). Unit cell dimensions were a = 52.0 Å, b = 62.7 Å, and c = 69.9 Å. The GFP S65T coordinate file (1EMA; Orm   et al. 1996) was used as the phasing model and was edited to reflect the mutations, with the introduced residues tyrosine 203 and leucine 68 initially modeled as alanines to prevent model bias. A model for the anionic chromophore was obtained by semiempirical molecular orbital calculations using AM1 in the program SPARTAN v4.1 (Wavefunction Inc., Irvine, CA). The minimized structure, which was planar, compared

very well with the model used during refinement of GFP S65T.

Using the program TNT (Tronrud et al. 1987), rigid-body refinement was performed to position the isomorphous model in the unit cell of YFP H148G. Positional refinement was carried out using the data to 4.0 Å, 3.5 Å, 3.0 Å, and finally to the limit of resolution, 2.6 Å. After each increase in resolution the electron density maps ($2F_o - F_c$ and $F_o - F_c$) were analyzed using the program O (Jones et al. 1991). Solvent molecules were added only if consistent with $F_o - F_c$ features and when in proximity of hydrogen bond partners. Due to the relatively low resolution data, B-factors were refined using a strong correlation between neighboring atoms. Since no B-factor library is available for the chromophore itself, the B-factors of all chromophore atoms were set to the values obtained in the 1.9 Å structure of GFP S65T and then refined as a group, with identical shifts for the grouped atoms.

Crystallization and Structure Determination of GFP S65T/H148D

The mutant GFP protein S65T/H148D was concentrated to approximately 13 mg mL⁻¹ in 20 mM HEPES (pH 7.9). Rod-shaped crystals grew in two days measuring 0.8 x 0.04 x 0.04 mm. Crystals were grown at room temperature from hanging drops containing 2 µL protein and 2 µL mother liquor. The mother liquor contained 50 mM

HEPES (pH 8.0), 100 mM MgCl₂, 24% PEG 4000.

X-ray diffraction data were collected at room temperature using an Raxis-IV image plate mounted on a Rigaku RUH3 rotating anode generator equipped with mirrors. Data sets were processed with Denzo and scaled with ScalePack (Otwinowski and Minor 1997). The space group is P2₁2₁2₁, with unit cell dimensions of $a = 51.65 \text{ \AA}$, $b = 63.14 \text{ \AA}$, and $c = 70.30 \text{ \AA}$. The GFP S65T coordinate file (1EMA; Orm   et al. 1996) was used as the phasing model and was edited to prevent model bias by initially modeling the mutation aspartic acid 148 as a glycine. A model for the chromophore was obtained in the same manner as above.

Using the program TNT (Tronrud et al. 1987), rigid-body refinement was performed to position the isomorphous model in the unit cell of GFP S65T/H148D. Positional refinement was carried out using the data to 4.0 \AA , 3.5 \AA , 3.0 \AA , 2.6 \AA , 2.4 \AA , 2.3 \AA , 2.2 \AA and finally to the limit of resolution, 2.1 \AA . After each increase in resolution the electron density maps ($2F_o - F_c$ and $F - F_c$) were analyzed using the program O (Jones et al. 1991). Solvent molecules were added only if consistent with $F_o - F_c$ features and when in proximity of hydrogen bond partners. B-factor refinement was performed using the default TNT B-factor correlation library. The B-factor correlation values for the chromophore atoms were derived from histidine and phenylalanine residues.

CHAPTER III

GREEN FLUORESCENT PROTEIN VARIANTS AS RATIOMETRIC DUAL-EMISSION pH SENSORS

Portions of the work presented in this chapter were done in collaboration with Shaoyou Chu, Lixuan Xi, and Marshall H. Montrose of the Department of Biology at Indiana University and Marla E. P. Rendell and S. James Remington of the Institute of Molecular Biology and Department of Physics at the University of Oregon. Portions of this chapter were submitted for publication to *Biochemistry* (2001).

This chapter describes the design and characterization of green fluorescent protein variants with ratiometric dual-emission properties in response to changes in pH.

Summary

Using structure-based design, several ratiometric-by-emission, pH-sensitive variants of the green fluorescent protein (GFP) have been engineered. They emit mainly blue fluorescence at acidic pH and mostly green fluorescence at alkaline pH. This new

class of GFPs display pK_a values ranging from 6.6 to 7.8. To explore the structural basis for the unique spectral properties of these variants, the high and low pH crystal structures were determined to 1.5 Å and 1.8 Å resolution, respectively. The structures revealed how the chromophore charge state was manipulated and gave insight into the nature of the fluorescence of the neutral chromophore species. PS120 fibroblasts were transiently transfected with one of the dual-emitting GFP variants, and the response of this variant to pH changes was compared to the commercially available, pH-sensitive dye, SNARF-1®. The dynamic range of the pH-sensitive GFP is comparable to that of SNARF-1® over the range examined and may even be better than SNARF-1® at lower pHs. Two-photon laser scanning microscopy greatly decreased the background cellular autofluorescence that precluded visible discernment of the shorter emission wavelength when using conventional fluorescence microscopy. As currently available instrumentation can more readily measure dual-emission wavelengths than dual-excitation wavelengths and as GFP is genetically encoded and thus targettable to subcellular compartments, these novel GFPs should make excellent probes for studying *in vivo* pH status.

Introduction

The *Aequorea victoria* green fluorescent protein (GFP) has become one of the most popular fluorescent indicators in cell and molecular biology research (for reviews, see: Tsien 1998; Remington 2000). This popularity stems largely from the fact that GFP is genetically encoded, making it targetable to subcellular compartments and ideal for fusion to proteins of interest, tasks that are not possible with most small molecule fluorescent indicators. While many researchers have used GFP exclusively for its idle fluorescent qualities, recent studies have utilized GFP as a dynamic fluorescent biosensor. An early report hinted at the pH-dependence of wild-type GFP's fluorescence (Ward et al. 1982), however it was not until the reports of Kneen et al. and Llopis et al. that GFP variants with more physiologically relevant chromophore ionization constants (pK_{aS}) were used to monitor pH *in vivo* (Kneen et al. 1998; Llopis et al. 1998). Since then, GFP has been circularly permuted and fused to calmodulin to report calcium ion fluctuations (Rosomer et al. 1997; Miyawaki et al. 1997; Baird et al. 1999), inserted within the Shaker potassium channel to optically observe membrane potential (Siegel and Isacoff 1997), altered to detect halide ion concentration (Wachter and Remington 1999; Wachter et al 2000), and engineered to indicate redox status in living cells (G.T.H, S.J.R, unpublished observation, see Chapter IV).

There are many factors that make fluorescent indicators useful, however when performing quantitative measurements, one of the most important factors is whether a probe is ratiometric (Haugland 1996). A ratiometric probe has either two excitation or emission peaks that elicit an opposite response to a given environmental factor.

Ratiometric measurements reduce or eliminate distortions of data caused by photobleaching, indicator concentration, variable cell thickness, illumination stability, excitation path length, and non-uniform indicator distribution within cells or between groups of cells (Grynkiewicz et al. 1985; Whitaker et al. 1991). We and others have reported pH-sensitive GFP variants that are ratiometric-by-excitation (Miesenbock et al. 1997; Elsliger et al. 1999), however, dual-excitation measurements are not readily adaptable to techniques which employ a single excitation wavelength such as flow cytometry and laser scanning microscopy. In general, these techniques are unable to rapidly switch excitation wavelength, but are proficient in observing several emission wavelengths simultaneously. Therefore, a pH-sensitive GFP that is ratiometric-by-emission is desirable.

This report describes both the spectral and structural attributes of a class of improved pH-sensitive GFP variants. The variants identified in this study display ratiometric emission properties in response to changes in pH and exhibit biologically

relevant pK_as. Crystal structure analysis of the low and high pH forms of one of the variants revealed a pH-dependent structural rearrangement that occurs near the chromophore. The details of how this rearrangement leads to blue and green fluorescence of the neutral chromophore will be discussed. Comparison of one of the GFP variants to the commercially available dye, SNARF-1®, showed that the dynamic range of the GFP in response to varying pHs was equivalent to that of SNARF-1®. To reduce the undesirable background autofluorescence that obscured the shorter wavelength emission in conventional fluorescence microscopy, two-photon laser scanning microscopy was performed and resulted in a clear picture of the blue emission peak.

Results

Design of Ratiometric pH-Sensitive GFPs

To create a ratiometric, pH-sensitive GFP with a pK_a near 7.0, we carried out mutagenesis of residues near the chromophore in the S65T variant of GFP. This background was chosen since GFP S65T exhibits profound fluorescence differences in response to pH changes (Kneen et al. 1998). However, we also wanted to create a mutant with ratiometric properties. On an ultra-fast time scale, wild-type GFP exhibits blue emission which rapidly decays as green emission concurrently arises (Chattoraj et al.

1996). This blue emission is thought to be due to neutral chromophore fluorescence (Brejc et al. 1997). Therefore, we wanted to stabilize the neutral chromophore in the S65T background. As histidine 148 has been shown to be crucial for stabilizing the deprotonated form of the chromophore, this site was chosen for the initial mutagenesis. The chromophore ionization constant of the S65T variant is quite acidic ($pK_a = 6$), therefore the H148G substitution was introduced as Wachter et al. have shown that this substitution in the yellow variant of GFP raises the pK_a from 7.0 to 8.0 (Wachter et al. 1998). The H148G mutation had a similar effect in the S65T variant, with the pK_a being raised one pH unit to 7.0 (see Chapter II). However, this mutant only exhibited fluorescence emission when excited at the longer absorbance wavelength, band B, and thus further modification was necessary to make the neutral chromophore species, band A, fluoresce.

Moreover, previous work has shown that substitution at position 203 can favor neutral chromophore fluorescence (Ehrig et al. 1995). Threonine 203 has been shown to be necessary for the formation and stabilization of the ionized chromophore (Elsliger et al. 1999). Consequently, threonine-203 was replaced with a cysteine. The resulting dual-emission GFP (deGFP1), S65T/H148G/T203C, had a substantially increased pK_a of 7.8, but more significantly, was ratiometric-by-emission. Thus, when excited at 400 nm

(band A), the emission spectra of this new variant displays two peaks, a shorter wavelength peak centered at 465 nm and a longer wavelength peak centered at 513 nm (Figure 10). In an attempt to create a mutant with a pK_a closer to neutral, various combinations of cysteine residues were placed at positions 148 and 203. This mutational analysis resulted in the identification of the mutant protein, C48S/S65T/H148C/T203C, whose ratiometric-by-emission properties display a pK_a of 7.0 (Figure 11). In addition to its more favorable pK_a , the deGFP4 variant has a 77% increase in the relative height of the blue emission peak (461 nm) relative to the green emission peak (515 nm) compared to the original deGFP1 variant. Table 3 summarizes the spectroscopic and biochemical properties of the different variants identified in this study.

Structural Basis for Dual-Emission

What structural differences could account for the dual-emission characteristics of these new GFP variants? Previous studies have shown that wild-type GFP fluoresces blue, but that this fluorescence rapidly decays to green emission on a pico-second time scale (Chattoraj et al. 1996). The rapid decay has been attributed to an excited state deprotonation of the chromophore phenolic hydroxyl (Brejc et al. 1997). In this process, glutamic acid 222 donates its charge to the chromophore by proton extraction through a

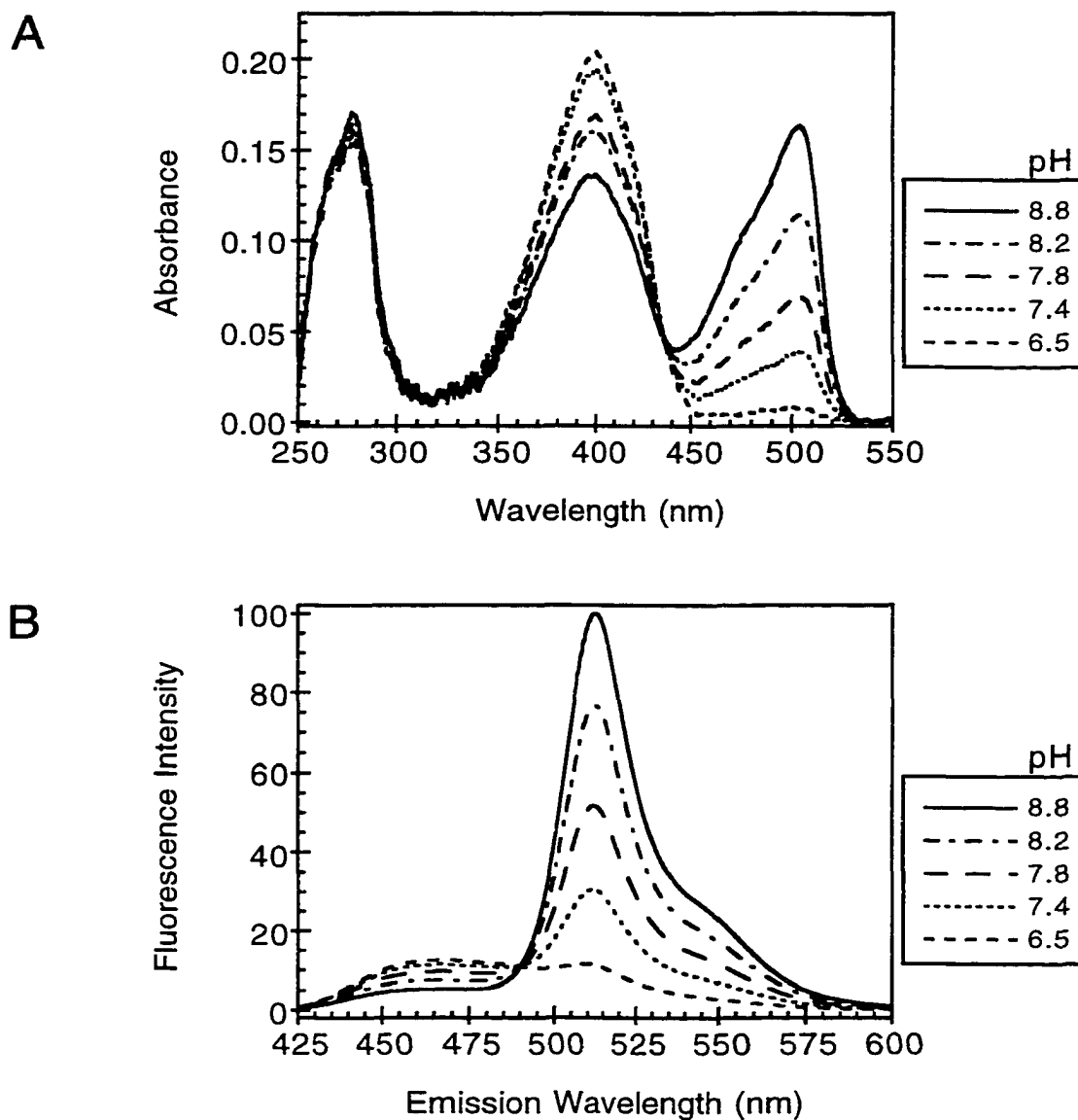


Figure 10. Absorbance and fluorescence emission spectra of deGFP1 as a function of pH. The absorbance scans (A), determined at the indicated pHs, indicate moderate ground-state conversion of neutral (band A; ~400 nm) to anionic chromophore (band B; ~510 nm) upon alkalization. Fluorescence emission spectra (B) were collected at an excitation wavelength of 400 nm, all traces were normalized according to the maximum intensity at pH 8.0, which was assigned the value of 100.

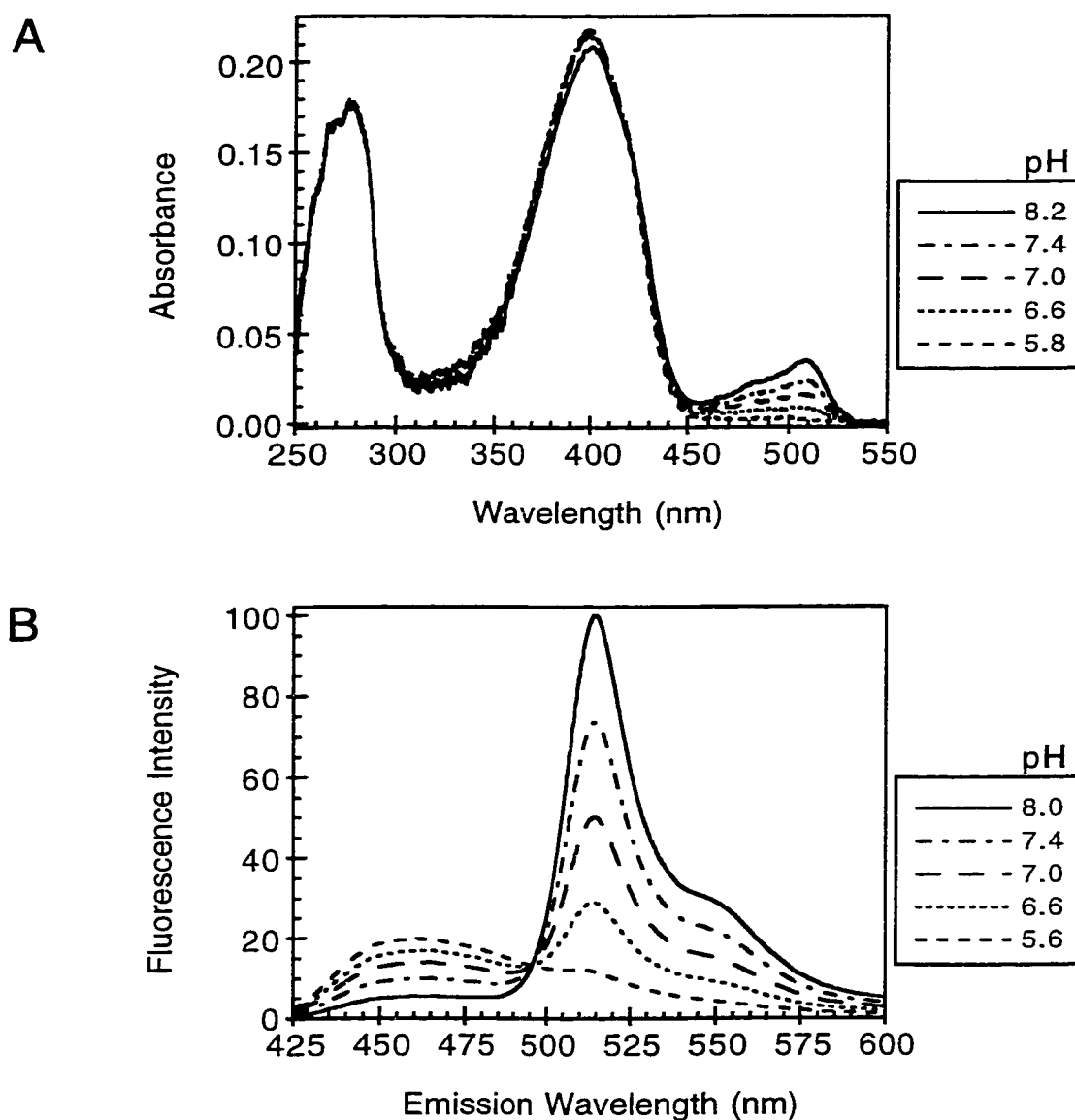


Figure 11. Absorbance and fluorescence emission spectra of deGFP4 as a function of pH. The absorbance scans (A), determined at the indicated pHs, indicate very little ground-state conversion of neutral (band A; ~400 nm) to anionic chromophore (band B; ~510 nm) upon alkalization. Fluorescence emission spectra (B) were collected at an excitation wavelength of 400 nm, all traces were normalized according to the maximum intensity at pH 8.0, which was assigned the value of 100.

Table 3. Spectroscopic and Biochemical Properties of deGFP Variants.

	<i>Variants</i>	λ_{Abs}^1		λ_{EM}^2		ϵ^3		Φ^4		pK_a^5	B^6
Name	Mutations	A	B	A	B	A	B	A_{460-5}	A_{512-5}	B	
	S65T/H148G	397	492	negligible	512	25,000	40,500	~0	~0	0.43	7.0
deGFP1	S65T/H148G/T203C	400	504	465, 513	516	24,500	21,000	0.04	0.20	0.32	7.8
deGFP2	S65T/H148C ⁷	398	496	461, 515	517	17,000	11,000	0.07	0.43	0.31	6.9
deGFP3	S65T/T203C	396	508	460, 512	518	20,500	22,000	0.10	0.20	0.51	6.6
deGFP4	S65T/H148C/T203C ⁷	400	509	461, 515	518	23,000	7,000	0.08	0.19	0.27	7.0
											20

¹ λ_{Abs} are the peaks in the absorbance spectrum in units of nanometers.

² λ_{EM} is the peak(s) in the emission spectrum in units of nanometers. Emission band(s) A and B result from excitation at the wavelength of absorbance band A and B, respectively.

³ ϵ is the molar extinction coefficient in units of $M^{-1} cm^{-1}$ and coincides with absorbance bands, A and B.

⁴ Φ is the fluorescence quantum yield, which is dimensionless. Values are given for the various emission peaks.

⁵ pK_a is the apparent mid-point in the pH titration of the chromophore.

⁶B is the percentage of the maximum fluorescence intensity of the higher energy to the lower energy emission bands arising from excitation of band A.

⁷These variants contain the phenotypically neutral mutation C48S. In addition all variants contain the Q80R substitution.

hydrogen bond network involving serine 205 and a bound water molecule. Recall that at high pH excitation of band A leads primarily to green fluorescence, which is consistent with chromophore deprotonation in the excited state. The blue fluorescence at low pH then appears to be caused by a lack of excited state proton transfer causing the neutral chromophore fluorescence to prevail. Given the role of glutamic acid 222 in wild-type GFP, it is predicted that the high pH chromophore environment would resemble wild-type GFP in which glutamic acid 222 is in position to donate its charge to the chromophore through proton extraction. On the other hand, at low pH, the chromophore surroundings are predicted to closely resemble the low pH S65T chromophore environment (Elsiger et al. 1999), with some exception that allows the neutral chromophore to fluoresce.

In order to resolve the structural basis for the pH dependence and dual-emission properties of this new class GFPs, the low and high pH crystal structures of the deGFP1 variant were solved to 1.8 and 1.5 Å resolution, respectively (Table 4). The fluorescence emission of the low pH (Figure 12A) and the high pH (Figure 12B) crystals are shown to visibly illustrate the convenient two-color reporting made available by these pH indicators. The crystals were isomorphous to the original S65T structure (Ormö et al. 1996), which simplified structure determination. Both the low and high pH structures

Table 4. Data Collection and Refinement Statistics for deGFP1 at Low and High pH.

<u>Data Collection</u>		Low pH	High pH
Crystal			
Total observations		83,420	120,478
Unique reflections		18,906	34,536
Cell dimensions (a, b, c; Å)		50.95, 62.24, 67.20	51.2, 62.37, 68.97
Resolution (Å)		19.5-1.80	19.9-1.50
Highest resolution shell (Å)		1.90-1.80	1.58-1.50
Completeness ¹ (%)		93.0 (87.2)	96.2 (93.6)
Multiplicity ¹		4.4 (4.3)	3.5 (3.3)
Average I/σ ¹		6.4 (2.7)	9.3 (2.3)
R _{merge} ^{1,2}		0.062 (0.273)	0.045 (0.319)
<u>Refinement</u>			
Spacegroup		P2 ₁ 2 ₁ 2 ₁	P2 ₁ 2 ₁ 2 ₁
Number of protein atoms		1,743	1,760
Number of solvent atoms		114	202
R _{factor} ³		0.194	0.177
Average B-factors (Å ²)		40.8	24.4
Protein atoms		40.4	22.5
Solvent		45.8	39.9
rms deviations			
Bond lengths (Å)		0.012	0.013
Bond angles (°)		2.076	2.233
B-factor correlations (Å ²)		5.345	3.989

¹Values in parentheses indicate statistics for the highest resolution shell.

²R_{merge} = $\sum|I - \langle I \rangle| / \sum \langle I \rangle$, where I is the observed intensity, and $\langle I \rangle$ is the average of intensity obtained from multiple observations of symmetry related reflections.

³R_{factor} = $\sum ||F_o - F_c|| / \sum |F_o|$, where F_o and F_c are the observed and calculated structure factors, respectively.

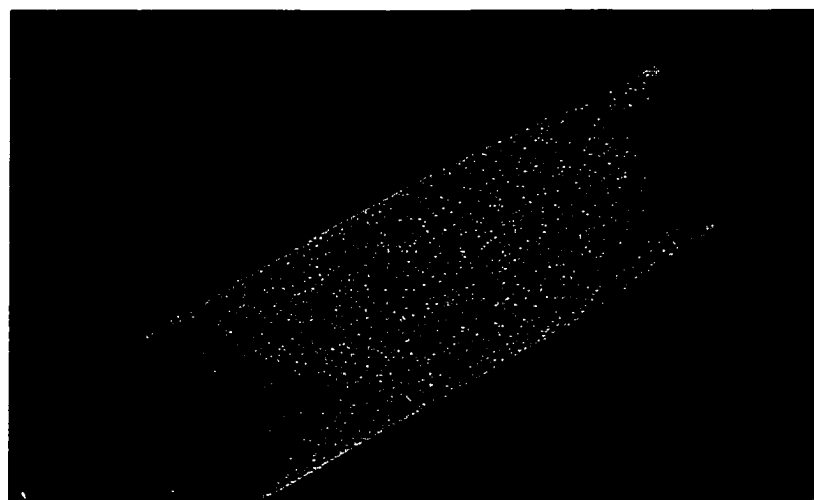
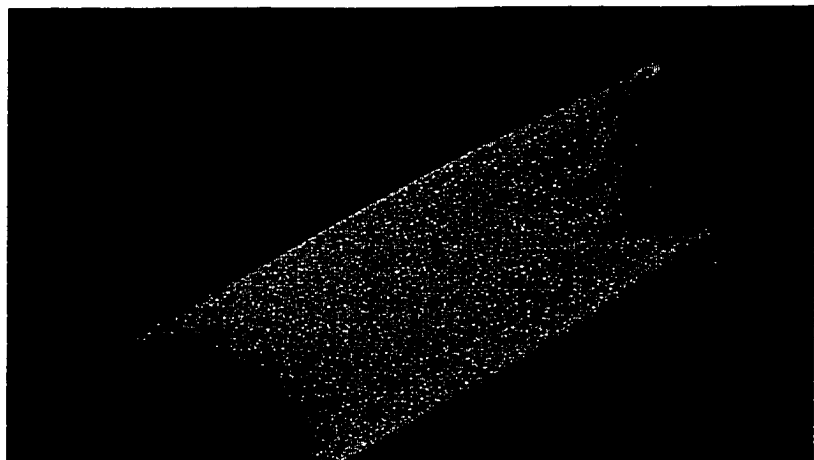
A**B**

Figure 12. Pictures of fluorescent deGFP1 crystals. A single crystal was excited with UV light and images were collected through filters transmitting only the blue (A) or green (B) fluorescence emission.

closely mimic the usual GFP-fold, retaining the 11-stranded β -barrel motif and coaxial helix upon which the centrally located fluorophore resides. Superimposition of the two structures quickly highlights the major differences. At high pH, the β -strand residues 143 through 150 undergo a shift in backbone atoms of up to 4 Å from the position seen at low pH (Figure 13). Interestingly, the low pH position is the normal location for this strand in previous GFP structures (Ormö et al. 1996; Wachter et al. 1997; Elsliger et al. 1999). At high pH, the strand motion places tyrosine 145 and serine 147 in position to interact with the phenolic end of the chromophore (Figure 14). Removal of the large imidazole side chain at position 148 (H148G), and replacement of the branched side chain of threonine 203 with a cysteine appears to have allowed the β -strand to adopt this new conformation and serine 147 to flip to the interior of the protein at high pH (Figure 15). Furthermore, the region adjacent to residue 148 is not involved in crystal contacts nor has this movement been seen in other high pH structures of GFP (Ormö et al. 1996; Elsliger et al. 1999), indicating the observed strand motion is due to the substitutions and not the crystallization conditions. At low pH, with the strand remaining unaltered, tyrosine 145 and serine 147 are positioned 4.0 Å and 5.8 Å away from the chromophore, respectively. In both structures, glutamic acid 222 has adopted the same conformation as seen in the S65T structure. Consequently, neither pH structure appears to have a proton relay

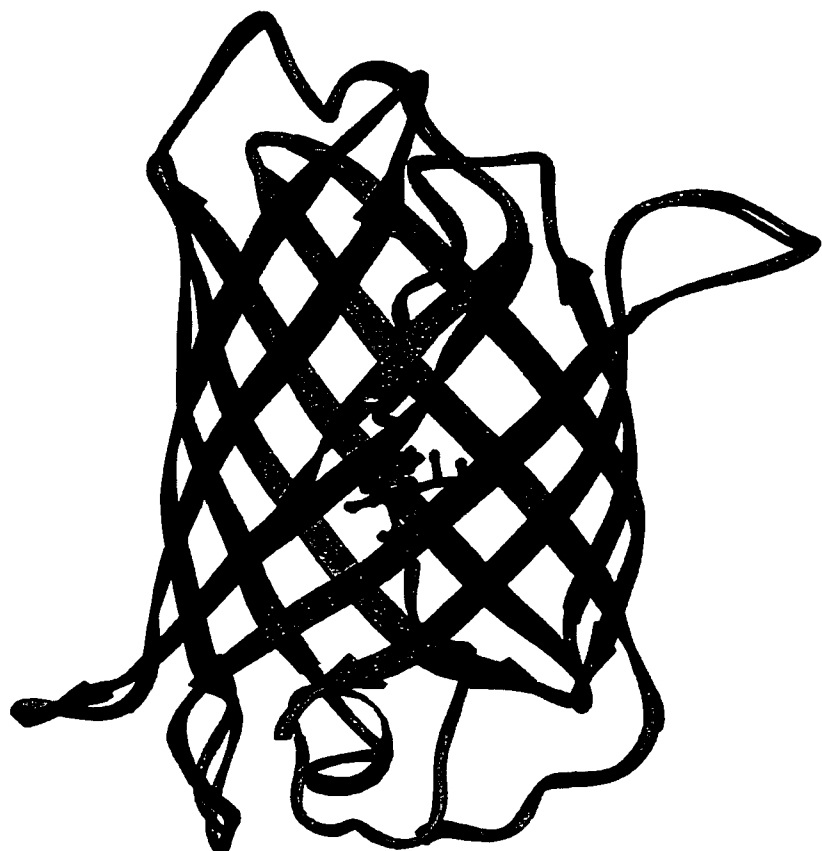


Figure 13. Overlay of low and high pH structures of deGFP1. Shown in green is a schematic diagram of the high pH structure superimposed upon the low pH structure (blue). Amino acid residues 143 through 150 reside along the strand shown in blue. Chromophore atoms are in ball-and-stick representation.

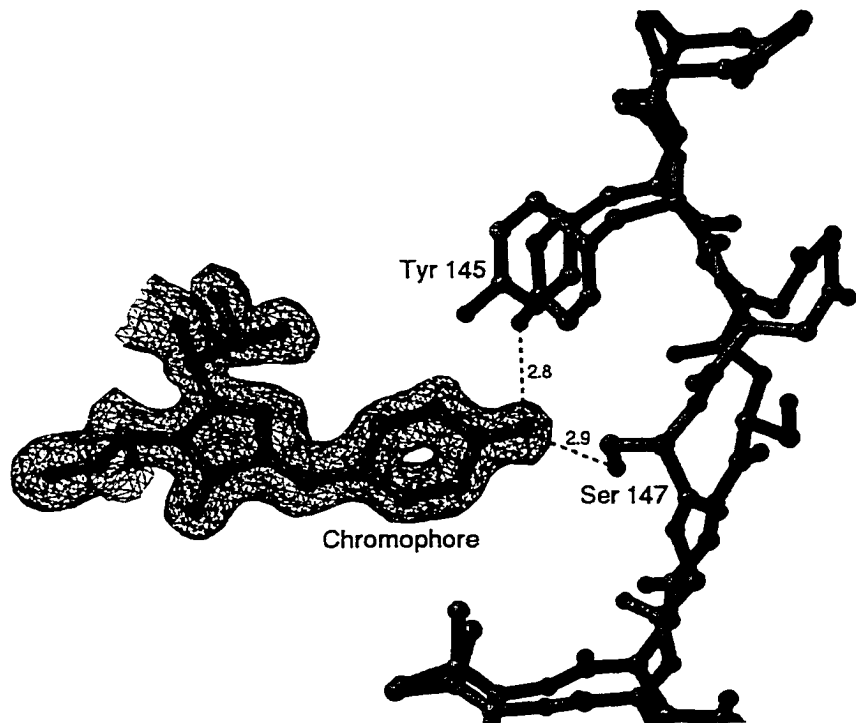


Figure 14. Overlay of the chromophore environment at low and high pH of deGFP1. The chromophore (same position in both models) is shown with a portion of the $2F_o - F_c$ electron density map of deGFP1 at high pH, contoured at 1 standard deviation (green bonds). Dashed lines indicate potential hydrogen bonds of Tyr 145 and Ser 147 to the chromophore, distances are in Ångstroms. The low pH model (blue bonds) is superimposed to show the new position adopted by these residues.

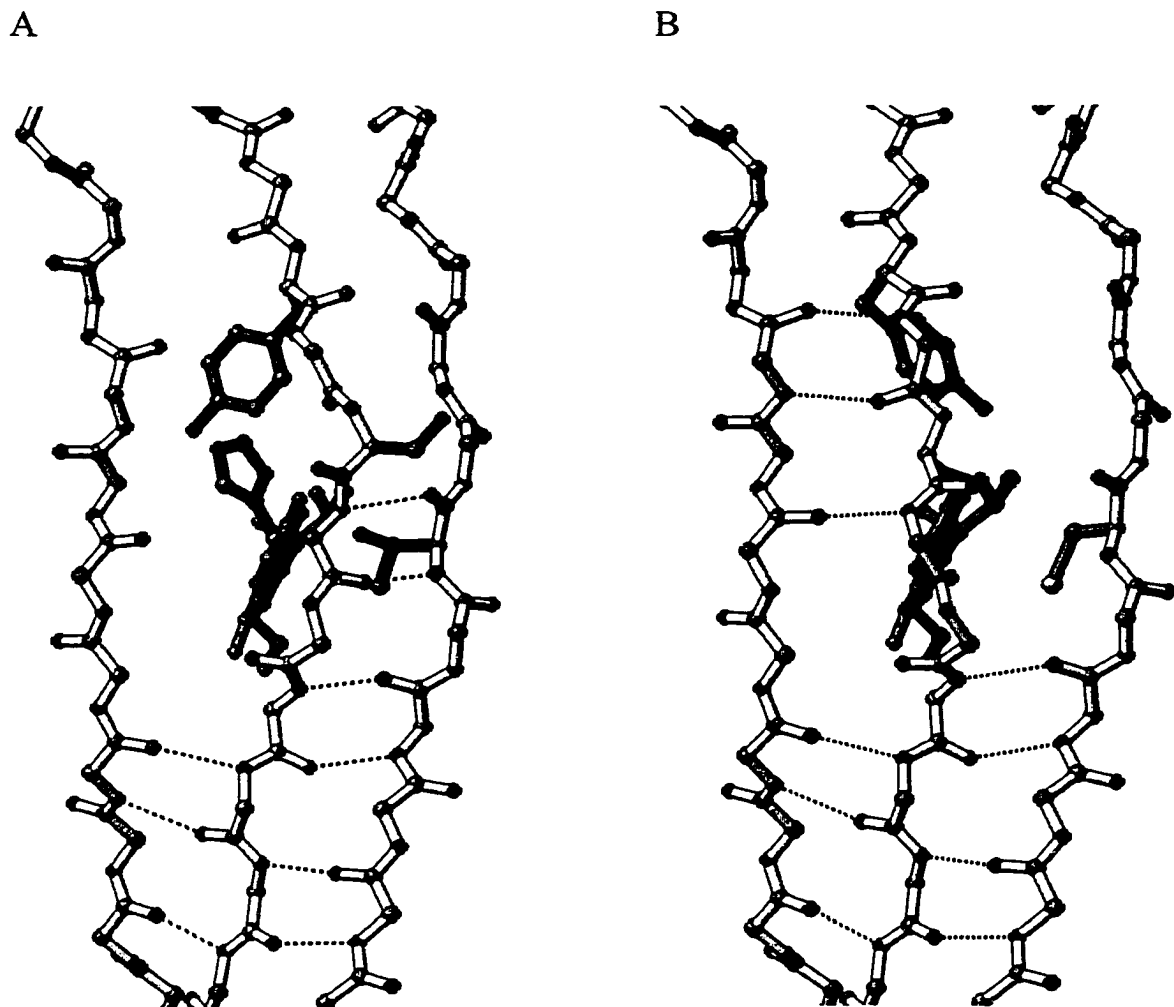


Figure 15. Structural comparison of S65T and the high pH structure of deGFP1. A view towards the interior of GFP with a portion of the backbone-atoms and chromophore (green) shown. In the S65T structure (A), the sidechains of amino acids Tyr 145 and Ser 147 (red bonds) and His 148 and Thr 203 (black bonds) are shown. In the deGFP1 structure (B), Cys 203 is highlighted in green. Dashed lines represent potential hydrogen bonds between adjacent backbone atoms.

network that resembles wild type GFP, as was predicted.

Close examination of the low and high pH chromophore environments has led to a proposed mechanism for dual emission. However, whether excited-state proton transfer occurs in deGFPs remains to be determined, it appears that pH-dependent excited-state proton transfer is responsible for the observed dual-emission properties. Upon excitation of the neutral chromophore at high pH, the phenolic hydroxyl of the chromophore most likely rapidly deprotonates via a hydrogen bond network. This network is certainly different from that seen in wild-type GFP (Brejc et al. 1997), because glutamic acid 222 is not in position to donate its charge to the chromophore (Figure 16A). Despite the existence of a network potentially involving proton transfer from the chromophore through serine 147 to either of two bound water molecules on the exterior surface of the protein, the high pH structure failed to illustrate a charged residue that may act analogous to glutamic acid 222 in wild-type GFP. At acidic pH, due to a pH-dependent structural rearrangement, there are no obvious proton relay networks leading away from the chromophore (Figure 16B). The hydroxyl of serine 147 is rotated 5.8 Å to the exterior of the protein and is replaced by a single water molecule. This water, located 3.2 Å from the chromophore hydroxyl, is also bound by serine 205 and the main chain carbonyl of asparagine 146. Since neither serine 205 or the carbonyl of asparagine 146 are likely to

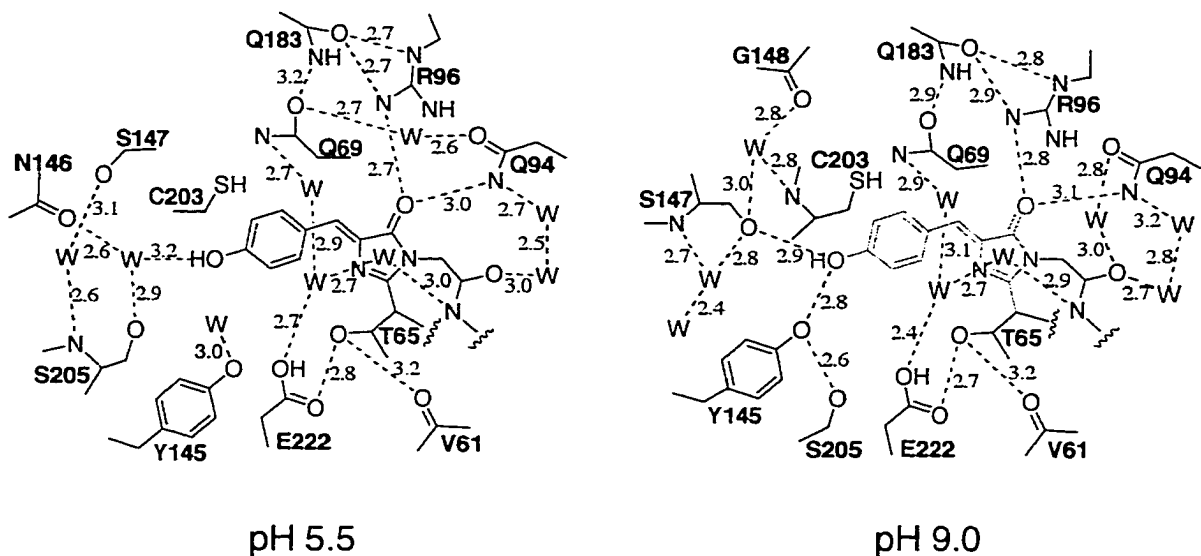


Figure 16. Schematic diagram showing the immediate chromophore environment of deGFP1 at low and high pH. Proposed hydrogen bonds are shown as dashed lines, labeled with approximate lengths in Ångstroms. Water molecules are abbreviated as Ws.

be charged, they are unable to pass the proton any further, and the chromophore likely remains protonated even in the excited-state and fluoresces blue. In the absence of a titrating group responsible for the pH-dependence of the proposed excited-state proton transfer, future studies will need to be performed to fully account for the dual-emission properties of the deGFP variants.

Fluorescence of the Neutral Chromophore

Excitation of the neutral chromophore in wild-type GFP leads to intense green fluorescence. Most GFP variants however, generally exhibit very little fluorescence upon excitation with UV light (Heim et al. 1995; Wachter et al. 1998). In fact, S65T emission is less than 5% of maximum fluorescence over the entire pH range of protein stability (see Chapter II Figure 2B). This loss of fluorescence upon chromophore protonation is apparently not due to a change in ground-state geometry, since high and low pH structures show the chromophore of S65T to be planar (Elsliger et al. 1999). Therefore, it has been suggested that the S65T neutral chromophore is only very weakly fluorescent because the excited state may be able to undergo out-of-plane distortions that could result in enhanced radiationless decay (Elsliger et al. 1999). Consistent with the general rule that rigid systems tend to fluoresce (Barltrop and Coyle 1978), the chromophore of wild-

type GFP appears to be embedded in a more rigid hydrogen bonding network that may disfavor such out-of-plane distortions (Elsliger et al. 1999).

The reason for neutral chromophore fluorescence in the dual-emission GFPs is suggested to be due to the introduction of a cysteine residue(s). As seen in the low and high pH structures of deGFP1, the introduced cysteine occupies a position only a few Ångstoms from the plane of the phenol ring of the chromophore (Figure 17). Given the close proximity of the introduced cysteine to the chromophore and the larger ionic radius of the sulfur atom of the cysteine as opposed to the normal threonine side chain at this position, the motion of the chromophore may be restricted and thus inhibited from radiationless energy transfer.

Dynamic Range of deGFP4

In order to explore the dynamic range of the new dual-emission variants, PS120 fibroblasts were transiently transfected with a plasmid expressing deGFP4 in the cytosol. Using fluorescence microscopy, cells expressing deGFP4 were shown to exhibit blue and green fluorescence when excited with 364 nm laser light (Figure 18A,B). The same cells were then exposed to the ratiometric, pH-sensitive dye, SNARF-1[®] (Figure 18C,D). Comparison of the signals from the four channels monitored before and after the cells

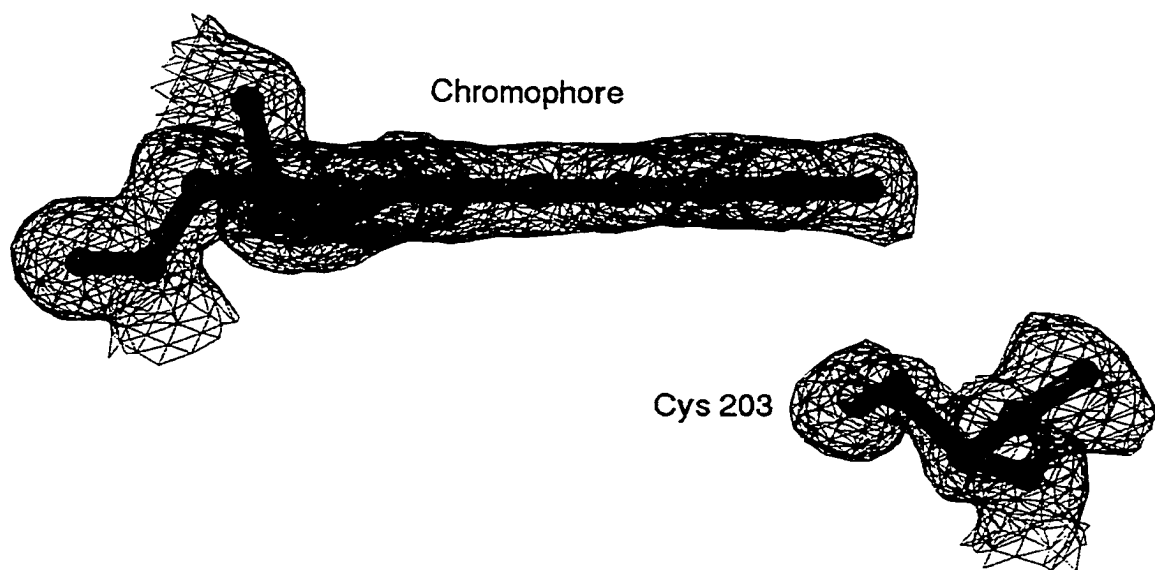


Figure 17. Electron density around the chromophore and Cys 203 of the high pH structure of deGFP1. The 1.5 Å, $2F_o - F_c$ electron density map was contoured to one standard deviation.

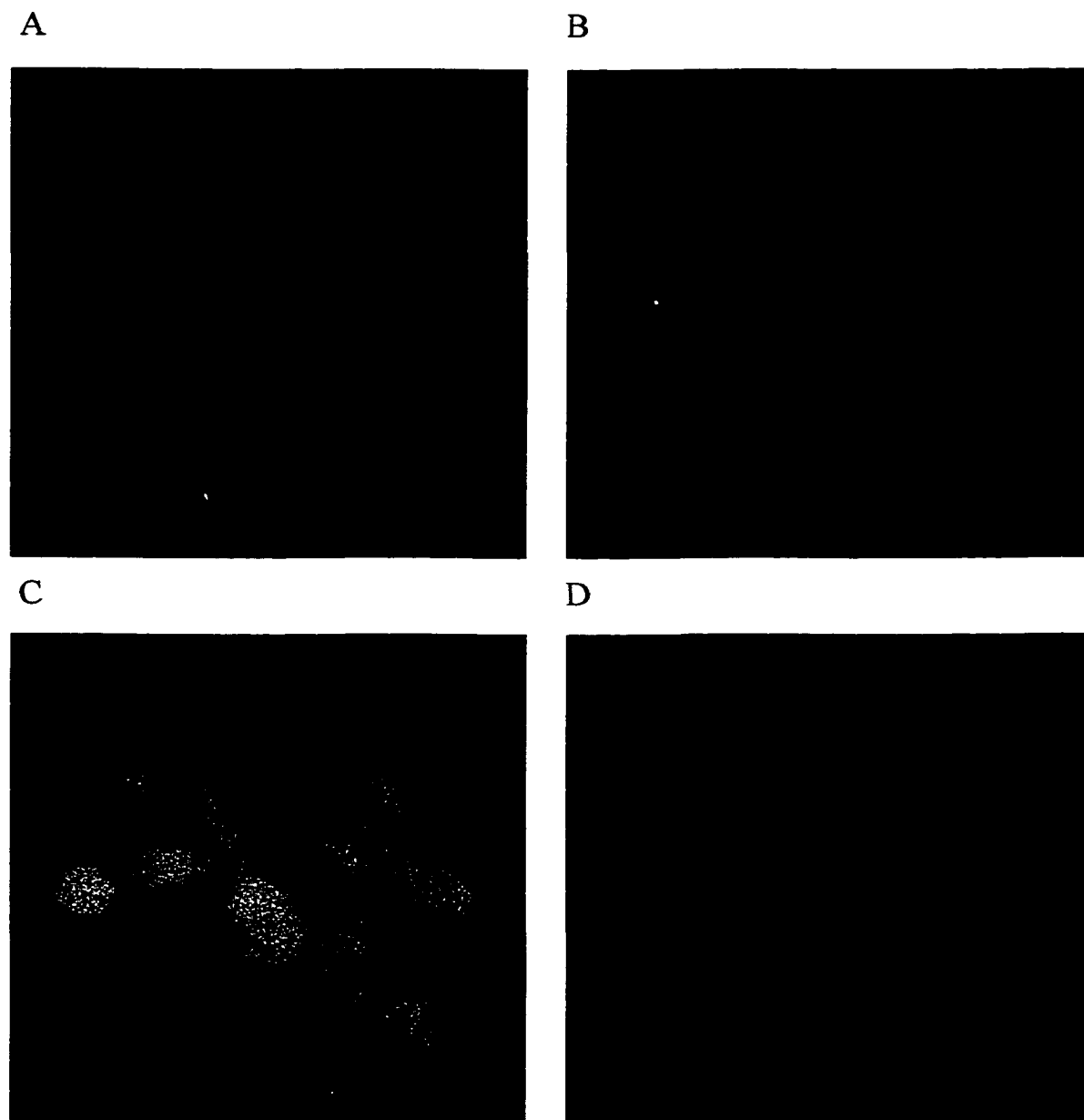


Figure 18. Images of PS120 cells transfected with deGFP4 and loaded with SNARF-1. Emission wavelengths for deGFP4 were 385–470 nm (A) and 475–525 nm (B) at an excitation of 364 nm. For SNARF-1 emission wavelengths were 560–615 nm (C) and 625–655 nm (D) and excitation was 514 nm. Cellular autofluorescence occludes much of the blue fluorescence of the cell expressing deGFP4 (see text).

were loaded with SNARF-1[®] shows that there is very little overlap in the signals from the GFP variant and SNARF-1[®]. A time-course experiment was carried out and the pH was simultaneously monitored with deGFP4 and SNARF-1[®] in the same cells. pH changes were introduced by addition and removal of NH₄Cl, which promptly alkalinizes (upon addition) and acidifies (upon removal) intracellular compartments because of rapid NH₃ transport and NH₃/NH₄⁺ equilibration (Kneen et al. 1998). Figure 19 shows the trace obtained from each probe after normalization. From this figure, it can clearly be seen that the deGFP4 has a dynamic range comparable to that of SNARF-1[®]. To illustrate the ratiometric properties of the GFP, the individual responses of the blue (385-475 nm) and green (475-525 nm) emission channels which give rise to the deGFP4 ratio shown in Figure 19 are shown in Figure 20. As cells are exposed to higher pH (addition of NH₄Cl), the intensity of fluorescence in the green channel increases, while the intensity of fluorescence in the blue channel decreases. The opposite is true as the cells are brought back to neutral pH.

Although a detectable signal was obtained from conventional fluorescence microscopy, two-photon laser scanning microscopy provides a much improved signal. Figure 21 shows PS120 cells transiently transfected with deGFP4 and imaged by using two-photon excitation at 810 nm. Unlike single-photon excitation at 364 nm, two-photon

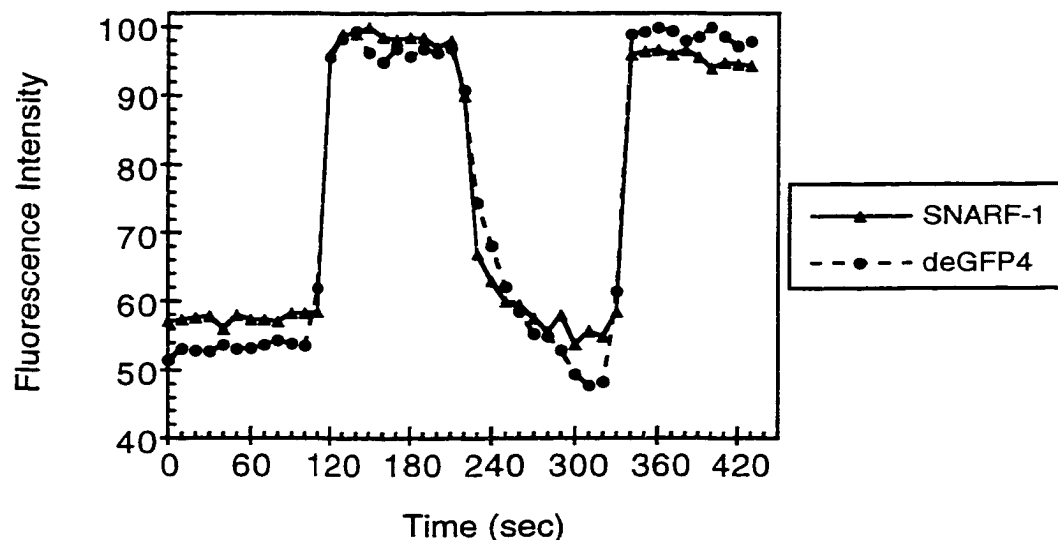


Figure 19. The normalized ratio of pH changes in PS120 cells as monitored with SNARF-1® and deGFP4. Cells were exposed to NH₄Cl (25 mM added to a physiologic saline solution containing; 130 mM NaCl, 20 mM HEPES (pH 7.4), 2 mM CaCl₂, 1 mM MgSO₄, 5 mM KCl, 1 mM NaPO₄, and 25 mM mannose) from 100-200 seconds and from 320 seconds to the end of the experiment. Ratio values were normalized to the maximum ratio observed with each indicator.

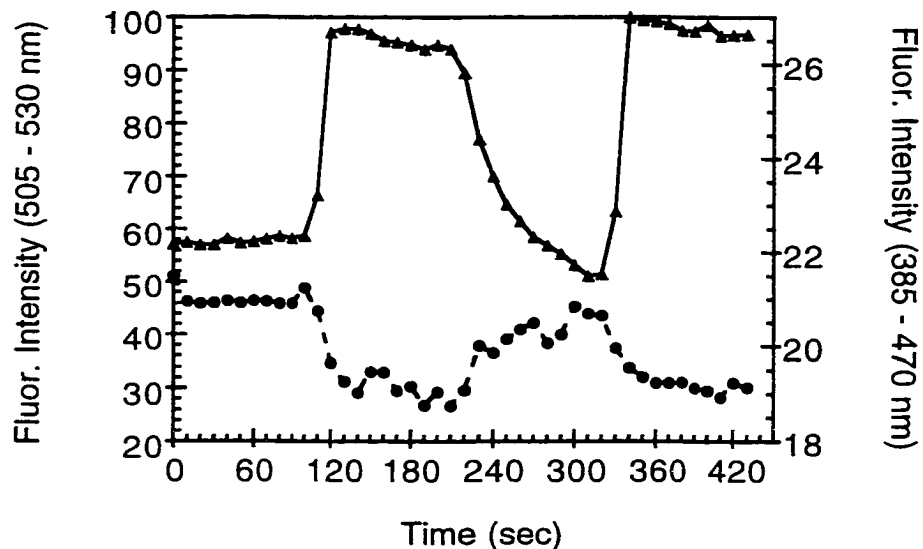


Figure 20. Individual wavelength signals of deGFP4 as a function of pH changes in PS120 cells. The y-axis on the left corresponds to the solid line with triangles and represents the emission intensity of the green channel (Figure 18B). The y-axis on the right has been expanded to show the emission intensity of the blue channel (Figure 18A) which corresponds to the dashed line with circles. Cells were exposed to NH₄Cl (25 mM added to a physiologic saline solution containing; 130 mM NaCl, 20 mM HEPES (pH 7.4), 2 mM CaCl₂, 1 mM MgSO₄, 5 mM KCl, 1 mM NaPO₄, and 25 mM mannose) from 100-200 seconds and from 320 seconds to the end of the experiment. Fluorescence intensity values were normalized to the maximum value observed in the green channel.

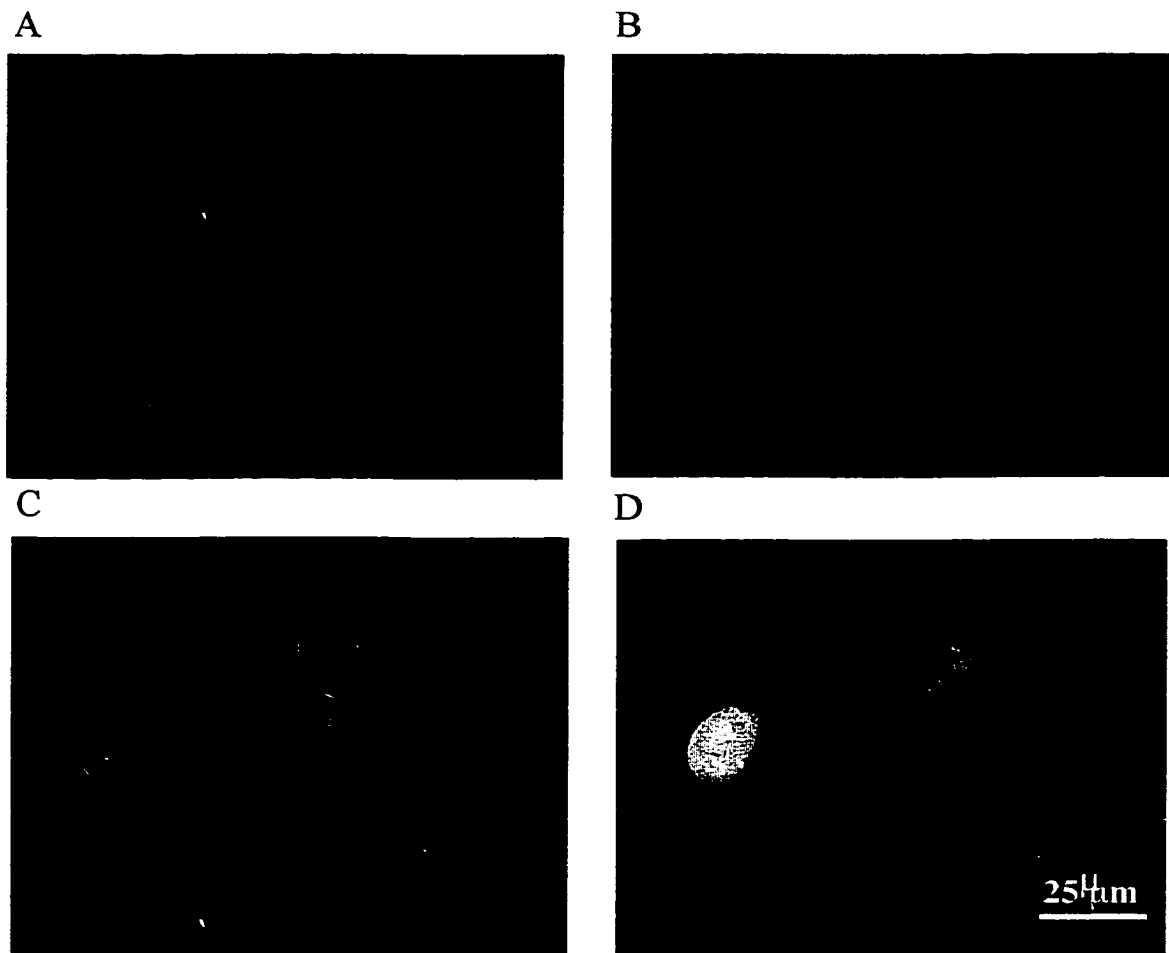


Figure 21. Two-photon excitation images of PS120 cells expressing deGFP4. Emission wavelengths for visualization of deGFP4 were 435-485 nm (A) and 490-685 nm (B), with a two-photon excitation wavelength of 810 nm. A transmitted light image (C) showing all cells, along with an overlay (D) of panels A, B, and C is shown.

excitation virtually eliminates background cellular autofluorescence, presumably by decreasing NADH fluorescence by a factor of at least 100 (Xu et al. 1996). This is made possible by the expanded choice of excitation wavelengths available with tunable lasers, such as a Titanium-Sapphire laser used in multi-photon experiments. By eliminating cellular autofluorescence, the blue emission peak from cells expressing deGFP4 is now easily distinguishable from the surrounding untransfected cells (compare Figure 21A to Figure 18A). Two-photon microscopy was also carried out on samples of the purified deGFP4 protein. Figure 22 shows the two-photon excitation spectra of deGFP4 as a function of pH, whereas Figure 23 shows the emission spectra of deGFP4 versus pH. Therefore, although it can be difficult to predict two-photon spectra from the single-photon data because of differences in selection rules and the effects of vibronic coupling (Xu et al. 1996), in the case of deGFP4 one and two-photon spectra are very similar (compare Figure 23 to Figure 11B).

Discussion

pH changes play important roles in many physiological processes. Cancer cells are known to have higher intracellular pH than normal tissues (Gillies et al. 1994). pH signaling has also been implicated in the modulation of caspase activation during

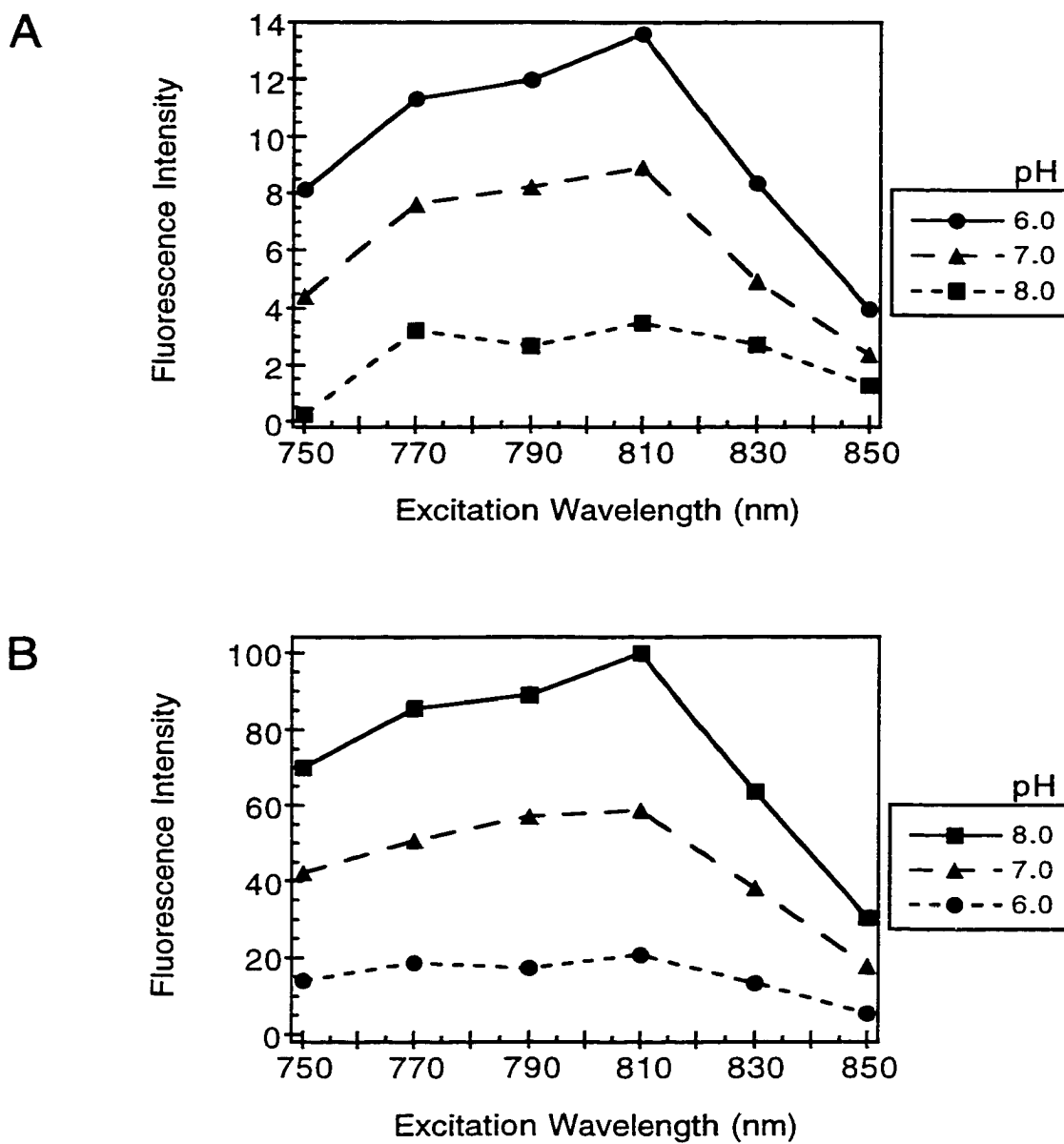


Figure 22. Two-photon excitation spectra of deGFP4 as a function of pH. Aliquots of purified protein were placed on the two-photon microscope stage while the excitation wavelength of a Coherent Titanium-Sapphire laser was varied (see Experimental Procedures). Emission intensities were monitored at 473 nm (A) and 514 nm (B) and normalized to 100, the maximum value obtained at pH 8.0 with 810 nm excitation and 514 nm emission.

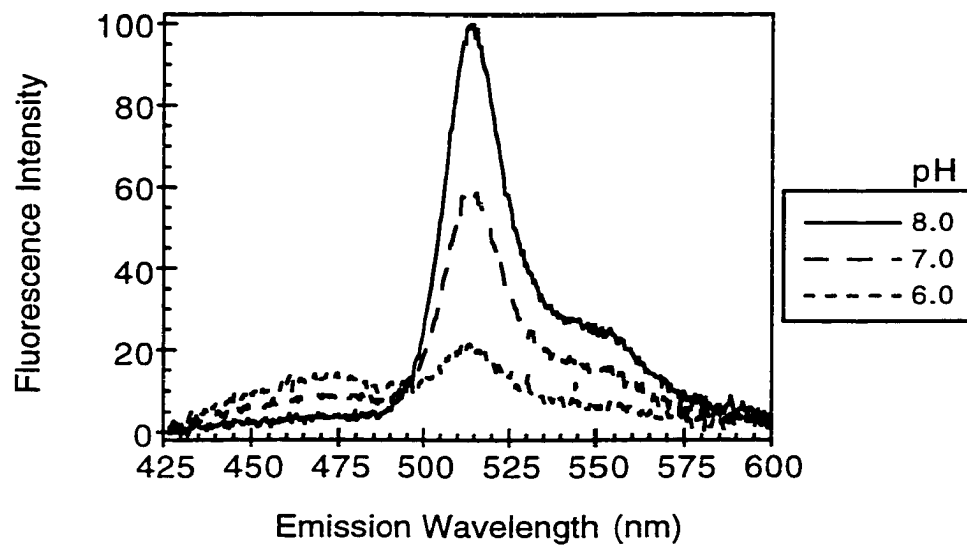


Figure 23. Two-photon emission spectra of deGFP4 as a function of pH. Fluorescence emission intensities were normalized to the maximum intensity of the pH 8.0 sample.

apoptosis (Matsuyama et al. 2000). In addition, in many mitochondrial disorders, dysfunction of the oxidative phosphorylation system leads to a build-up of lactic acid caused by anaerobic respiration (Taylor et al. 1997). To better understand pH changes that take place *in vivo*, a good intracellular “pH meter” is needed. Ratiometric-by-emission dyes like SNARF-1[®] have been available for some time now (Whitaker et al. 1991), however these dyes stain the whole cell, precluding experiments on individual organelles. Ratiometric-by-excitation pH-sensitive GFPs have been described (see Chapter II; Miesenbock et al. 1997; Elsliger et al. 1999). They have the advantage of being targettable to subcellular organelles, however these GFPs are incompatible with techniques which use a single wavelength like flow cytometry and laser scanning microscopy.

The observation that excitation of the neutral chromophore leads to fluorescence, suggests an excited state proton transfer reaction occurs. Since the dual-emission is pH dependent, this indicates that there is likely a titrating group that is part of a proton transfer pathway leading to the chromophore phenolic hydroxyl. It is unlikely to be the same proton transfer network that exists in wild-type GFP, since structural analysis showed that glutamic acid 222 is in a different position with respect to wild-type GFP and since a pK_a of 4.25 (typical for a free glutamic acid in solution; Lehninger et al 1993)

is far too low for glutamic acid 222 to be the titrating group. Considering the pK_a of a cysteine is around 8.4 (Voet and Voet 1994), it cannot be excluded as the determinant of the pK_a of the deGFPs and potentially the titrating group. By understanding the structural aspects and the titrating group responsible for the dual-emission of these variants, it may be possible in the future to design even brighter deGFPs for increased signal in the absence of two-photon excitation equipment.

Nonetheless, we have shown that the dynamic range of these GFPs is comparable to that of SNARF-1[®]. In fact, the pK_a of the SNARF-1[®] dye favors the alkaline range examined in this study by NH₄Cl exposure. Therefore, the deGFP4 variant which has a lower pK_a should perform even better than the SNARF-1 dye at lower pH ranges. Moreover, the deGFP3 variant with a pK_a of 6.6, should be an excellent dual-emission probe for studying acidic pH compartments, like the Golgi apparatus and the vacuole whereas the deGFP1 variant with a pK_a of 7.8, would likely make a good pH sensor for alkaline environments, such as the mitochondrial matrix. Given the sensitivity and non-invasiveness of fluorescence measurements, these deGFPs are likely to become popular *in vivo* pH indicators.

Experimental Procedures

Mutagenesis and Protein Preparation

Mutagenesis was carried out on a histidine-tagged version of the S65T variant of GFP in the plasmid pRSET_B. Mutations were introduced via the QuikChange™ Site-Directed Mutagenesis Kit (Stratagene, La Jolla, CA), following the manufacturer's protocol. All mutations were verified by DNA sequencing of the entire GFP coding sequence. Mutant protein was expressed in *Escherichia coli*, strain JM109(DE3), by use of the pRSET_B expression system with an N-terminal six histidine tag. The cells were resuspended in 50 mM HEPES, pH 7.9, 300 mM NaCl, 10% glycerol, and sonicated for seven minutes. Cell lysate was centrifuged and the supernatant was applied to a column of Ni-NTA agarose resin (Qiagen, Hilden, Germany). The N-terminal histidine tag was cleaved with $1/_{50}$ (w/w) γ -chymotrypsin overnight at room temperature. Samples were concentrated by filtration (Centricon 10; Amicon Inc., Beverly, MA) and buffer exchanged with PD-10 Sephadex columns (Amersham Pharmacia, Piscataway, NJ) into 20 mM HEPES, pH 7.9.

Spectroscopy and pH Titrations

pH titrations were performed using approximately $200 \mu\text{g mL}^{-1}$ mutant GFP in 75 mM buffer and 140 mM NaCl. According to the desired pH, an appropriate buffer was chosen from MES, HEPES, or CHES and the final pH was adjusted by HCl or NaOH addition. The absorbance was then scanned between 250 and 550 nm on a Shimadzu 2101 spectrophotometer. Molar extinction coefficients were determined using the Beer-Lambert law. Protein concentrations were carried out using the A_{280} and the theoretical ε_{280} ($19,890 \text{ M}^{-1} \text{ cm}^{-1}$) for S65T which is in good agreement with protein concentrations determined using the BCA assay kit (Bio-Rad, Hercules, CA) with bovine serum albumin as the standard. The extinction coefficients for band A were evaluated at pH 5.5 and for band B at pH 9.0.

Fluorescence measurements were performed on a Hitachi F4500 fluorescence spectrophotometer at a protein concentration of approximately $100 \mu\text{g mL}^{-1}$ in the same buffers used for absorbance measurements. For emission scans, the excitation wavelength was set to the absorbance maximum of band A for each mutant (see Table 3). Apparent chromophore pK_a values were determined by plotting the emission intensity of the major emission peak when excited at band A as a function of pH and fitting the data to a titration curve (Kaleidagraph, Abelbeck Software). Quantum yield measurements

were performed using equal 400 nm optical densities of the reference standard, 9-aminoacridine, in water and each variant at pH 5.5 and 9.0. Fluorescence emission profiles spanning 405-600 nm (excitation 400 nm) for pH 5.5 and for pH 9.0 were summed and compared with the 9-aminoacridine standard ($\Phi = 0.98$) to give the quantum yield for each of the dual emission peaks of the GFP variants.

Crystallization

The mutant GFP protein, S65T/H148G/T203C, was further concentrated to approximately 48 mg mL⁻¹ in 20 mM HEPES (pH 7.9) and 0.2 μ m-filtered. Rod-shaped crystals were grown at room temperature in 1-2 days by hanging drop vapor diffusion against 100 mM Citrate-NaOH (pH 4.5), 100 mM ammonium acetate, 14% polyethylene glycol 1550 for the low pH crystals and 50 mM Tris (pH 9.0), 100 mM MgCl₂, 22% polyethylene glycol 4000 for the high pH crystals. Drops contained 4 μ L protein solution and 4 μ L well solution. For low-temperature diffraction data collection, low pH crystals were then exchanged over three days into a solution of 100 mM Citrate-NaOH (pH 4.5), 100 mM ammonium acetate, and 40% polyethylene glycol 1550, and the high pH crystals were exchanged into 50 mM Tris (pH 9.0), 100 mM MgCl₂, 22% polyethylene glycol 4000, and 40% ethylene glycol.

Data Collection and Refinement

X-ray diffraction data were collected from a single frozen crystal for each pH using an Raxis-IV image plate mounted on a Rigaku RUH3 rotating anode generator equipped with mirrors for the low pH data set and using a Mar 345 detector at the Stanford Synchrotron Radiation Laboratory beamline 7-1 for the high pH data set. Data sets were indexed and reduced with Mosflm (Leslie 1996) and intensities were scaled with SCALA (CCP4 1994). The GFP S65T coordinate file (PDB code: 1EMA) was used as the phasing model. Positional refinement was carried out using the data to 4.0 Å, 3.0 Å, 2.5 Å, 2.1 Å, 1.8 Å and finally to the limit of resolution, using the program TNT (Tronrud et al. 1987). After each increase in resolution the electron density maps ($2F_o - F_c$) and $F_o - F_c$) were analyzed using the program O (Jones et al. 1991). B-factor refinement was performed using the default TNT B-factor correlation library. The B-factor correlation values for the chromophore atoms were derived from histidine and phenylalanine residues. Solvent molecules were added only if consistent with $F_o - F_c$ features and when in proximity of hydrogen bond partners. The atomic coordinates and structure factors have been deposited in the Research Collaboratory for Structural Bioinformatics Protein Data Bank (<http://www.rcsb.org/>).

Fluorescence Microscopy

PS120 cells were transiently transfected with a plasmid containing GFP C48S/F64L/S65T/H148C/T203C. Cells were imaged 1-2 days after transfection on a Zeiss LSM 510 confocal microscope before and after loading with 2 μ M SNARF-1 AM[®] (Molecular Probes, Eugene, OR). During imaging, cells were exposed to physiologic saline: 130 mM NaCl, 5 mM KCl, 2 mM CaCl₂, 1 mM MgSO₄, 1 mM NaPO₄, 25 mM mannose, and 20 mM HEPES (pH 7.4). 25 mM NH₄Cl was added to induce pH changes. All images were collected simultaneously during excitation at 364 nm and 543 nm by an Ar-ion laser (Coherent Enterprise), while monitoring emission at 385-470 nm and 475-525 nm for deGFP4 and 560-615 nm and 625-655 nm for SNARF-1[®]. Data were analyzed using Metamorph software (Universal Imaging, PA).

Two-Photon Laser Scanning Microscopy

PS120 cells expressing deGFP4 from the mammalian expression plasmid pEGFP-N1 (CLONTECH Laboratories Inc., Palo Alto, CA) were excited with 810 nm light from a Coherent Titanium-Sapphire laser. The titanium-sapphire laser was pumped by a Verdi frequency doubled Nd:YAG laser running at 5-6 W output power. For the excitation and emission scans 90 μ g μ L⁻¹ drops of purified deGFP4 were placed on the two-photon

microscope stage. At each indicated excitation wavelength, 56 mW of laser power was input into the scan head of the Zeiss LSM510 NLO microscope (measured by Coherent Lasermate laser power detector). Two-photon fluorescence was descanned prior to collection at a fiber optic, which was used to steer emission light to an imaging spectrograph (Model Triax 320, JY Horiba). Within the Triax, a liquid nitrogen cooled, back-thinned CCD was used to collect the entire emission spectrum simultaneously at any given condition (data collection time was fixed at 15 seconds of scanning). No photobleaching of fluorescence was detectable under these conditions, even when scanning continuously for several minutes. A background spectrum at each excitation wavelength was collected from solutions without added deGFP4 and subtracted from the appropriate experimental spectrum.

CHAPTER IV

OXIDATION REDUCTION SENSITIVE GREEN FLUORESCENT PROTEIN VARIANTS WITH RATIO METRIC REDOX AND pH INDICATING CAPABILITIES

Portions of the work presented in this chapter were done in collaboration with Robert J. Aggeler and Roderick A. Capaldi of the Institute of Molecular Biology and Department of Biology at the University of Oregon. Portions of this chapter were submitted for publication to *Biochemistry* (2001).

This chapter describes the design and characterization of green fluorescent protein variants with ratiometric-by-excitation properties in response to changes in redox potential and ratiometric-by-emission characteristics as a function of pH as well as the usefulness of redox-sensitive GFPs as indicators of redox status in living cells.

Summary

To create a redox sensor that overcomes many of the drawbacks of other methods of *in vivo* redox status determination, site-directed mutagenesis was carried out on the

green fluorescent protein (GFP). By mutating key residues near the chromophore in GFP to cysteines, novel *redox*-sensitive GFPs (rosGFPs) were constructed. They display ratiometric dual-wavelength excitation of fluorescence as a function of redox state, with apparent redox potentials of -0.272 to -0.299 V depending on pH. Unexpectedly, these rosGFPs also exhibited ratiometric dual-emission properties in response to pH changes, providing the unique possibility to simultaneously monitor redox potential and pH changes with the same probe. T65S reversion leads to pH-independent redox sensors with altered redox potentials and large UV excitation peaks, which should help to overcome background levels of cellular autofluorescence. Crystal structure analysis of an oxidized and reduced rosGFP to 1.9 and 2.0 Å, respectively, indicate that dual-wavelength excitation is likely the result of manipulating the position of glutamic acid 222. These findings unveil that the key to dual-wavelength excitation GFP biosensor design is modulation of glutamic acid 222. Using cultured HeLa cells, we demonstrate that rosGFPs can reversibly respond to exogenous redox stimuli and have redox potentials near that of mitochondria, with the apparent redox potential of mitochondria estimated to be -0.368 ± 0.004 V. In addition, the apparent redox potential of the cytosol was found to be more reducing than -0.330 V. The chemistry of two distinct types of

two-electron transfer reactions and how this chemistry helps cells maintain a very reducing environment is discussed.

Introduction

Oxidation-reduction (redox) processes are very important in living organisms. The formation of disulfide bonds during protein folding relies upon a well maintained redox buffering system of glutathione and oxidized glutathione (Cuozzo and Kaiser 1999). There also exists a thioredoxin-like family of enzymes that catalyze the formation and isomerization of disulfide bonds in proteins (Debarbiex and Beckwith 1999). In addition, redox signaling during apoptosis has been implicated in activating mitochondrial permeability transition, leading to cytochrome c release (Hall 1999). Redox changes in the form of cellular oxidation have also been suggested to be a final step in the apoptotic process leading to degradation of apoptotic bodies (Cai and Jones 1999). Given the importance of *in vivo* processes such as protein folding and apoptosis that are dependent upon redox status, a non-invasive, convenient method for studying redox changes within living cells is needed.

Current methods of determining *in vivo* redox status have many limitations. Many present techniques require cells to be harvested before their contents can be analyzed. This type of procedure is not only very invasive but is also not a very accurate

measure of the redox state of within live cells. Moreover, it would be impossible with this technique to monitor redox changes within the same cell over a period of time.

Recently, Keese et al. (1999) have developed an indicator of redox state in which glutathione reductase crystals were microinjected into the cytosol of human fibroblasts, and by detecting a color change of the crystals, they were able to determine the redox potential of the cytosol to be more reducing than -0.270 V. While this method may allow redox determination within single living cells, the cumbersome nature of the technique is still a major drawback. The most reasonable protocol for determining redox status is probably still that of Hwang et al. (1992). They employed the tetrapeptide N-Acetyl-Asn-Tyr-Thr-Cys-NH₂ to measure the concentration ratio of free thiols to disulfides in the cytosol and secretory pathway of cultured cells. They concluded that the cytosol is more reducing than the secretory pathway with an approximate redox potential of -0.221 to -0.236 V for the cytosol compared to -0.170 to -0.185 V for the secretory pathway. However, this method requires harvesting the cells and like all the other methods, it is very labor intensive. Moreover, this technique determined redox potentials based only upon the ratio of reduced glutathione (GSH) to oxidized glutathione (GSSG), potentially ignoring other redox buffering components.

To create a redox sensor that overcomes many of these drawbacks, we modified the *Aequorea victoria* green fluorescent protein (GFP). GFP is a 238 amino acid, spontaneously fluorescent protein that has become extremely popular in molecular and cell biology (for reviews: Tsien 1998; Remington 2000). Originally GFP was used as a passive indicator of gene expression and protein localization. However more recently, GFP has taken on the role of an active indicator of such things as intracellular H⁺, Ca²⁺, and halide ion concentrations (Kneen et al. 1998; Llopis et al. 1998; Baird et al. 1999; Jayaraman et al. 2000). In addition to GFP being highly fluorescent, protease resistant, and very stable throughout a wide range of pH and solvent conditions, it also has the advantage of being genetically encoded. These characteristics result in a probe that can not only be expressed in nearly all organisms, but is also targetable to organelles within the host cell. GFP is a non-invasive indicator, which allows experiments to be conducted and monitored in a single cell over a period of time.

In this chapter, we describe the engineering and application of a fluorescent ratiometric indicator of redox state based on *Aequorea* GFP. By mutating key residues near the chromophore of GFP to cysteines, novel redox-sensitive GFPs were created. They display ratiometric-by-excitation fluorescent properties as a function of redox state, with apparent redox potentials of -0.272 to -0.299 V. Analysis of the oxidized and

reduced crystal structure of one redox-sensitive GFP variant revealed that positional modulation of glutamic acid residue 222 is responsible for the dual-wavelength excitation property of the variants identified in this study. Using cultured mammalian cells expressing a redox-sensitive GFP, we show that the GFP can reversibly respond to redox changes in response to exogenous stimuli. The *in vivo* results indicate that the apparent redox potential of the cytosol of cultured mammalian cells is more reducing than -0.330 V and the apparent redox potential of mitochondria is approximately -0.368 ± 0.004 V. Possible mechanisms for how the reducing environments of the cytosol and mitochondria are maintained is discussed.

Results

Design of Redox-Sensitive GFPs

In order to create redox-sensitive GFPs, we sought to introduce two cysteine residues into GFP that would be within disulfide bonding distance of each other, near the chromophore, and on the surface of the protein. It was thought that differing oxidation states of the cysteine residues would result in fluorescence changes due to changes in the chromophore environment. In addition, the surface location of the cysteines would permit them to be solvent accessible, which should enable reversible response to redox

changes in the surrounding environment. After close examination of the crystal structure of GFP, several suitable sites for the introduction of pairs of cysteines were chosen. The first site chosen was positions 147 and 204, while the second site chosen was positions 149 and 202. All four amino acid side chains at these positions pointed away from the protein's interior. The distance between the C_{α} - C_{α} and C_{β} - C_{β} positions for site one were 4.6 Å each, and for site two the distance between these positions were 4.8 and 5.9 Å, respectively. Although these distances did not perfectly agree with previous reports on ideal geometry for the introduction of disulfide bridges in proteins and neither of these sites were chosen by a disulfide bridge modeling program (Sowdhamini et al. 1989), there were still indications that one or both of these pairs of cysteines may be able to form a disulfide bond. Such evidence came from the irregular "bulging" nature of the β -strand encompassing the positions 147 and 149, which has previously been shown to move in response to substitution at position 148 (see Chapter II; Wachter et al. 1998). Considering that flexibility has been suggested to help ensure that a protein can both adjust to the perturbation due to replacements with cysteine residues as well as to allow the disulfide bridge to assume near-optimal geometry (Matsumura et al. 1989), the 147/204 and 149/202 sites best fit the criteria.

Disulfide-Bond Formation and Redox Sensitivity of Engineered Cysteines

To verify that the introduced cysteines formed disulfide bonds and to show that the disulfide bonds were intramolecular, SDS-PAGE was run on redox-sensitive GFP #1 (rosGFP2), harboring the mutations C48S/S65T/S147C/Q204C and on a control GFP (C48S/S65T) under reducing and non-reducing conditions (Figure 24). If an intramolecular disulfide bond forms, the resulting polypeptide would be expected to migrate further based on its slightly more compact structure in the denatured form. However, if an intermolecular disulfide bridge forms, then a large molecular weight band (~60 kDa) corresponding to a disulfide-linked dimer, would be expected. The results indicate that the introduced cysteines do indeed form intramolecular disulfide cross-links, but are unable to produce disulfide-linked dimers. This can be seen by comparing lanes 11 and 12 with lanes 14-16 or lanes 21 and 22 with lanes 17-19.

To test whether the introduced cysteines affected the spectral properties of GFP, absorbance and fluorescence scans were collected at different redox potentials. To establish these various redox potentials, GFP was equilibrated with varying concentrations of dithiothreitol (DTT) and oxidized DTT (DTT_{ox}). Figure 25 shows the absorbance and fluorescence excitation spectra of rosGFP2 as a function of redox potential. With a disulfide bond formed under oxidizing conditions, the 400 nm peak

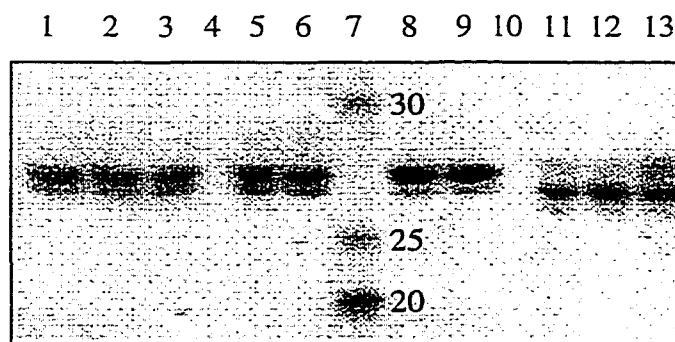


Figure 24. SDS-PAGE reveals disulfide linkage in rosGFP2. Lanes 1 – 6, control (C48S/S65T) and lanes 8 – 13 rosGFP2 were incubated with 1 μ M CuCl₂ (with or without 2 mM *N*-ethylmaleimide; lanes 2, 3, 11, 12) or with 1 mM DTT (with or without 2 mM *N*-ethylmaleimide; lanes 5, 6, 8, 9). Lane 7 shows approximate molecular weights in kDa. Lanes 4 and 10 were left empty.

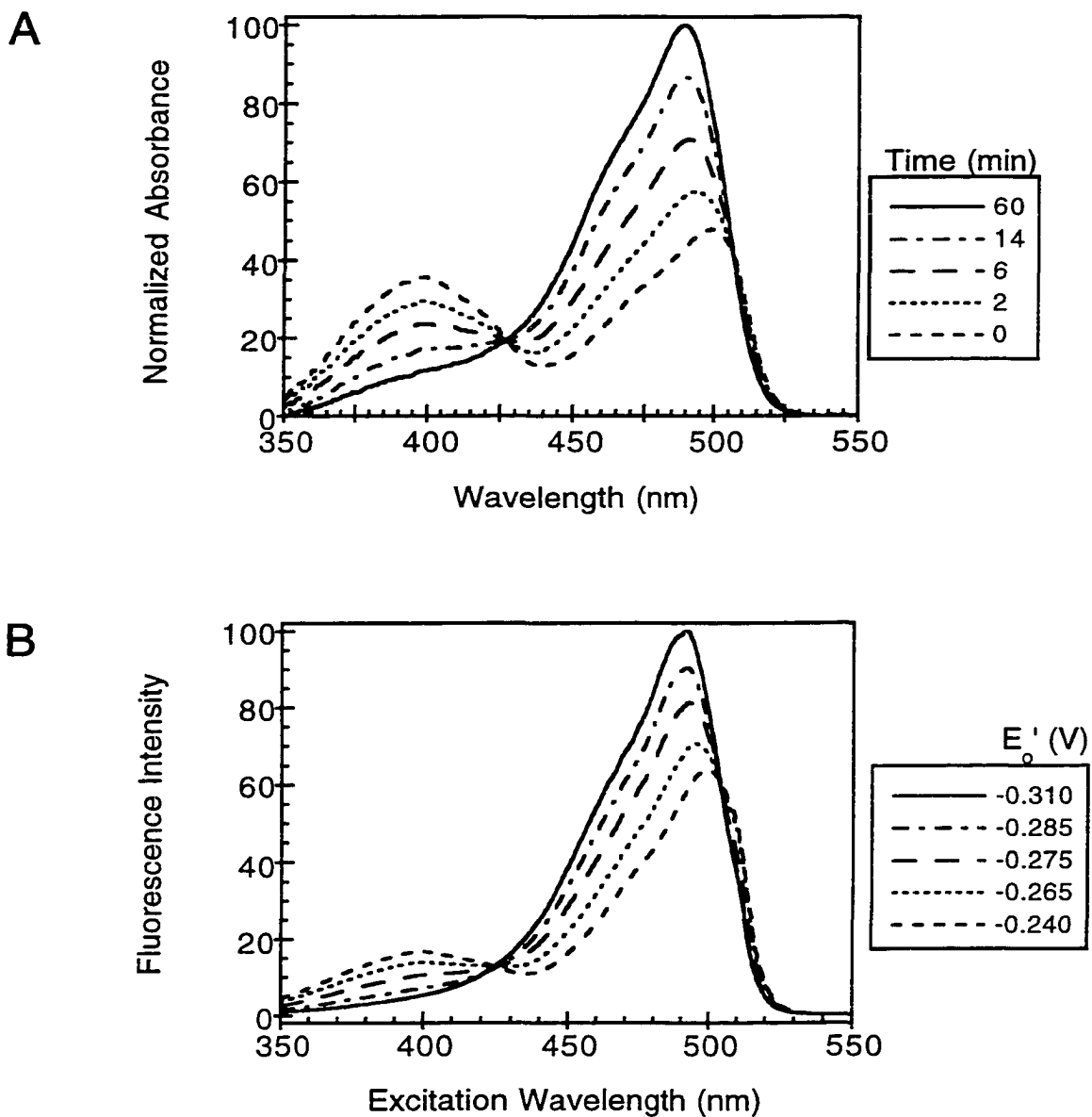


Figure 25. Absorbance and fluorescence excitation spectra of rosGFP2 at various redox states. The absorbance spectra (A) show the conversion of the neutral (band A; 400 nm) to the anionic (band B; 490 nm) chromophore species over time in the presence of 1 mM DTT. Band A is maximized under oxidizing conditions, whereas band B is favored under reducing conditions. Fluorescence spectra (B) were collected at various redox potentials and also show the interconversion of chromophore charge states. Absorbance and fluorescence spectra were both normalized to the intensity of the fully reduced protein.

(band A) was maximized whereas the 490 nm peak (band B) was minimized.

Conversely, in the absence of a disulfide cross-link achieved with reducing conditions,

band B was at a maximum, while band A was at a minimum. The two peaks were

separated by a clean isosbestic point at 425 nm, indicative of only two interconvertable

species. The redox potential of rosGFP2 was then determined from the equilibrium

constant obtained by plotting the fraction of reduced protein versus the ratio of DTT_{red} to

DTT_{ox} (see Appendix) and discovered to be -0.272 V.

Introducing a pair of cysteines at the alternative site also yielded a mutant protein whose fluorescent properties varied in response to redox potential (Figure 26A). The rosGFP4 variant, having the mutations C48S/S65T/N149C/S202C, displayed increased band B fluorescence over rosGFP2, however band A fluorescence intensity was almost non-existent. The fluorescence isosbestic point of rosGFP4 was shifted to approximately 400 nm (Figure 26B).

Combining the two pairs of cysteine substitutions resulted in a variant (C48S/S65T/S147C/N149C/S202C/Q204C, rosGFP6), whose properties appeared to be an average of both rosGFP2 and rosGFP4. Figure 27 shows the fluorescence excitation spectra of rosGFP6. In this variant the dynamic range of the two excitation peaks as well as the isosbestic point lie in the middle of the values observed for either rosGFP2 or

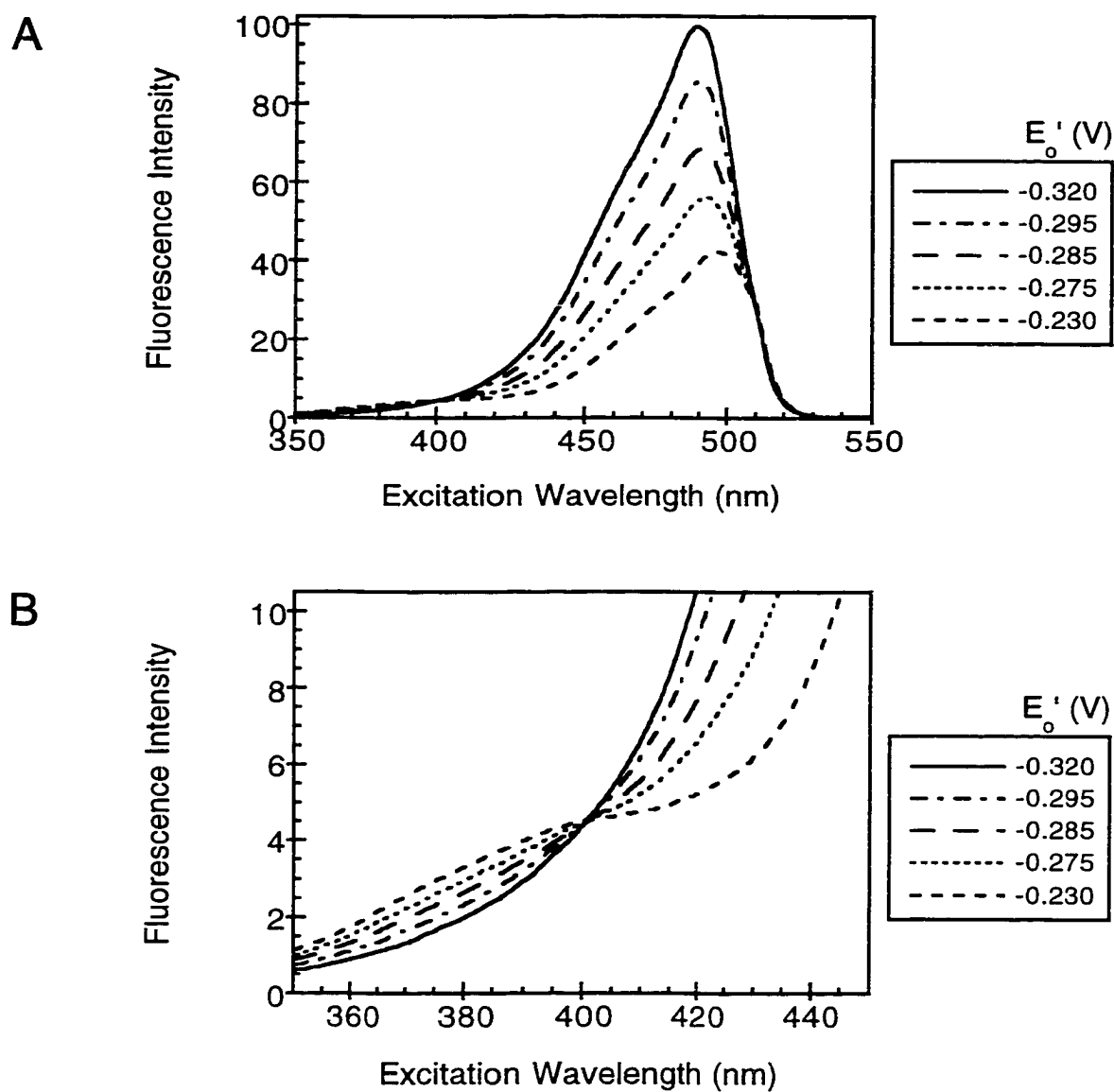


Figure 26. Fluorescence excitation spectra of rosGFP4 as a function of redox potential. The entire spectrum (A) shows the redox potential dependence on the excitation spectra of rosGFP4. Expanded the region around 400 nm (B), reveals a well resolved isosbestic point. Fluorescence intensity values were normalized to the maximum intensity at E'_o -0.320 V and emission was monitored at 510 nm.

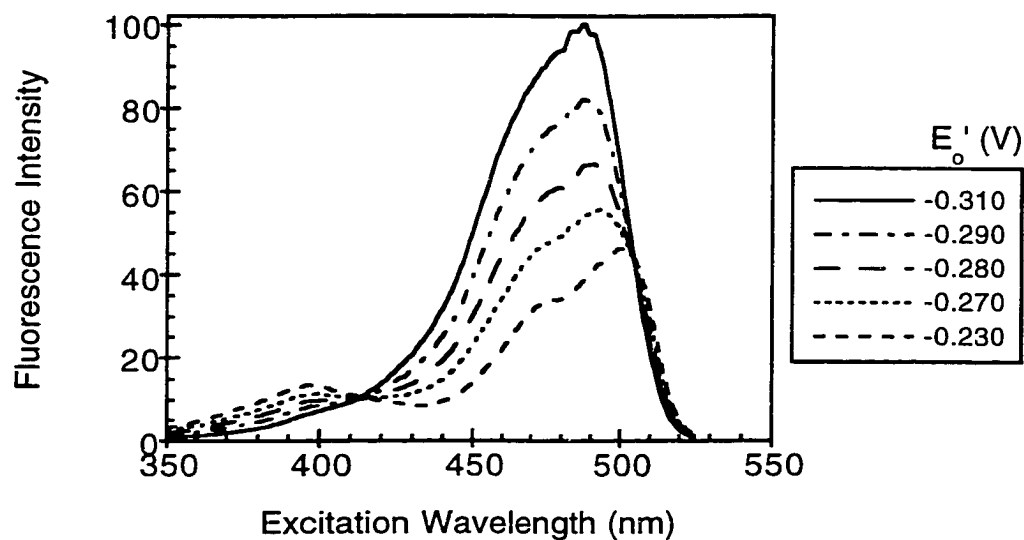


Figure 27. Fluorescence excitation spectra of rosGFP6 as a function of redox potential. Fluorescence intensity values were normalized to the maximum intensity at $E'_o = -0.310$ V and emission was monitored away from the peak at 535 nm.

rosGFP4. The overall dynamic range of the excitation ratio (δ), determined by dividing the maximum and minimum possible excitation peak ratios, was found to be 5.4 for rosGFP6. Table 5 summarizes the spectroscopic and biochemical parameters of the rosGFP variants.

pH-Sensitivity of rosGFPs

Previous work has shown that while the fluorescence of wild-type GFP is unaffected throughout the biologically relevant pH range from 6 to 8 (Ward et al. 1982), GFP variants harboring the S65T mutation often exhibit dramatic fluorescence changes over this pH range (Kneen et al. 1998; Wachter et al 1998; Elsliger et al 1999). To determine if the rosGFPs were also pH-sensitive, their absorbance and fluorescence was scanned over a wide range of pHs. Figure 28 shows both absorbance and fluorescence excitation spectra of oxidized rosGFP2 versus pH. The spectra show that as the pH is increased from 5.2 up to 9.0 the fluorescence intensity of both excitation peaks increases. Plotting the intensity at 490 nm as a function of pH and fitting to a titration curve with a single ionization constant gave a pK_a value of 6.0 (Figure 29). Interestingly, titration of rosGFP2 in the reduced state shifted the pK_a to 5.6 (Figure 30).

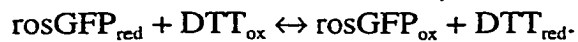
Initially it appeared that the pH-sensitivity of the rosGFPs may pose a problem for

Table 5. Spectroscopic and Biochemical Properties of rosGFPs.

WT ¹	K _{eq} ²	E _{o'} (V) ³	δ ⁴	K _{eq} ²	E _{o'} (V) ³	δ ⁴	S65T ⁵
147/204 (rosGFP1)	0.0702	-0.288	6.1	0.0205	-0.272	5.8	147/204 (rosGFP2)
149/202 (rosGFP3)	0.1505	-0.299	4.3	0.0561	-0.286	2.6	149/202 (rosGFP4)
Double ⁶ (rosGFP5)	0.1341	-0.296	7.8	0.0385	-0.280	5.4	Double ⁶ (rosGFP6)

¹Variants in this column contain the phenotypically neutral substitutions C48S and Q80R in addition to the introduced cysteines.

²Equilibrium constant values (K_{eq}) are listed for the reaction:



³Apparent redox potential values (E_{o'}) are given for pH 7 and 30°C.

⁴The dynamic range values (δ) are the maximum excitation peak ratio change in number of fold (ie. the quotient of the maximum and minimum possibly ratio of peak excitation wavelengths).

⁵Variants in this column contain the S65T mutation in addition to the phenotypically neutral substitutions C48S and Q80R and the introduced cysteines.

⁶The rosGFPs contain four introduced cysteines at positions 147, 149, 202, and 204.

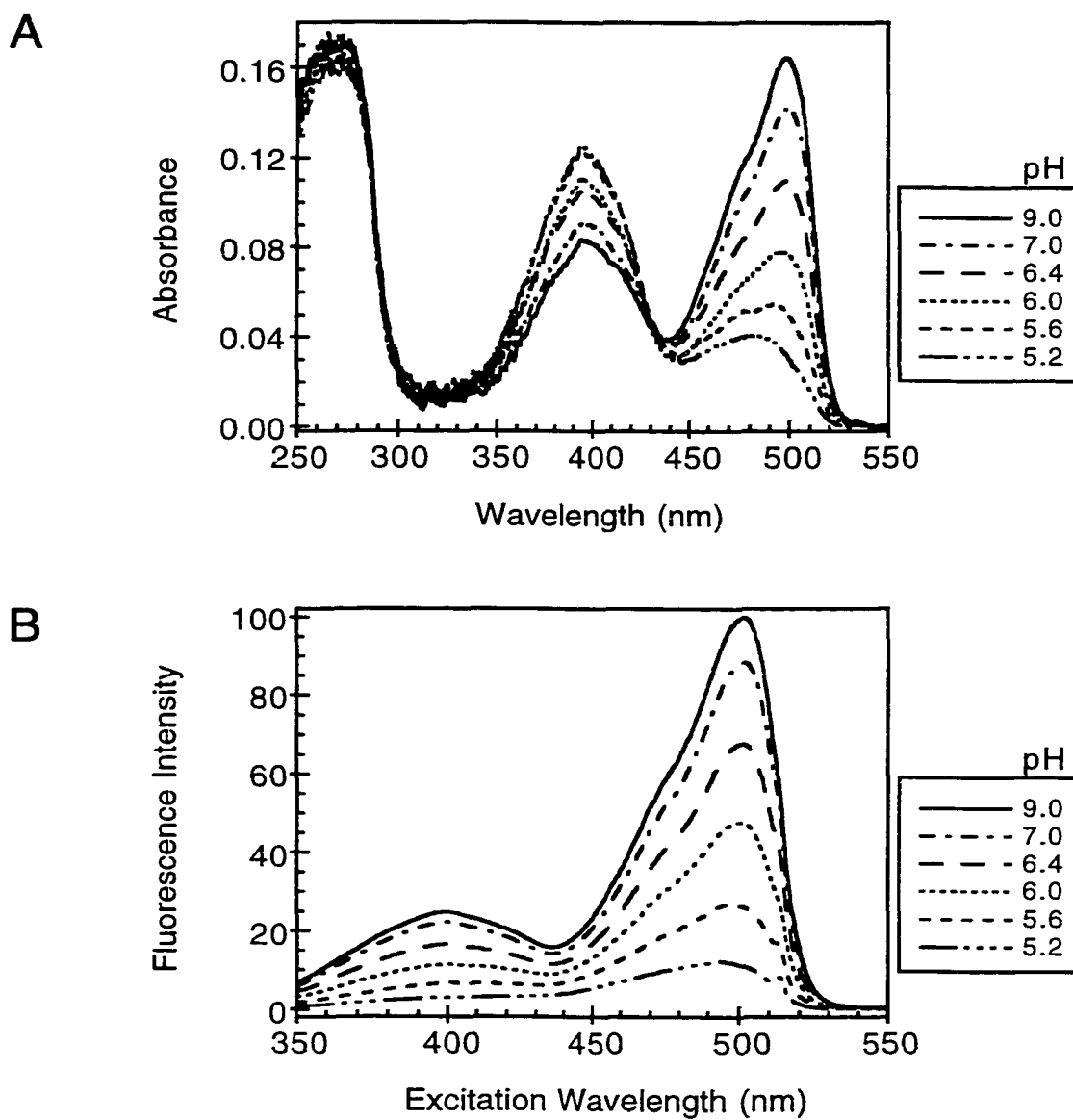


Figure 28. Absorbance and fluorescence excitation spectra of oxidized rosGFP2 as a function of pH. Absorbance scans (A) were taken on samples of rosGFP2 containing 0.5 μM CuCl_2 at the indicated pHs. These samples were then diluted in the same buffer and their fluorescence excitation spectra (B) were collected. Fluorescence intensity values were normalized to the maximum intensity at pH 9.0 and emission was monitored at 510 nm.

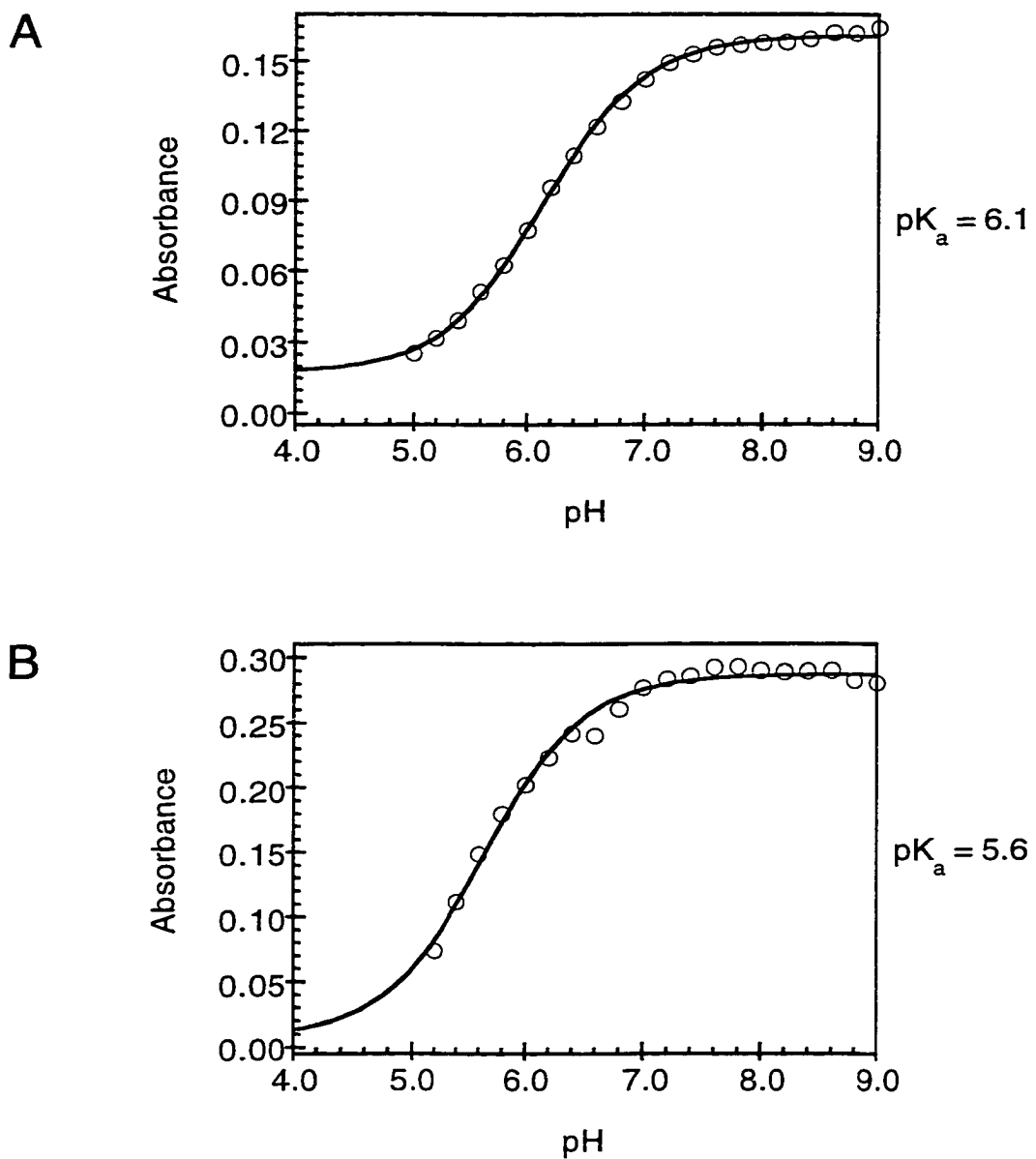


Figure 29. pH titration of oxidized and reduced rosGFP2. Absorbance values at 490 nm (band B) were plotted versus pH for oxidized (A) and reduced (B) rosGFP2. The data were then fitted to a titration curve with a single pK_a value.

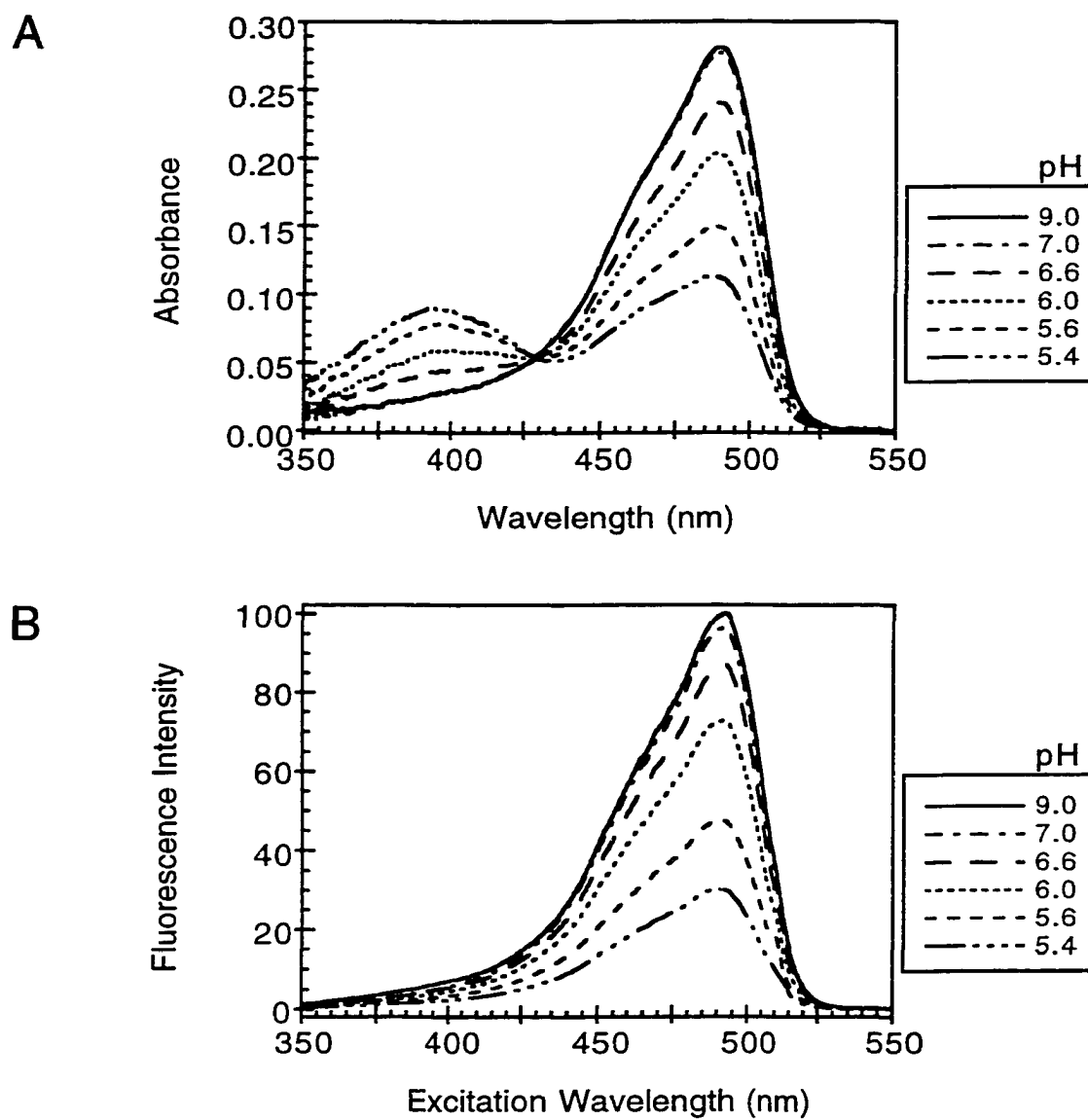


Figure 30. Absorbance and fluorescence excitation spectra of reduced rosGFP2 as a function of pH. Absorbance scans (A) were taken on samples of rosGFP2 containing 1 mM DTT at the indicated pHs. These samples were then diluted in the same buffer and their fluorescence excitation spectra (B) were collected. Fluorescence intensity values were normalized to the maximum intensity at pH 9.0 and emission was monitored at 510 nm. Absorbance readings around 280 nm are greatly altered due to the presence of DTT and thus are not shown.

using them as tools to determine *in vivo* redox potentials by introducing pH artifacts. Therefore, to produce a pH-insensitive rosGFP, threonine 65 was reverted back to serine, which is the amino acid found at this position in wild-type GFP. Not only did the T65S reversion completely eliminate pH-sensitivity over the range of 6 to 8 (data not shown), but it greatly altered the spectral properties of the rosGFPs. Figures 31, 32, and 33 show the fluorescence excitation spectra of rosGFP1 (C48S/S147C/Q204C), rosGFP3 (C48S/N149C/S202C), and rosGFP5 (C48S/S147C/N149C/S202C/Q204C) at varying redox potentials. The most striking difference between these rosGFPs and threonine 65 containing rosGFPs is the favoring of band A over band B fluorescence. There is also a tendency toward more even excitation of both bands, which is especially evident in the rosGFP3 and rosGFP5 variants. Unexpectedly, the T65S reversion led to a 13-16 mV more reducing redox potential (see Table 5).

Subsequent to the T65S reversion, it was determined that by using a fluorescence excitation ratio any effects induced by pH changes were virtually eliminated. Figure 34 illustrates how a ratio of excitation wavelengths remains a constant over a large pH range in both the fully reduced or fully oxidized protein. In other words, the fluorescence increase due to alkalization or fluorescence decrease upon acidification seen in the excitation spectra of rosGFP2 affects the entire spectrum in the same manner, and hence

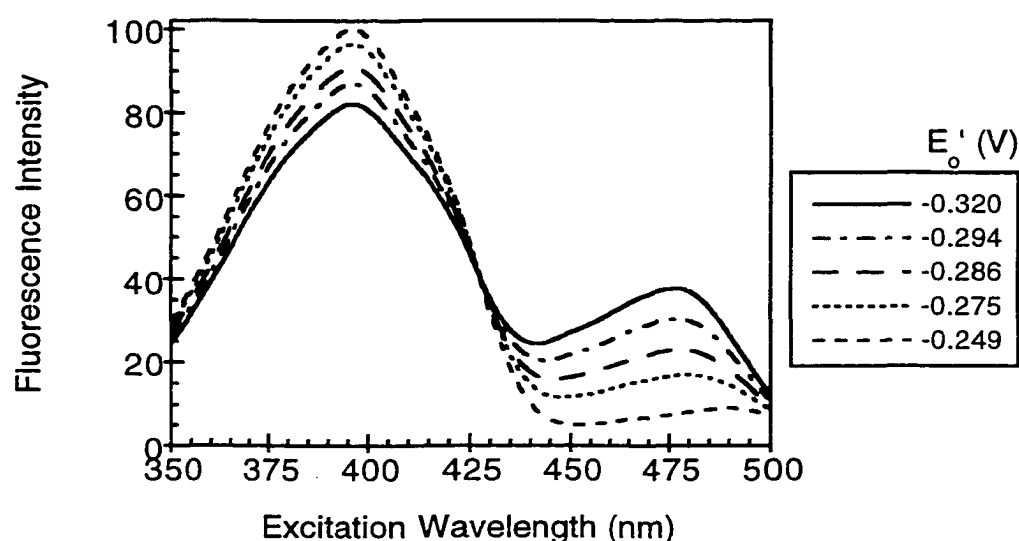


Figure 31. Fluorescence excitation spectra of rosGFP1 at various redox potentials. Fluorescence intensity values were normalized to the maximum intensity at E'_o -0.320 V and emission was monitored at 510 nm.

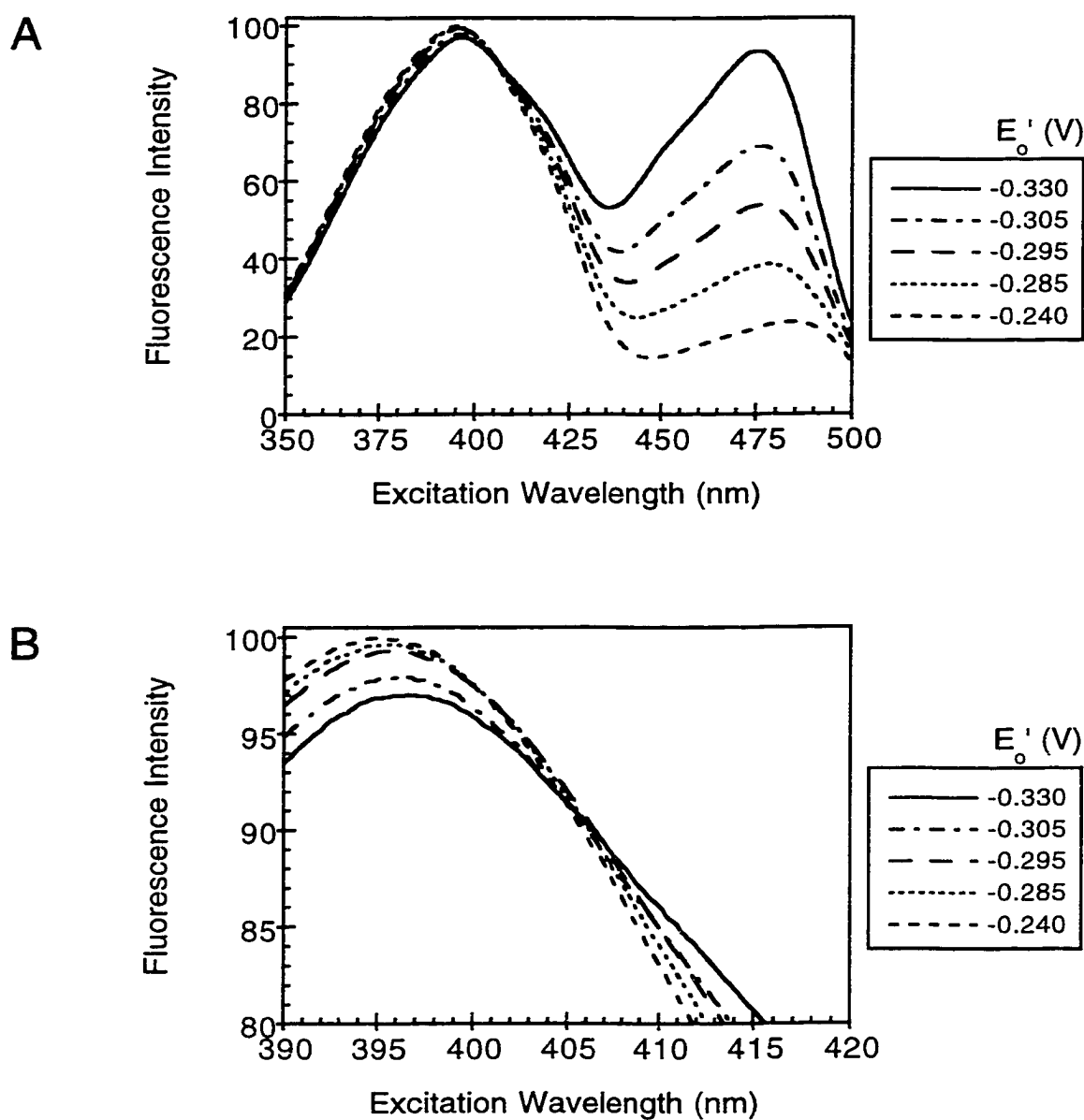


Figure 32. Fluorescence excitation spectra of rosGFP3 at various redox potentials. The entire spectrum (A) shows the redox potential dependence on the excitation spectra of rosGFP4. Expanded the region around 405 nm (B), reveals the existence of an isosbestic point. Fluorescence intensity values were normalized to the maximum intensity at E'_o -0.330 V and emission was monitored at 510 nm.

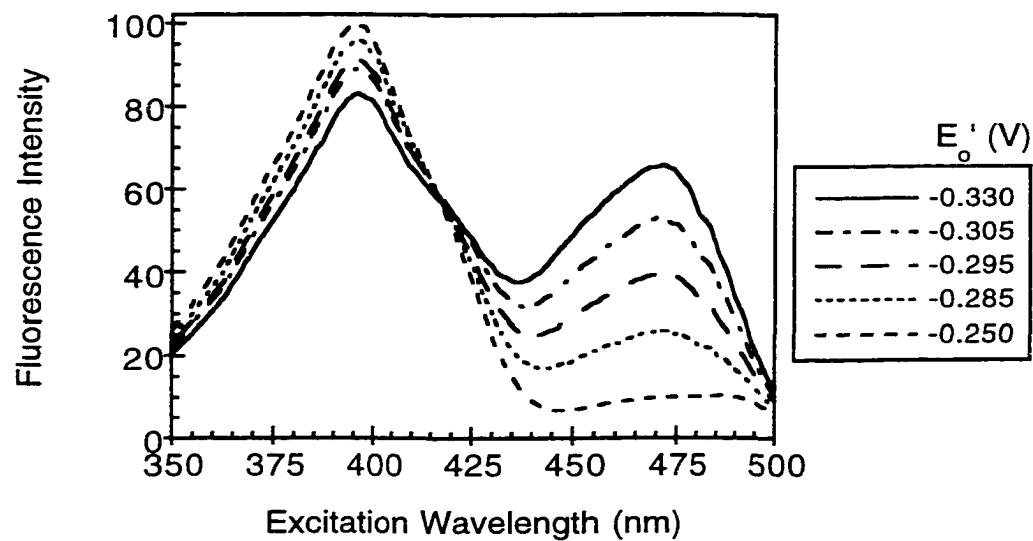


Figure 33. Fluorescence excitation spectra of rosGFP5 at various redox potentials. Fluorescence intensity values were normalized to the maximum intensity at $E_o' = -0.330$ V and emission was monitored off the peak at 535 nm.

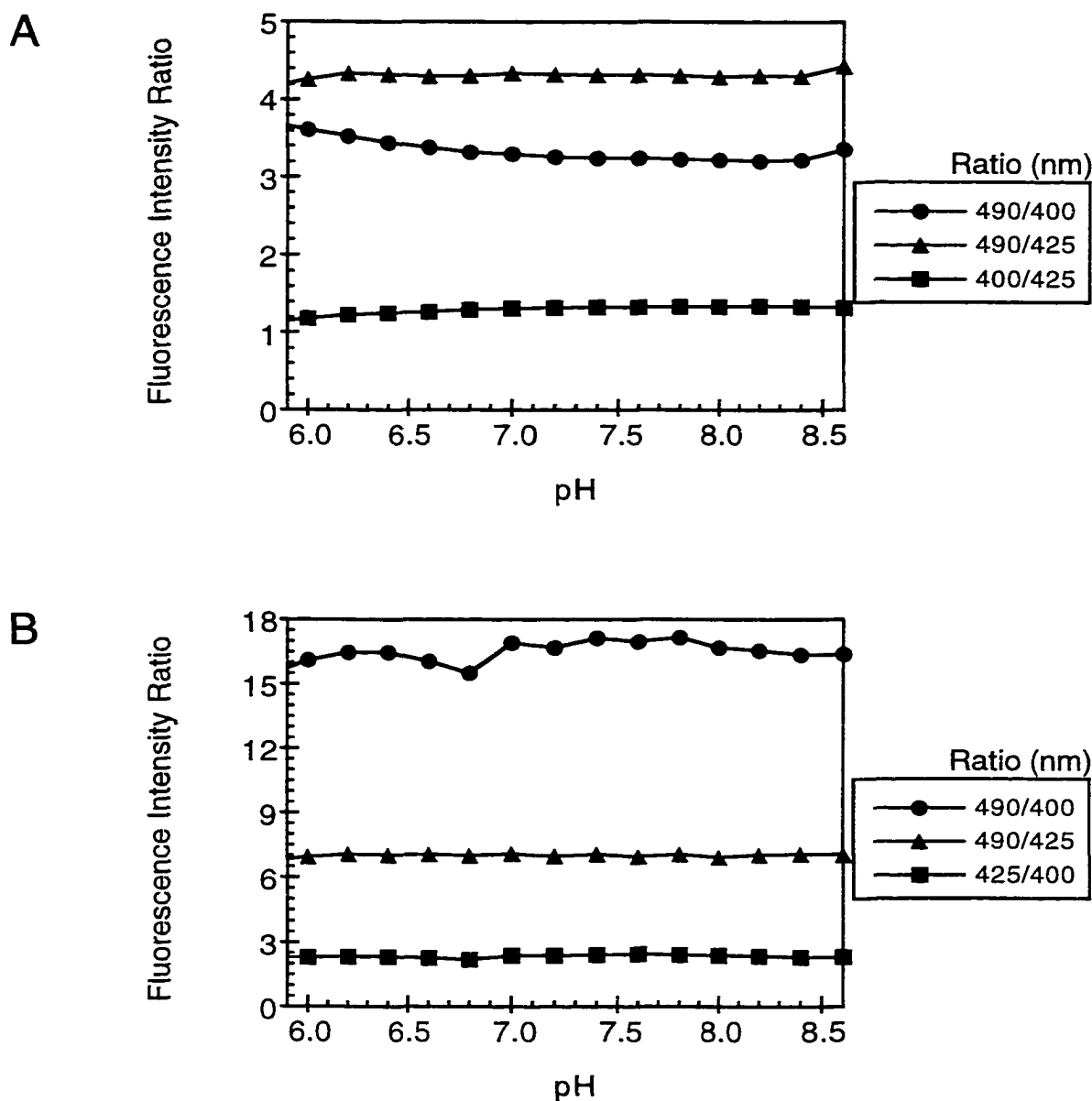


Figure 34. A fluorescence excitation ratio results in the cancellation of pH artifacts. In the oxidized (A) or reduced (B) state, a ratio of fluorescence intensities at various excitation wavelengths of rosGFP2 is independent of pH.

the ratio of intensities is unaffected by pH changes in the range of at least pH 6 to 8.5.

Therefore, a ratio of the excitation wavelengths cancels out variations due to pH fluctuations and allows for redox status determination in the absence of pH artifacts.

Since redox reactions involving the liberation of H⁺ ions are intrinsically based on pH (see Appendix) and consequently the pH of the cellular compartment of study must be determined, the ability to separate out the pH and redox sensing capabilities of rosGFP2 was investigated. Excitation of band A was found to result in pH-dependent dual-emission (Figure 35). In other words, at low pH, blue emission prevails and at high pH, green emission dominates, with pK_as of 5.6 (reduced) to 6.0 (oxidized) dependent upon the redox state of rosGFP2. This phenomenon has been seen in other GFP variants (see Chapter III), where it was shown to be a useful means of monitoring pH changes *in vivo*. By utilizing a ratio of emission wavelengths, pH variations due to the redox state of the probe are minimized (Figure 36). Therefore, it is possible to experimentally separate out the pH and redox contributions to the fluorescent signal, and thus simultaneous monitoring of redox and pH should be possible with the same probe.

Structural Basis for Dual-Wavelength Excitation

The crystal structure of rosGFP2 was solved in order to better understand how

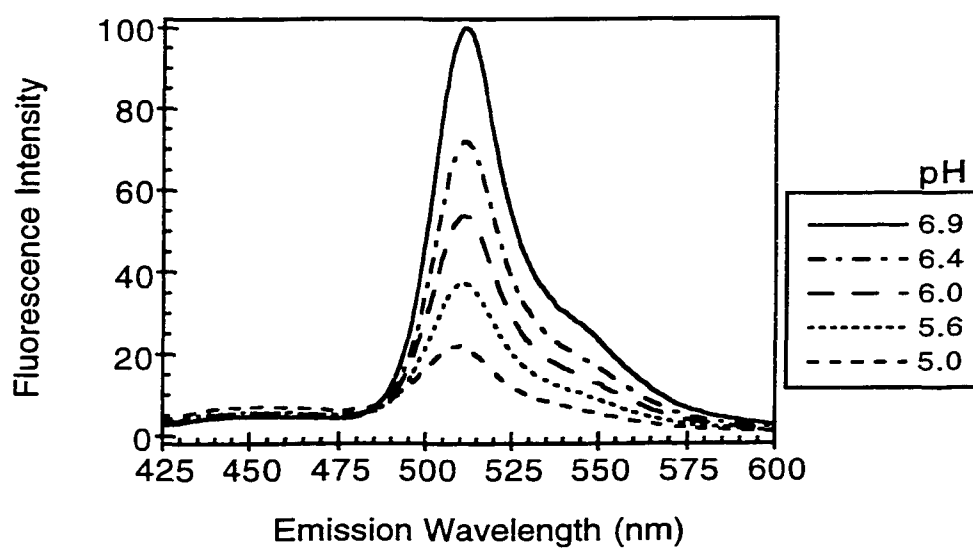


Figure 35. Dual-emission characteristics of rosGFP2. Excitation at 400 nm results in emission peaks centered near 450 and 510 nm, which have an opposite response to pH changes.

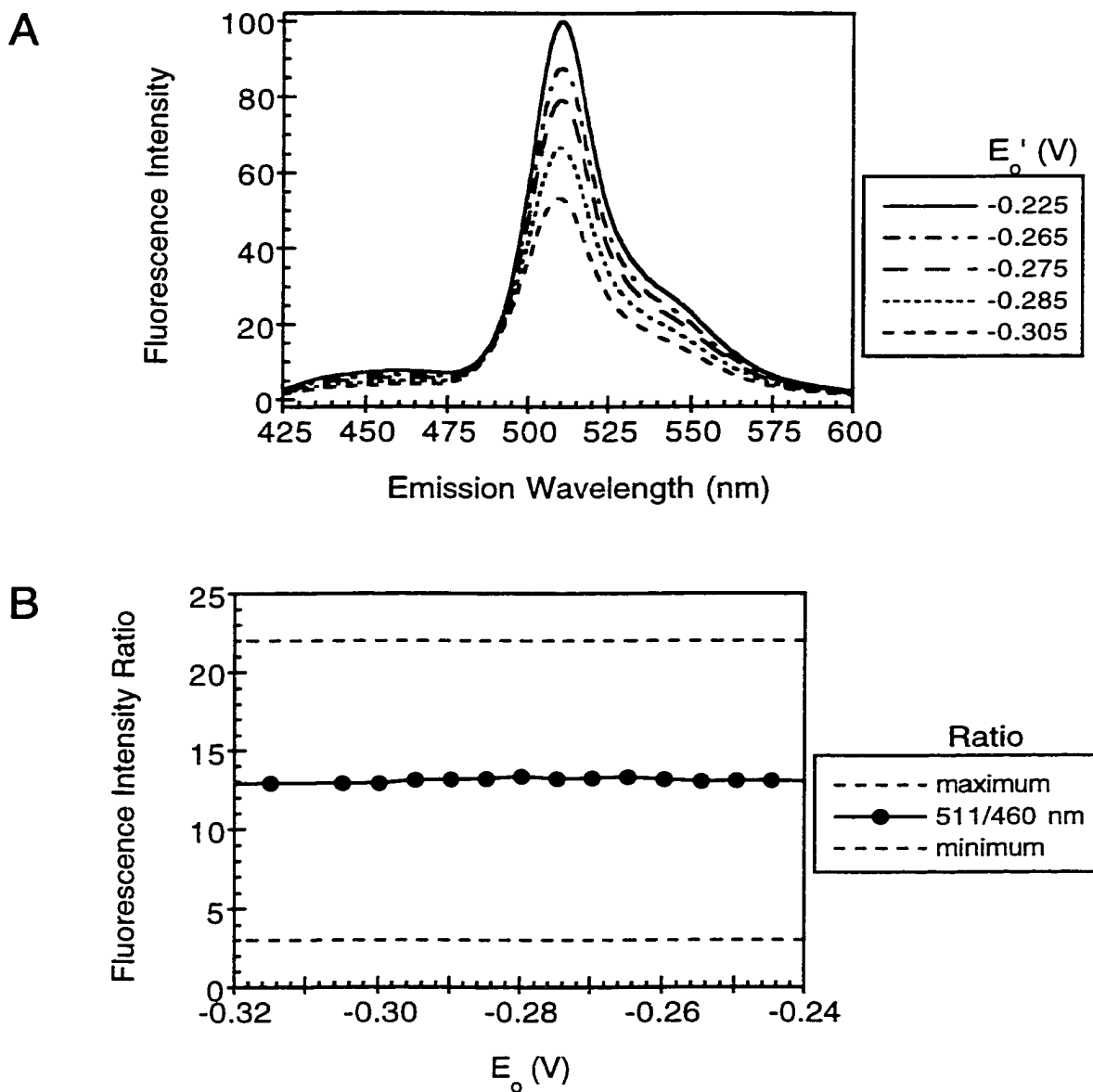


Figure 36. A fluorescence emission ratio results in the cancellation of redox potential changes on pH determination. The fluorescence emission spectra (A) of rosGFP2 were collected at various redox potentials (ratios of DTT and DTT_{ox}) and at a constant pH of 6.0. Plotting the ratio of the two emission peaks results in a constant ratio over a large range of redox states (B). The dashed lines in B represent the maximum and minimum ratios to illustrate the possible dynamic range of rosGFP2 as a function of pH.

disulfide bond formation leads to changes in fluorescence and dual-wavelength excitation. Crystals belonging to the space group P2₁2₁2 were grown of both the oxidized and reduced forms of rosGFP2 and the crystal structures were solved by molecular replacement to 1.9 Å and 2.0 Å resolution, respectively. The protein crystallized as a dimer (Figure 37), with three molecules in the asymmetric unit. One molecule is related to its dimer partner by a crystallographic two-fold axis of symmetry, while the other two molecules in the asymmetric unit were related by a non-crystallographic two-fold axis of symmetry. Since the resolution limit of the data collected was fairly high, refinement was performed without imposing non-crystallographic symmetry restraints, and therefore the three molecules in the asymmetric unit were independently refined. Analysis of the different molecules in the asymmetric unit after refinement revealed only very subtle differences, all of which were within experimental error (approximately 0.2 Å) for the atomic positions at this resolution. Interestingly, the surface residues of one of the molecules comprising the non-crystallographic symmetry dimer, adjacent to a solvent channel, were poorly ordered. This disorder is most certainly reflected in many of the refinement statistics presented in Table 6.

The dimer interface is essentially the same as seen for wild-type GFP and the yellow variant of GFP (Yang et al. 1996; Wachter et al. 1998). One molecule of the

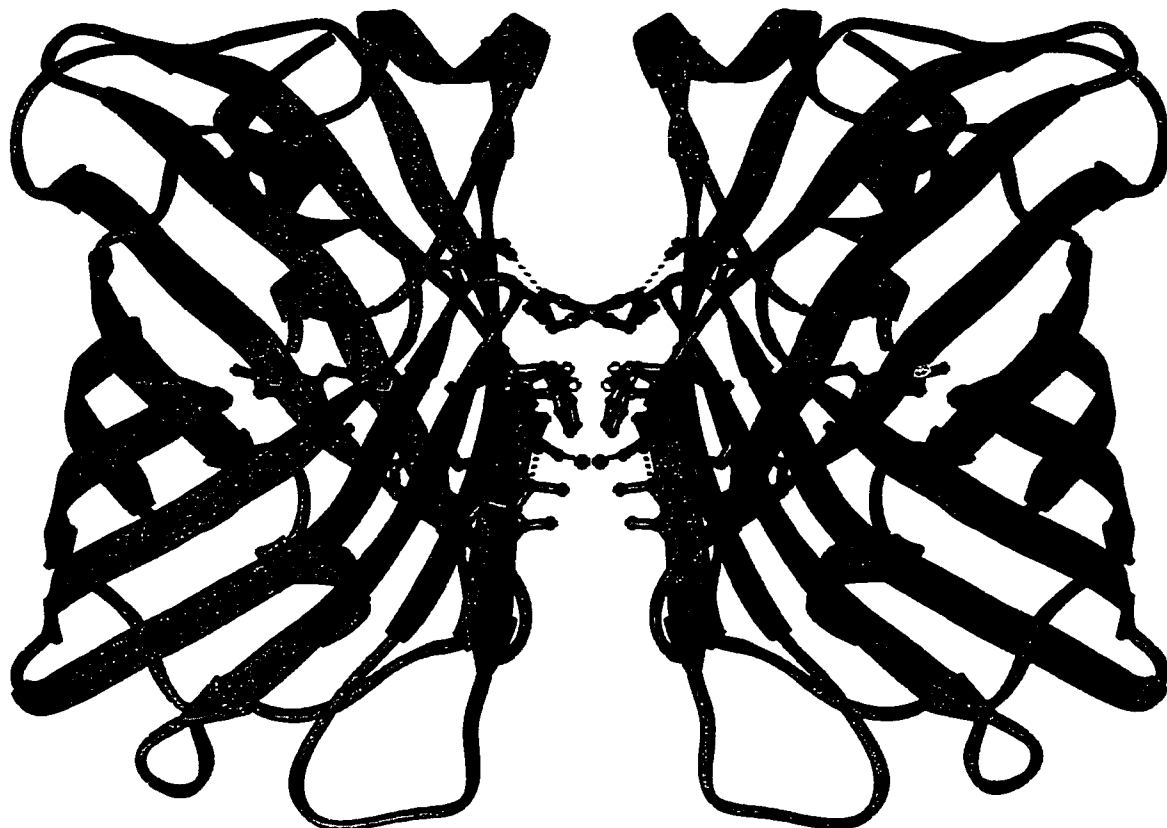


Figure 37. Ribbon diagram of rosGFP2 dimer. A view orthogonal to the two-fold axis of symmetry with residues comprising the dimer interface highlighted. Shown are hydrophobic side chains (cyan bonds), hydrophilic side chains (blue bonds) and water molecules (blue spheres), and the interaction of Tyr 39 with Asn 149 (red bonds), which comprise the dimer interface. Potential hydrogen bonds are shown as dashed lines (blue or red). The position of the introduced cysteines (black) and the disulfide cross-link (black dashed line) are also shown. Furthermore, the chromophore (green bonds) and a ribbon diagram (green) of secondary structure elements are depicted.

Table 6. Data Collection and Refinement Statistics for
Oxidized and Reduced rosGFP2.

<i>Data Collection</i>	Oxidized	Reduced
Crystal		
Total observations	203,865	194,884
Unique reflections	56,854	38,346
Cell dimensions (a, b, c; Å)	186.84, 67.61, 56.08	185.63, 67.86, 56.38
Resolution (Å)	29.7-1.90	28.7-2.00
Highest resolution shell (Å)	1.95-1.90	2.10-2.00
Completeness ¹ (%)	99.8 (100)	78.2 (74.3)
Multiplicity ¹	3.6 (3.6)	5.1 (5.5)
Average I/σ ¹	7.2 (2.3)	8.7 (2.2)
R _{merge} ^{1,2}	0.058 (0.247)	0.053 (0.304)
<i>Refinement</i>		
Spacegroup	P2 ₁ 2 ₁ 2	P2 ₁ 2 ₁ 2
Number of molecules ³	3	3
Number of protein atoms ³	5,220	5,216
Number of solvent atoms ³	174	132
R _{factor} ⁴	0.229	0.223
Average B-factors (Å ²)	46.6	49.7
Protein atoms	46.7	49.7
Solvent	44.2	47.4
rms deviations		
Bond lengths (Å)	0.020	0.014
Bond angles (°)	3.111	2.436
B-factor correlations (Å ²)	7.019	5.779

¹Values in parentheses indicate statistics for the highest resolution shell.

²R_{merge} = Σ|I - <I>| / Σ<I>, where I is the observed intensity, and <I> is the average of intensity obtained from multiple observations of symmetry related reflections.

³Per asymmetric unit.

⁴R_{factor} = Σ||F_o - F_c|| / Σ|F_o|, where F_o and F_c are the observed and calculated structure factors, respectively.

dimer is tilted approximately 70 degrees with respect to the other molecule based on an imaginary axis drawn from one end of the GFP barrel structure through the center and out the other end. The dimer interface is comprised of a small hydrophobic patch consisting of alanine 206, leucine 221 and phenylalanine 223, a hydrogen bond interaction between tyrosine 39 and asparagine 149, as well as a number of hydrophilic contacts involving several bound water molecules (Figure 38). At present it is not known whether the dimer is solution relevant or simply an artifact created by the crystallization conditions (Palm et al. 1997). At any rate, knowledge of the dimer interface residues permits future mutational studies aimed at disrupting dimers without affecting protein stability and folding.

As designed, the introduced cysteines are positioned facing the exterior of the protein and are in an appropriate arrangement to form a disulfide bond under oxidizing conditions. They reside along the edge of the dimer interface and adjacent to bulk solvent. The individual disulfides are separated by 14 Å from the cysteines on the closest adjacent molecule, and thus do not form intermolecular disulfides during crystallization. The disulfide bond present in the oxidized structure has close to ideal geometry (Figure 39) with an average C_{α} - C_{α} distance of 4.0 Å, C_{β} - C_{β} distance of 4.2 Å, S-S distance of 2.0 Å, C_{α} - C_{β} -S angle of 112°, and C_{β} -S-S angle of 106°. These parameters closely

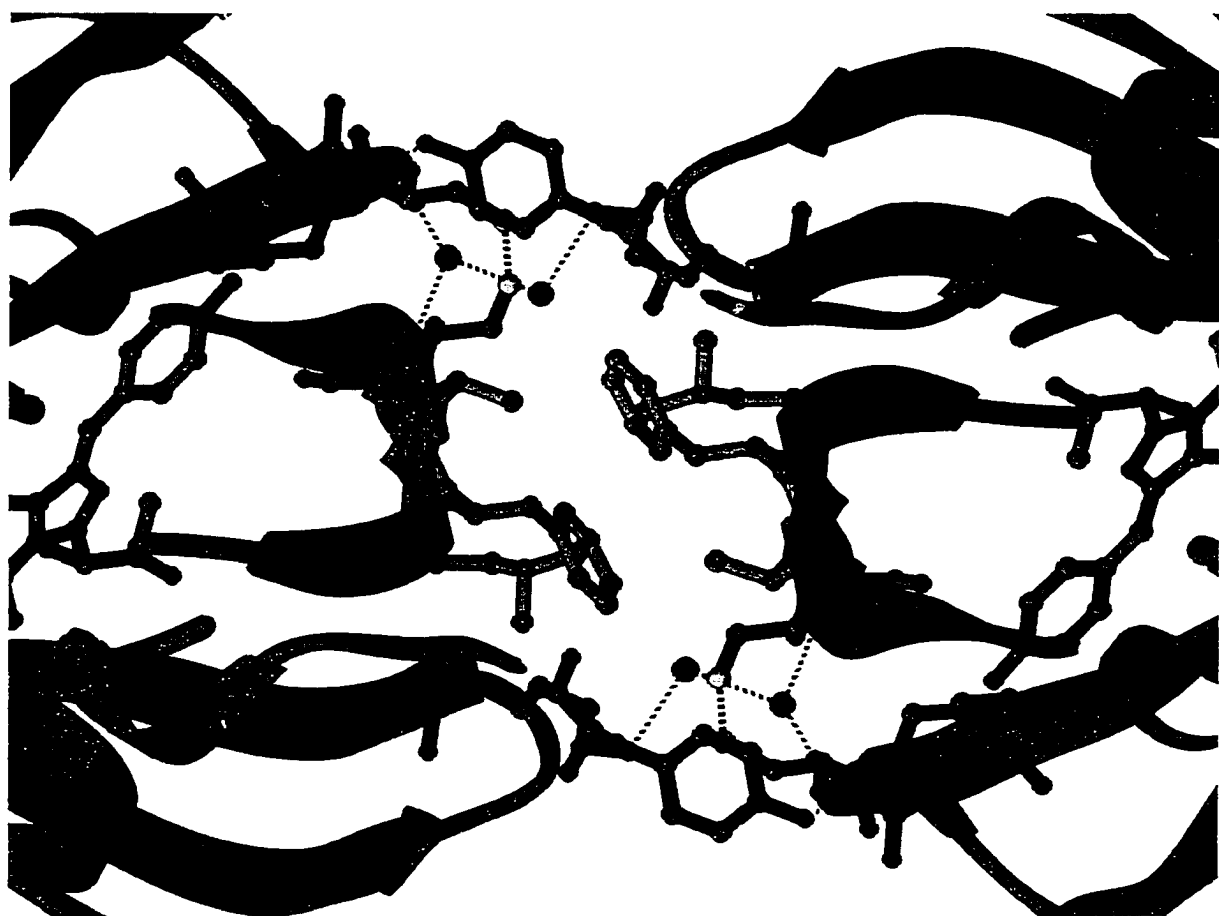


Figure 38. Dimer interface of rosGFP2. A view down the two-fold axis of symmetry highlighting the dimer interface residues. Shown are hydrophobic side chains (cyan bonds), hydrophilic side chains (blue bonds) and water molecules (blue spheres), and the interaction of Tyr 39 with Asn 149 (red bonds), which comprise the dimer interface. Potential hydrogen bonds are shown as dashed lines (blue or red). The position of the introduced cysteines (black) and the disulfide cross-link (black dashed line) are also shown. Furthermore, the chromophore (green bonds) and a ribbon diagram (green) of neighboring secondary structure elements are depicted.

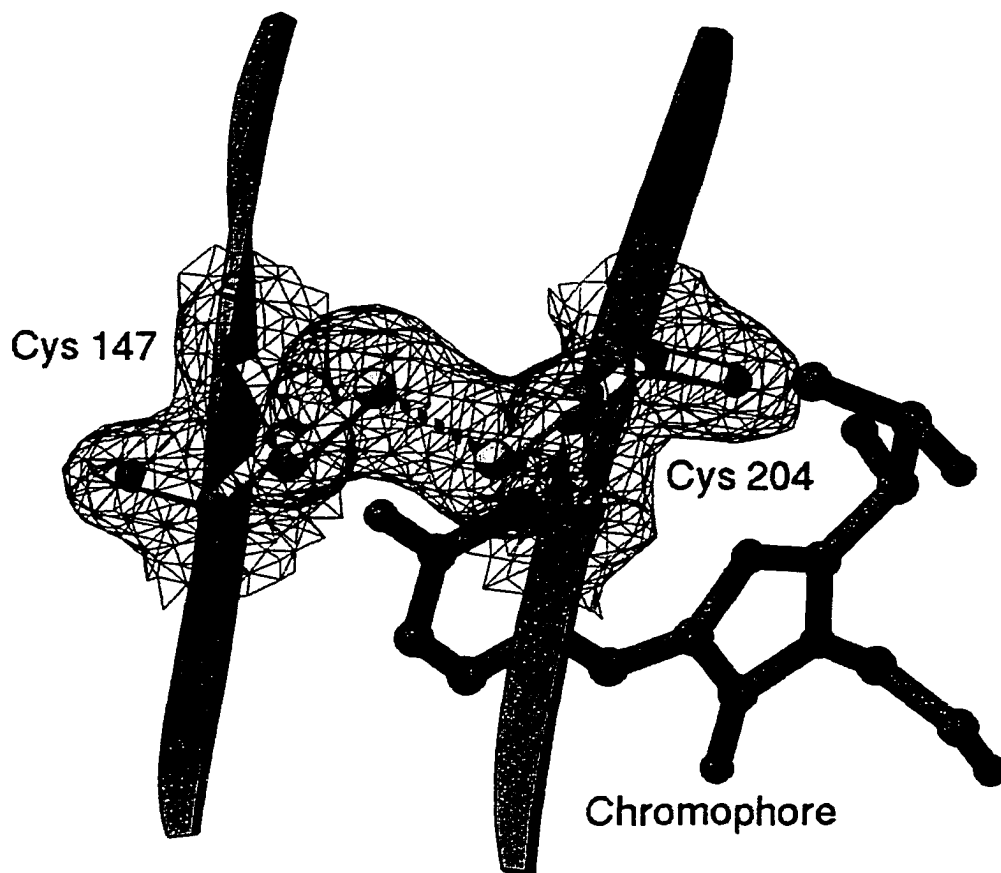


Figure 39. Electron density surrounding the disulfide bridge in the oxidized structure of rosGFP2. A view from the exterior toward the engineered cysteines (white bonds) residing on β -strands (green ribbons) adjacent to the chromophore (green bonds). The 1.9 Å resolution, $2F_o - F_c$ electron density map surrounding the disulfide bond (dashed line), is contoured to one standard deviation.

resemble those values seen in protein structures containing natural disulfides

(Sowdhamini et al. 1989; Matsumura et al. 1989).

In the absence of a disulfide bond and as with the GFP S65T variant, the longer wavelength (low energy) excitation band due to the anionic form of the chromophore, is favored (Figure 25B and Chapter II Figure 2B). Structurally, this is reflected by the position of the side chain of glutamic acid 222, which in this conformation is unable to interact with serine 205 as part of the proton relay pathway proposed by Brejc et al. (1997). The presence of a disulfide favors the high energy excitation band. In wild-type GFP, where the shorter wavelength band is also favored, glutamic acid 222 forms a hydrogen bonding network to the chromophore phenolic hydroxyl through serine 205 and a bound water molecule (Brejc et al. 1997). In the oxidized rosGFP2 structure, glutamic acid 222 is also observed to be hydrogen bonded to serine 205, which in turn interacts with a bound water molecule adjacent to the chromophore phenolic hydroxyl (Figure 40). As a result, the variable dual-wavelength excitation properties of rosGFP2 can be attributed to the positional rearrangements of glutamic acid 222 upon disulfide bond formation.

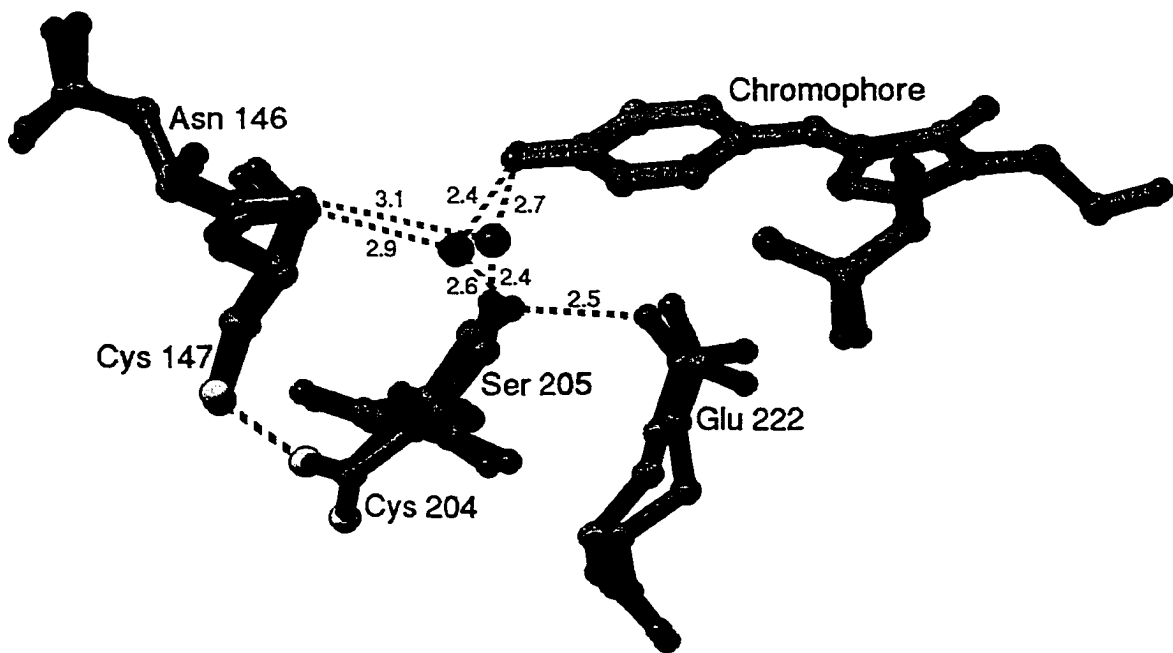


Figure 40. Overlay of the chromophore environment of oxidized and reduced rosGFP2. The oxidized structure (blue bonds) and the reduced structure (red bonds) are shown. Water molecules are depicted as individual spheres. Potential hydrogen bonds are shown as blue or red dashed lines, with approximate lengths in Ångstroms. The black dashed line represents the engineered disulfide bond.



Figure 41. A HeLa cell expressing rosGFP1 localized to the mitochondria.

In Vivo Redox Status

To determine if redox-sensitive GFPs work as indicators of redox status within mammalian cells, rosGFP1 was expressed in the mitochondria of cultured HeLa cells. Figure 41 shows the reticular localization pattern of rosGFP1 expressed in the mitochondrial matrix via fusion at the DNA level to the mitochondrial targeting sequence of the E₁α subunit of pyruvate dehydrogenase. Upon addition of an oxidizing agent (H_2O_2) the fluorescence excitation ratio (400 nm/490 nm) increased, as expected for an oxidation event (Figure 42). Conversely, the addition of a reducing agent (DTT) decreased the elevated ratio to a level below the initial ratio. From this experiment several conclusions can be made. First, rosGFP1 is able to rapidly and reversibly respond to induced redox changes within living cells. As seen in Figure 42, large fluorescence changes accompany the addition of H_2O_2 or DTT. Second, the results demonstrate that initially rosGFP1 is not fully reduced or oxidized within mitochondria. Therefore rosGFP1 is able to equilibrate with the intrinsic redox potential inside mitochondria, presumably by interacting with endogenous oxidizing and reducing agents. Moreover, the redox potential of rosGFP1 is close to that of mitochondria and hence rosGFP1 should make an excellent probe for studying redox changes in mitochondria. Finally, given the initial fluorescence excitation ratio, the percentage of reduced to oxidized

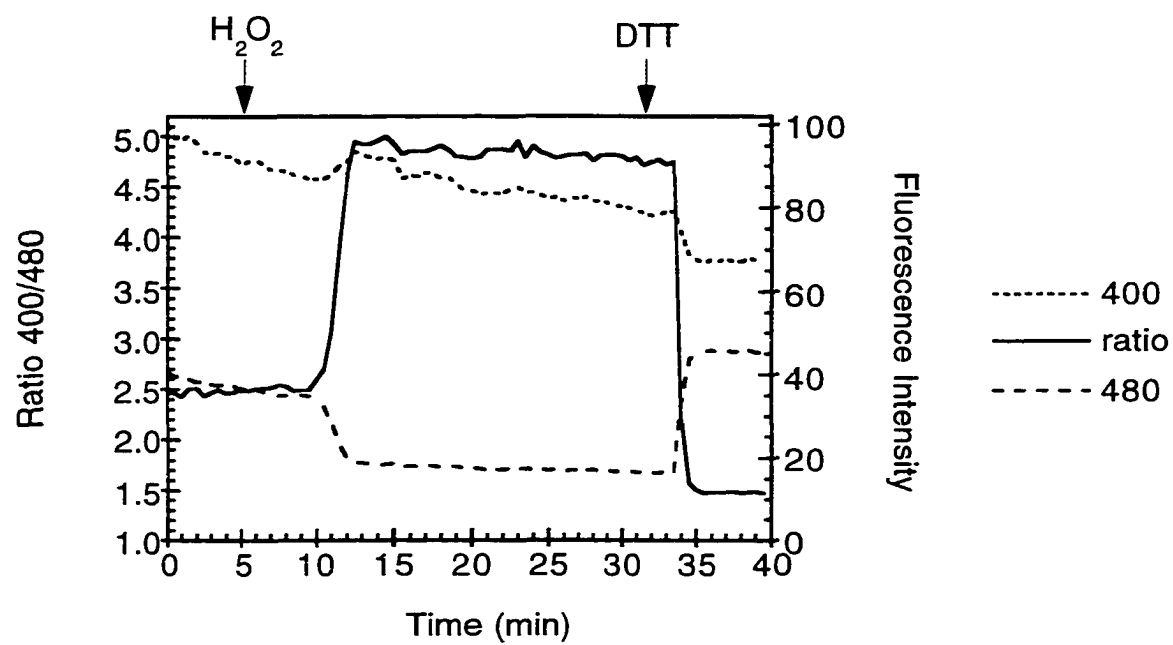


Figure 42. Response of rosGFP1 to H_2O_2 and DTT induced redox potential changes in HeLa cell mitochondria. H_2O_2 and DTT were added at the indicated time points to a final concentration of 1 mM and 30 mM, respectively. The Fluorescence Intensity axis corresponds to the individual wavelengths, whereas the Ratio 400/480 axis corresponds to the ratio of the two wavelength channels.

rosGFP1 could be estimated and thus the *in vivo* redox potential of mitochondria could be calculated.

Since redox potentials involving the liberation of H⁺ ions are intrinsically based on pH (see Appendix), we put to use the GFP S65T/H148D variant (see Chapter II; Wachter et al. 1998) with a pK_a of 7.8 to examine the pH within the mitochondria. The inherent pH sensing abilities of rosGFP2 was not utilized in this instance, due to the high pH nature of mitochondria and the high levels of autofluorescence. The fluorescence excitation ratio of GFP S65T/H148D changed as function of pH inside the mitochondrial matrix. The addition of oligomycin, carbonylcyanide-*p*-trifluoromethoxyphenylhydrazone (FCCP), or hydrochloric acid resulted in an acidification of the mitochondrial matrix (data not shown). On the other hand, addition of NH₄Cl caused the matrix pH to increase. From these types of additions, the resting pH of the mitochondrial matrix of HeLa cells was estimated to be 7.65 ± 0.15 (n = 110 cells from seven experiments). However due to a slow acidification process during the experimental setup and data collection process, this value is likely to be an underestimate of the true mitochondrial matrix pH. Therefore, the pH value of 7.98 ± 0.07 estimated by Llopis et al. for the mitochondrial matrix of HeLa cells was used in subsequent calculations (1998). Based on an average of 23 cells from seven independent

experiments, and accounting for the 60.2 mV per pH unit change in redox potential for a reaction involving two protons (see Appendix), the redox potential in normal resting HeLa cell mitochondria was determined to be -0.368 ± 0.004 V.

To investigate the redox potential of the cytosol, we expressed rosGFP2 in the cytosol of HeLa cells. The starting fluorescence amplitude ratio of 400/480 nm excitation was low as expected for the reducing environment of the cytosol of healthy cells (data not shown). Again, there was a marked increase and decrease in ratio upon addition of H₂O₂ and DTT, respectively. However the ratio only recovered to the starting value, indicating that rosGFP2 was fully reduced in the cytosol. Hence the redox potential of the cytosol was estimated to be more reducing than -0.330 V, assuming a pH of 7.34 (Llopis et al. 1998).

What Factors Influence the Redox State of rosGFPs *In Vivo*?

It is generally thought that the major redox buffer in cells is glutathione and that the ratio of reduced glutathione (GSH) to glutathione disulfide (GSSG) is the crucial parameter for determining redox status (Meister 1995; Deneke 2000). On average, the ratio of GSH to GSSG is greater than 100:1 for whole cell determinations on a wide variety of tissue types and total glutathione levels are believed to be around 1–10 mM

(Kosower and Kosower 1978; Voet and Voet 1995; Meister 1995). To investigate whether glutathione may contribute to the redox state of rosGFPs *in vivo*, fluorescence experiments were conducted *in vitro*. Incubation of reduced rosGFP1 with GSSG resulted in complete oxidation of rosGFP1 in the absence of air oxidation (data not shown). From this experiment it was concluded that rosGFPs expressed *in vivo* can indeed become oxidized by GSSG. However, since rosGFPs have a lower affinity for electrons than does glutathione, then GSH is unable to reduce oxidized rosGFPs. Therefore, given the large number of oxidizing agents present in the mitochondrion, due in part to the respiratory chain, what factors contribute to the very reducing environment of this organelle? Specifically, what factors are responsible for maintaining rosGFP1 in a reduced form?

Several reports concur that the ratio of GSH to GSSG in mitochondria is between 6:1 to 33:1, with total glutathione approximately 1-2 mM (Lê-Quôc and Lê-Quôc 1989; Bindoli et al. 1997; Lenton et al. 1999). Substituting these values into the Nernst equation (assuming a mitochondrial pH of 7.98, 37°C, and a standard redox potential of -0.205 V (Szajewski and Whitesides 1980) for the GSH/GSSG couple) results in a mitochondrial redox potential in the range of -0.210 to -0.230 V. Since the present work suggests that the redox potential of mitochondria is more reducing (-0.368 ± 0.004 V)

than these estimates, glutathione alone may not be a major factor accounting for the observed potential. Therefore, other potential redox active agents were investigated.

The NAD⁺/NADH (nicotinamide adenine dinucleotide) couple was considered, because it is present at high concentrations in mitochondria and has a very reducing redox potential. The ratio of NAD⁺ to NADH in the presence or absence of glucose has been variously estimated to be between 1:6 to 10:1 in mitochondria (Lê-Quôc and Lê-Quôc 1989; Ramirez et al. 1996; Robinson 1996). These ratios translate into redox potentials in the range of -0.328 to -0.382 V at pH 7.98 and 37°C using -0.320 V as the standard potential of the NAD⁺/NADH couple at pH 7. As a result, this redox couple appears to be a good candidate for maintaining the very reducing environment of the mitochondrion. However, redox reactions involving nicotinamides carry out concerted two-electron transfers, whereas thiols undergo two sequential one-electron transfers. *In vitro*, NADH is unable to directly reduce rosGFP1 (data not shown).

However, there exists a family of pyridine nucleotide-disulfide oxidoreductases comprising lipoamide dehydrogenases (LDH), glutathione reductases, thioredoxin reductases, trypanothione reductase, and alkylhydroperoxide reductase. These enzymes all perform homologous reactions ultimately involving the transfer of NADH or NADPH (nicotinamide adenine dinucleotide phosphate) reducing equivalents to thiols (Carothers

et al. 1989). In general terms, the reducing equivalents are transferred from NADH or NADPH through a concerted two-electron transfer reaction to a bound FAD (flavin adenine dinucleotide) cofactor. The FAD then reduces a nearby disulfide bridge through two sequential one-electron transfer reactions. In some cases, the electrons are transferred by disulfide exchange to other nearby disulfides (Ellis and Poole 1997; Calzi and Poole 1997). Finally, the reduced pair of thiols participate in the reduction of a substrate such as lipoamide, glutathione, thioredoxin, or various peroxides. The essential key to these electron transfer reactions resides in the chemistry of the FAD cofactor, which is able to undergo either two sequential one-electron transfers or a simultaneous two-electron transfer.

To determine if rosGFPs may be in an enzyme-coupled equilibrium with redox active agents other than glutathione, we constructed an *in vitro* system of linked enzymatic reactions analogous to a portion of the pyruvate dehydrogenase complex. The system consisted of LDH, oxidized lipoamide, NADH, and oxidized rosGFP1. The rationale behind this experimental setup was to monitor the reduction of rosGFP1 by NADH, coupled by LDH and free lipoamide. Figure 43 shows that with all four components of the system present, nearly 75% of rosGFP1 is reduced, however removal of any one of the components; LDH, lipoamide, or NADH results in less than 5%

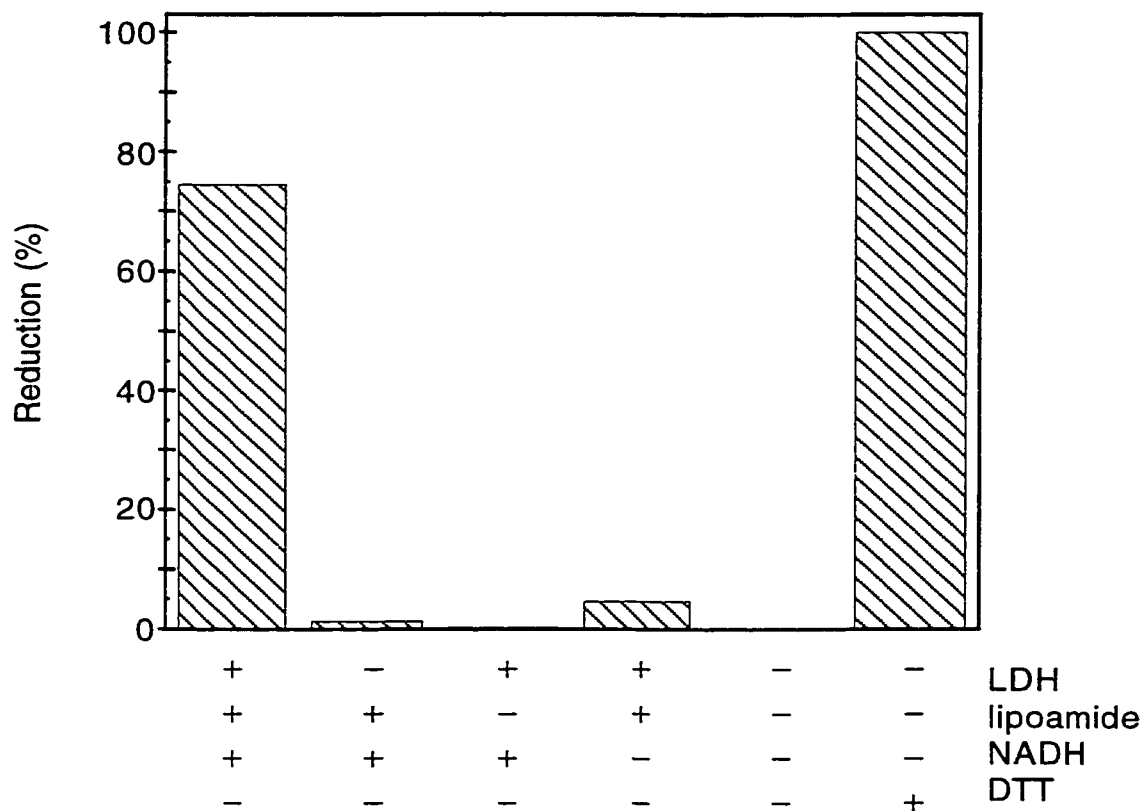


Figure 43. NADH-dependent reduction of rosGFP1 via lipoamide dehydrogenase. Each bar represents the percent reduction of oxidized rosGFP1 by 1-2 μ L LDH, 1 mM oxidized lipoamide, 1 mM NADH, and/or 1 mM DTT. Samples were equilibrated at 22°C for one hour after which the fluorescence excitation was scanned from 325 to 525 nm. Percent reduction values were determined by the fluorescence at 490 nm with 100% corresponding to reduction by DTT.

reduction of rosGFP1. Incomplete reduction was expected since the redox potential of rosGFP1 (-0.288 V) and the lipoic acid/dihydrolipoic acid couple (-0.29 V; Szajewski and Whitesides 1980) are very similar. Air oxidized and DTT reduced rosGFP1 were used as standards for obtaining the zero and 100 percent values. The results of this experiment indicate that it is possible for NADH reducing equivalents, through a variety of possible enzymes such as pyruvate dehydrogenase, to be ultimately imposed on rosGFPs *in vivo*.

Discussion

Many fundamental biological processes rely upon a properly maintained intracellular redox environment (Cuozzo and Kaiser 1999; Debarbiex and Beckwith 1999; Hall 1999; Cai and Jones 1999). Moreover, reactive oxygen species like O_2^- , HO^- , or H_2O_2 , arise in cells by a variety of processes including light, radiation, or the respiratory chain. These radical species present major threats to organisms by damaging DNA, membranes, or other cellular components. This would imply that researchers have numerous well established techniques for monitoring redox potentials *in vivo*. However, this is not the case. Current methods are invasive, require large sample sizes, are labor intensive, and do not allow for real-time determinations on living cells. In this work we

have described a new class of GFP variants that display ratiometric excitation properties as a function of redox potential. Such GFP biosensors allow for real-time redox potential determinations on small groups of cells, individual cells, or even within certain cellular organelles. They are non-invasive and easy to use. Consequently, redox-sensitive GFPs may become the standard tool for measurement of redox status within living cells. Finally, their ratiometric behavior has the advantage of reducing or eliminating distortions of data caused by photobleaching, indicator concentration, variable cell thickness, illumination stability, excitation pathlength, and non-uniform indicator distribution within cells or between groups of cells (Grynkiewicz et al. 1985; Whitaker et al. 1991). Moreover, a ratio of excitation wavelengths greatly minimizes the contribution of pH artifacts to the fluorescent signal over a pH range from 6 to 8.5. Similarly, a ratio of emission wavelengths can result in pH monitoring without artifacts introduced by the redox state of the biosensor.

The “pseudo-wild-type” rosGFPs with more closely matched excitation peak amplitudes may aid in fluorescence microscopy experiments by allowing the same camera/detector settings to capture both images that constitute the ratio. Furthermore, the second generation rosGFPs have a larger 400 nm fluorescence amplitude which is desirable for detection of the rosGFP probe over background levels of cellular

autofluorescence. In the future, mutational screening of rosGFP2 may lead to rosGFPs with altered redox potentials for future studies in very oxidizing or reducing compartments or for studies of certain cell types or cellular processes which may have very different redox potentials than the currently available rosGFPs. Moreover, if the crystallographic dimer is discovered to be problematic in solution, albeit unlikely, straightforward site specific mutagenesis can be performed to reduce rosGFPs to monomers in solution.

Accuracy of Standard Redox Potentials

The main problem in the determination of standard redox potentials is given by the fact that E_o values cannot be measured directly, but rather are calculated from the known E_o of another redox couple equilibrated with the redox couple of unknown E_o . The standard redox potential can thus vary over a large range depending on experimental conditions and the choice of redox couple. In this study, the value of -0.323 V for the dithiothreitol couple was chosen, because it has been very accurately determined in 0.05-0.02 M phosphate buffer at pH 7.0 and 30.0° +/- 0.5°C using the lipoamide-lipoamide dehydrogenase couple (Szajewski and Whitesides 1980). Because redox potentials are pH and temperature dependent, all redox equilibria were measured at the same pH (7.0)

and temperature (30°C) as was used to evaluate the standard redox potential of the dithiothreitol couple. Another reason to use the value of -0.323 V for the dithiothreitol couple is that the standard potentials of other commonly used thiol reagents (including the GSH-GSSG couple) have been determined under identical conditions (Szajewski and Whitesides 1980). In the future, this will allow for the direct comparison of redox potentials determined by use of rosGFPs to those determined by other methods, provided the experimental conditions are reproduced.

For the DTT_{red}-DTT_{ox} couple, the standard potential throughout literature is well accepted to be about -0.330 V at near biochemist's standard state of pH 7 and 25°C. However, such agreement is not always the norm. In the case of the glutathione redox couple, very different values for the standard redox potential have been reported. The published values deviate from a somewhat oxidizing value of -0.205 V to a more reducing value of -0.250 V (Szajewski and Whitesides 1980; Rost and Rapoport 1964; Torchinskii 1981). The 45 mV difference in literature values is a problem when trying to compare redox potentials of rosGFPs to previously determined estimates of the redox potential inside cells.

Even with the large discrepancy in the standard potential of GSH-GSSG, our results suggest that *in vivo* redox potentials may be more reducing than previous

estimates. Hwang et.al., using the tetrapeptide N-Acetyl-Asn-Tyr-Thr-Cys-NH₂ to measure the ratio of thiol to disulfide in the cytosol and secretory pathway of cultured cells, concluded that the cytosol is more reducing than the secretory pathway with an approximate redox potential of -0.221 to -0.236 V versus -0.170 to -0.185 V, respectively (1992). In addition, based on prior determinations of the concentration and ratio of GSH to GSSG in mitochondria, the redox potential of this compartment is calculated to be -0.210 to -0.230 V. However, Keesee et al. recently developed an indicator of redox state in which they transfer glutathione reductase crystals into the cytosol of living cells and then detect a color change in the crystals (1999). Using this method they determined the redox potential of the cytosol of human fibroblasts to be more reducing than -0.270 V at pH 7.4 and 37°C. This result is in agreement with our estimate of the cytosolic redox potential for HeLa cells being more negative than -0.330 V.

Clearly there must be some rationale explanation for the disparity between redox potentials determined for cells. It is unlikely given the magnitude of the disagreement between values that conditions (pH and temperature), different cell types, or known redox potential differences for couples could be the sole contributors to the problem. More likely, a combination of factors involving these inaccuracies in conjunction with errors introduced by the methods used for obtaining redox potentials give rise to the

unacceptably large differences between values of *in vivo* redox potentials. For example, glutathione reductase crystals and rosGFP may be indirectly detecting reducing equivalents from NADH or NADPH, whereas methods that rely only on the ratio of GSH to GSSG are underestimating the true redox potential within cells.

Redox-sensitive GFPs may provide a solution to the widely varying estimates of cellular redox potentials. The ability to characterize rosGFPs *in vitro*, with specific attention paid to the standard redox potential, pH sensitivity, reversibility, kinetics, and oxidant/reductant specificity should be a sizeable advantage in determining if rosGFPs are suitable indicators of redox status. Further *in situ* calibration by clamping the redox potential to known values within intact cells and measuring the excitation ratio will also help to demonstrate the usefulness of rosGFPs. Finally, with the *in vitro* characteristics and *in situ* calibration resolved, experiments can be conducted to address what the true redox potential of a living cell is and to investigate redox changes in association with biological processes including plasticity of glutamatergic synapses, induction of apoptosis, and growth factor and cytokine induction of transcriptional responses such as via NF-κB (Tsien R.Y. personal communication).

Experimental Procedures

Construction and Expression of Redox Sensitive GFPs

Wild-type GFP contains two cysteine residues at positions 48 and 70. To avoid possible thiol/disulfide interchange reactions with the newly engineered cysteines, cysteine 48 and cysteine 70 were replaced with serine and alanine, respectively. Although the substitution C48S did not alter the properties of GFP (data not shown), C70A appeared to be deleterious to obtaining soluble, fluorescent protein. Since position 70 is located within the interior of GFP and is in close proximity to the chromophore, it was deemed a mutation-sensitive position and was therefore left as a cysteine. The C48S mutation was introduced into a histidine-tagged version of the S65T variant of GFP in the plasmid pRSET_B. This construct served as the template for introduction of the cysteines at sites one (S147C/Q204C) and site two (N149C/S202C). All mutations were introduced via the QuikChange™ Site-Directed Mutagenesis Kit (Stratagene, La Jolla, CA), following the manufacturer's protocol. Mutations were verified by DNA sequencing of the entire GFP coding sequence.

Mutant protein was recombinantly expressed in *Escherichia coli*, strain JM109(DE3). Transformed bacteria were grown in four liters of S-LBH media at 37°C,

stirred at 450 rpm, with 5 liters per minute air flow, and in the presence of 0.27 mM ampicillin. After the culture reached a density of approximately OD₅₉₅ equal to 0.8, then protein expression was induced by addition of isopropyl-β-D thiogalactopyranoside (IPTG) to a final concentration of 1 mM. At the same time the temperature of the culture was reduced to 16°C and allowed to grow for an addition 16 hours. Cells were then harvested by centrifugation at 4°C in a Beckman KA-9.1000 rotor at 11,800 × g for 10 minutes. The bacterial cell pellet was resuspended in 100 mL of 50 mM HEPES (pH 7.9), 300 mM NaCl, 10% glycerol, and 0.1 mM phenylmethylsulfonyl fluoride (PMSF). The resuspended cells were then sonicated for a total of five minutes. The cell lysate was clarified twice by centrifugation at 35,000 × g in a Beckman JA-20 rotor at 4°C for 20 minutes. Next, the supernatant was loaded onto a pre-equilibrated nickel-nitrilotriacetic acid (Ni-NTA) metal-affinity column (Qiagen, Hilden, Germany). The equilibration and subsequent washing of the column was performed with washing buffer (50 mM HEPES (pH 7.9) and 300 mM NaCl). Proteins were eluted from the column by a step gradient of washing buffer plus 20 mM imidazole to remove mostly unwanted proteins and then with washing buffer plus 100 mM imidazole to elute the mutant GFP. To remove the amino-terminal histidine tag and as a further purification step the eluted protein was incubated with 1/50 w/w γ-chymotrypsin at 22°C for 22 hours. The protein was finally buffer

exchanged on a Sephadex® G-25 column. Characteristic yields of mutant GFP protein were in the range of 15 to 100 milligrams and with a purity greater than 95%.

SDS-PAGE

Samples of rosGFP2 and GFP S65T (control) were treated with 1 mM DTT or 1 μ M CuCl₂ and incubated at room temperature for 3-4 hours at which time 2 mM N-ethyl maleimide was added to prevent disulfide exchange reactions. Molecular weights were determined by comparison to BenchMark™ protein ladder (Invitrogen, Carlsbad, CA). The gel was visualized with coomassie blue stain.

Spectroscopy and pH Titrations

Absorbance measurements were performed on a Shimadzu 2101 spectrophotometer. The molar extinction coefficient of GFP S65T ($\epsilon_{280\text{ nm}} = 19,890 \text{ M}^{-1}$ cm⁻¹) was calculated from its amino acid sequence as described (Gill and von Hippel 1989), and used to determine protein concentrations of the rosGFPs. pH titrations were performed using approximately 200 μ g mL⁻¹ mutant GFP in 75 mM buffer, 140 mM NaCl and either 1 μ M CuCl₂ or 5 mM DTT. According to the desired pH, an appropriate buffer was chosen from MES, HEPES, or CHES and the final pH was adjusted by HCl or

NaOH addition. The absorbance was then scanned between 250 and 550 nm and the optical density of the long-wave band B was plotted as a function of pH and fitted to a titration curve to obtain pK_a values. Fluorescence excitation spectra at various pHs were attained on a Hitachi F4500 fluorescence spectrophotometer or a Perkin Elmer LS 55 luminescence spectrometer at protein concentrations of approximately 100 µg mL⁻¹ in the same buffers used for absorbance measurements. Apparent chromophore pK_a values were determined by plotting the emission intensity when excited at band B as a function of pH and fitting the data to a titration curve (Kaleidagraph). In all cases, the pK_a values determined by absorbance and fluorescence differed by no more than +/- 0.05 of a pH unit. All plots and curve fits were made with Kaleidagraph (Abelbeck Software).

Redox Titrations

Fluorescence measurements were performed at 30°C using a thermostated cuvette holder. Samples consisted of 1 µM GFP in 75 mM HEPES (pH 7.0), 140 mM NaCl, 1 mM EDTA, and 1 mM total DTT (mixture of oxidized and reduced forms). To exclude air oxidation, the solutions were degassed and subsequently flushed with nitrogen. In general equilibration was reached within 1 hour at pH 7.0. Equilibration of rosGFPs was ensured by incubating the samples at 30°C for 4 hours. The reaction appeared to be at

equilibrium, since the ratio of oxidized and reduced protein, as determined by fluorescence, did not change between 4 and 16 hour incubation times.

Crystallization

rosGFP2, C48S/F64L/S65T/Q80R/S147C/Q204C, was concentrated to approximately 20 mg mL⁻¹ in 20 mM HEPES (pH 7.9) and 0.2 μm-filtered. Flat plate-like crystals grew at room temperature in 1-2 days by hanging drop vapor diffusion against 0.1 M Tris (pH 8.5), 0.07-0.1 M LiSO₄, 17-22% polyethylene glycol 4000, and 0.5 μM CuCl₂ or 5 mM DTT for the oxidized and reduced crystals, respectively. Drops contained 4 μL protein solution and 4 μL well solution. For low-temperature diffraction data collection, crystals were exchanged into a solution of 0.1 M Tris (pH 8.5), 0.07-0.1 M LiSO₄, 20% polyethylene glycol 4000, 20% ethylene glycol, and either 0.5 μM CuCl₂, or 5 mM DTT.

Data Collection and Refinement

X-ray diffraction data were collected from a single frozen crystal for each redox state at beamline 7-1 at the Stanford Synchrotron Radiation Laboratory. Data sets were indexed and reduced with Mosflm (Leslie 1996) and intensities were scaled with SCALA

(CCP4 1994). Molecular replacement solutions were found using the computer program EPMR, using the GFP S65T coordinate file (PDB code: 1EMA) as the search model. Positional refinement was carried out using the data to 3.5 Å, 3.0 Å, 2.6 Å, 2.3 Å, 2.1 Å and finally to the limit of resolution, using the program TNT (Tronrud et al. 1987). After each increase in resolution the electron density maps ($2F_o - F_c$ and $F_o - F_c$) were analyzed using the program O (Jones et al. 1991). B-factor refinement was performed using the default TNT B-factor correlation library. The B-factor correlation values for the chromophore atoms were derived from histidine and phenylalanine residues. Solvent molecules were added only if consistent with $F_o - F_c$ features and when in proximity of hydrogen bond partners. The atomic coordinates and structure factors have been deposited in the Research Collaboratory for Structural Bioinformatics Protein Data Bank (<http://www.rcsb.org/>)

Mammalian Cell Expression and Fluorescence Microscopy

The mutations C48S/T65S/S147C/Q204C were introduced into the mammalian expression plasmid pEGFP-N1 (Clontech, Palo Alto, CA). This plasmid has the “folding mutation” F64L, which was found not to alter the spectral or redox properties of the rosGFPs (data not shown). HeLa cells transiently transfected with this plasmid using

Fugene (Boehringer-Mannheim, Germany) were imaged one day post-transfection on a motorized Zeiss Axioscope 2 microscope. The temperature of the cells was maintained at 37°C using an open perfusion micro-incubator (Harvard Apparatus Inc., Holliston, MA). Dual-wavelength excitation ratio imaging required 400(10) and D480/30x excitation filters, a 505DCXR dichroic mirror, and a D535/40m emission filter (Edmund Scientific Company, Omega Optical and Chroma Technologies, Battleboro, VT) alternated by a fast filter changer. Images were collected with a PentaMax cooled CCD camera (Princeton Instruments). Data were collected and processed using the program Openlab (Improvision, Lexington, MA).

CHAPTER V

CONCLUSION

Green Fluorescent Protein Homologues

Although fluorescent proteins had been discovered in the related coelenterates *Obelia* and *Renilla*, a hydroid and a sea pansy, respectively (Morin and Hastings 1971), the *Aequorea victoria* green fluorescent protein (avGFP) was the only fluorescent protein (FP) to gain popularity. The reason for this popularity was due solely to the cloning of avGFP's DNA sequence and the finding that avGFP was fluorescent in the absence of any other FP DNA sequence. The DNA sequence eliminated the need to extract avGFP from the jellyfish, since molecular biology techniques allowed for the protein to be expressed and purified from bacteria. Not only did the cloning provide researchers with an efficient means for producing the protein, but this also permitted the manipulation of the avGFP through mutagenesis of the DNA sequence. Alteration of avGFP led to blue, cyan, improved green, and yellow emission variants as well as redox potential, H⁺, Ca²⁺, and halide ion indicators (for review, Tsien 1998; Remington 2000). With such a large

number of functional proteins having been created from just one FP coding sequence, it is no wonder that “Rosy Dawn for Fluorescent Proteins” was the title of an October 1999 article appearing in the same journal as a report describing the cloning of six new FPs (Tsien 1999). The article’s title in some sense suggests that all the designed FPs based on avGFP may have been just the beginning.

The six new FPs were unique from *Aequorea*, *Obelia*, and *Renilla* FPs in that they were cloned from non-bioluminescent *Anthozoa* species of reef coral (Matz et al. 1999). The other exciting difference was that two of the proteins zFP538 (species initial, FP, and peak emission wavelength in nanometers) and drFP583 emitted yellowish/orange and red fluorescence, respectively. Longer wavelength FPs were desired because they are easily distinguished from background levels of cellular autofluorescence, and their lower energy excitation wavelengths are less harsh on the biological system of study. For the most part, longer wavelength variants of avGFP were elusive, with the longest wavelength variant emitting at 527 nm (Ormö et al. 1996). It was interesting to learn from the recent crystal structure of drFP583 that the structural basis for the red fluorescence is due to the formation of a *cis* peptide bond that leads to an extra oxidation reaction (Wall et al. 2000; Yarbrough et al. 2001). This oxidation event, not seen in any avGFP variant, further extends the conjugation of the chromophore and results in red fluorescence emission.

Since the initial reports of the cloning of other FPs, a number of concerns have arisen. Both the crystal structure and analytical ultracentrifugation of drFP583 and zFP538 have unveiled that these proteins exist as tetramers (Baird et al. 2000; Heikal et al. 2000; Wall et al. 2000; Yarbrough et al. 2001; Wachter, R.M. personal communication). Likewise, the *Renilla* FP has been shown to exist as an obligate dimer (Ward and Cormier 1979). Hence, it appears that of the known FPs, only the avGFP may exist as a monomer. The requirement for multimeric states makes fusion with other proteins of interest problematic by forming non-physiological pseudo-oligomers or altogether impossible due to steric hindrance. Another drawback of the longer wavelength FPs, is the slow maturation time of the chromophore. The extra oxidation step can take up to 18 hours and usually does not go to completion (Terskikh et al. 2000; Yarbrough et al. 2001). This greatly reduces or eliminates the possibility of using these FPs to follow host protein localization and fate. However, modification especially through designed mutagenesis, may be able to overcome some or all of these drawbacks.

Structure-Based Design

Even though many of the original avGFP variants that displayed enhanced properties were identified by random mutagenesis, most of the active indicators based on

avGFP have been designed. The engineering of redox sensitive avGFPs by introducing pairs of cysteine residues was made possible only by close examination of the three dimensional structure of avGFP (see Chapter IV). Since these indicators rely on disulfide bond formation of two cysteine residues, it is very unlikely that random mutagenesis would have ever identified such variants. In the absence of the crystal structure, selecting positions 148 and 203 to create dual-emitting GFPs would have been improbable, since these residues lie far away from the chromophore residues (65-67) in the linear amino acid sequence (see Chapter III). However, it is now apparent that the peptide chain uniquely folds up to place many residues that lie far from the fluorophore in the linear chain, neighboring it in the folded protein.

In the case of the newly cloned FPs, it should be possible to enhance many of their characteristics by utilizing structure-based design. Although the tetramer interfaces of drFP583 are quite extensive, replacement of hydrophobic patches with hydrophilic residues and substituting uncharged polar amino acids for those involved in salt-bridges, could result in a monomeric red fluorescent protein. Similarly, mutational analysis of specific sites near the chromophore of zFP538 and drFP583 may expedite fluorophore maturation. Obviously if some of the drawbacks can be overcome, it would be advantageous to use the knowledge gained in avGFP biosensor design to create

multicolored fluorescent indicators of redox potential and H⁺, Ca²⁺, and halide ion concentration. Having indicators of different color would permit simultaneous reporting of various intracellular conditions.

Concluding Remarks

The goal of this dissertation work has been to rationally design environmentally sensitive avGFP variants and to use x-ray crystallography to link protein structure to spectroscopic function. To date, ratiometric-by-excitation-and-emission pH sensitive GFPs as well as ratiometric-by-excitation redox-sensitive GFPs have been engineered. High and low pH structures of a dual emitting GFP have been solved and show that a pH dependent structural rearrangement near the chromophore is likely to be involved in the altered fluorescent properties observed in this class of avGFPs. Additionally, the structures of both oxidized and reduced redox-sensitive avGFP show that positional manipulation of glutamic acid 222 in response to disulfide bond formation is responsible for the dual excitation characteristics of this variant. Through collaboration, the dynamic range of a dual emitting avGFP was found to be comparable to the commercially available, pH-indicating dye, SNARF-1®. Furthermore, a greatly improved fluorescent signal of avGFP over background cellular autofluorescence was found with two-photon

laser scanning microscopy when compared to conventional confocal microscopy.

Finally, with the assistance of the Capaldi and Marcus labs here at the University of Oregon, we have shown that the apparent redox potential of the redox sensing avGFPs fall within the biologically relevant range of potentials found in cultured mammalian cells.

Future Directions

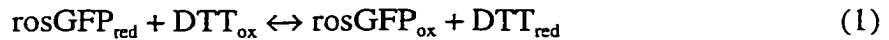
In addition to improving and designing biosensors of coral FPs, much work still remains on avGFP to fully comprehend how its structure relates to its spectroscopic function. In the case of dual-emitting avGFPs, the exact molecular details of dual emission remain elusive. If the details surrounding this phenomenon can be understood, dual-emission variants of redox-sensitive avGFP and perhaps coral FPs can be designed. Since the atomic details of the dual-excitation process are known, it may be possible to engineer dual-excitation attributes into already existing Ca^{2+} and halide ion indicators as well as future FP sensors. New biosensor design for metal ions such as Mg^{2+} , Zn^{2+} , $\text{Cu}^{2+}/\text{Cu}^+$, $\text{Fe}^{3+}/\text{Fe}^{2+}$, Na^+ , and K^+ may depend on exploiting the H148G mutation, which opens up a solvent channel to the chromophore in avGFP.

Most small molecule fluorescent probes are essentially naked fluorophores in solution and as was seen in avGFP, single amino acid substitution near the chromophore can strongly affect fluorophore properties. Therefore, avGFP and its homologues provide a unique opportunity to study the perturbation of a fluorescent chromophore. For all these reasons, the future of fluorescent proteins looks bright!

APPENDIX

Determination of Redox Potentials

Apparent redox potential values for the rosGFPs were found by exploiting the fact that the fluorescence of the rosGFP chromophores are strongly dependent upon the redox state of the introduced cysteines. Therefore the redox equilibrium of the rosGFPs with dithiothreitol (DTT_{red}) and oxidized dithiothreitol (DTT_{ox}) was analyzed. The equilibrium for the oxidation of reduced rosGFP by DTT_{red} and its equilibrium constant (K_{eq}) are given by equations 1 and 2.



$$K_{\text{eq}} = [\text{rosGFP}_{\text{ox}}] [\text{DTT}_{\text{red}}] / [\text{rosGFP}_{\text{red}}] [\text{DTT}_{\text{ox}}] \quad (2)$$

When rosGFPs were incubated in the presence of varying concentrations of DTT_{red} and DTT_{ox} (total $\text{DTT}_{\text{red}} + \text{DTT}_{\text{ox}} = 1 \text{ mM}$), the fractional amount of reduced rosGFP at equilibrium (R) could be measured over the whole range from the oxidized to the reduced protein using the chromophore fluorescence (Figure 44). Based on the SDS-PAGE result that indicated rcsGFPs only form intramolecular disulfide bonds, R can be related to K_{eq}

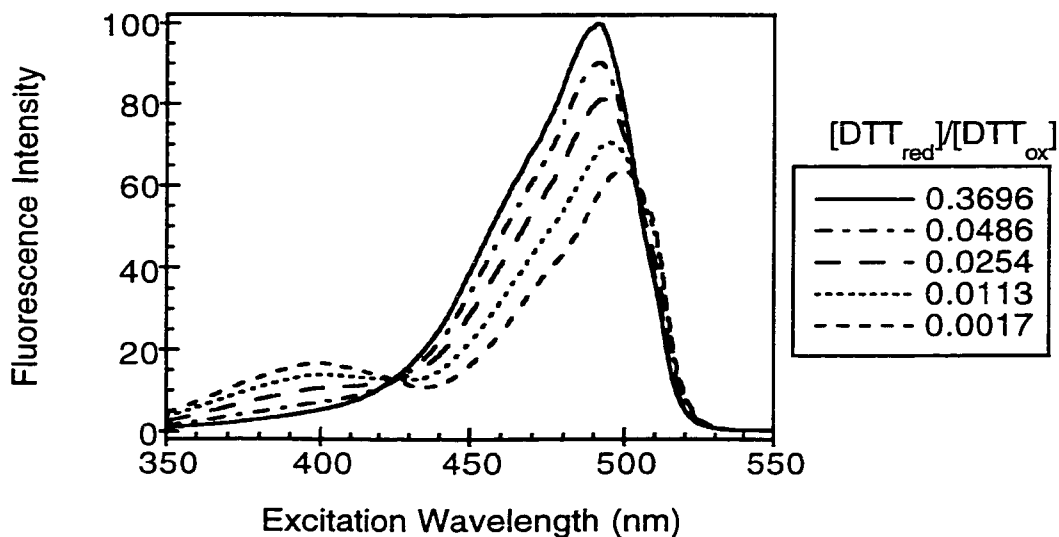


Figure 44. Fluorescence excitation spectra of rosGFP2 at varying concentrations of DTT_{red} and DTT_{ox} . Fluorescence emission intensity was monitored at 510 nm and normalized to the maximum intensity of the fully reduced spectrum (solid line).

by equation 3 (Hawkins et al. 1991).

$$R = ([\text{DTT}_{\text{red}}] / [\text{DTT}_{\text{ox}}]) / (K_{\text{eq}} + [\text{DTT}_{\text{red}}] / [\text{DTT}_{\text{ox}}]) \quad (3)$$

For experimental determination of the equilibrium constants of the GFP:dithiothreitol system, the equilibrium concentrations of DTT_{red} and DTT_{ox} were calculated according to equations 4-6, where $[\text{DTT}_{\text{red},0}]$ and $[\text{DTT}_{\text{ox},0}]$ are the initial concentrations of DTT_{red} and DTT_{ox} , respectively, R is the fractional amount of reduced rosGFP at equilibrium, $[\text{rosGFP}_0]$ is the initial concentration of oxidized rosGFP, F is a fluorescence intensity ratio of band B excitation (490 nm) versus the isosbestic point (425 nm), and F_{ox} and F_{red}

are the 490:425 nm ratios of the completely oxidized and reduced protein, respectively.

$$[DTT_{red}] = [DTT_{red,0}] - R [rosGFP_o] \quad (4)$$

$$[DTT_{ox}] = [DTT_{ox,0}] + R [rosGFP_o] \quad (5)$$

$$R = (F - F_{ox}) / (F_{red} - F_{ox}) \quad (6)$$

By plotting R against the $[DTT_{red}]/[DTT_{ox}]$ ratio and fitting the data to a titration curve according to equation 3 (Figure 45), the K_{eq} for the rosGFP2:dithiothreitol system was found to be 2.05×10^{-2} . The redox potential of rosGFP2 at pH 7 and 30°C ($E'_{rosGFP2}$) was

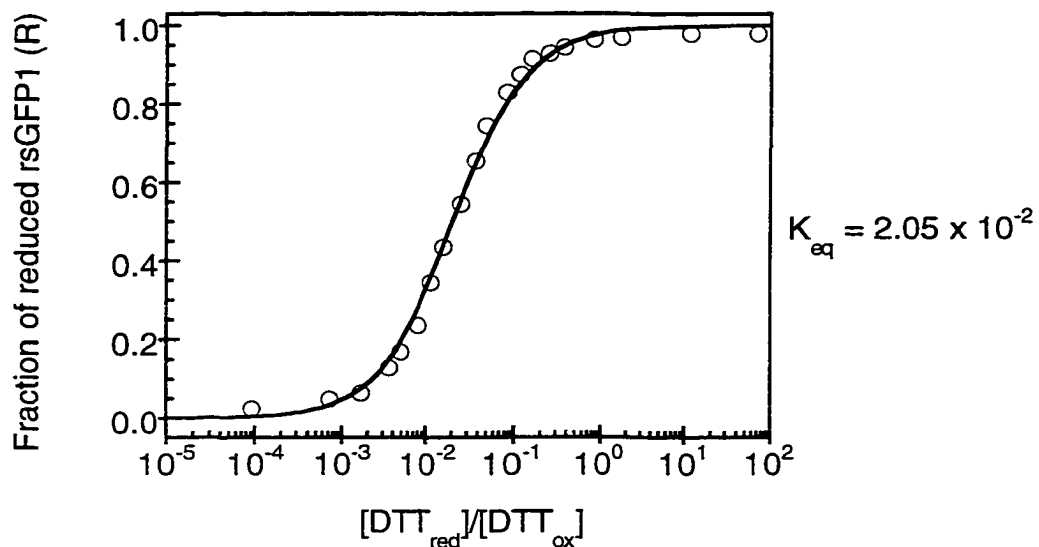


Figure 45. Redox equilibrium titration of rosGFP2 with dithiothreitol. The relative amount of reduced rosGFP2 at equilibrium (R) was measured using a ratio of the rosGFP2 fluorescence at 510 nm (excitation 490:425 nm). Oxidized rosGFP2 (1 μM) was incubated for 4 hours in 75 mM HEPES (pH 7.0), 140 mM NaCl, and 1 mM EDTA, containing varying ratios of DTT_{red} to DTT_{ox} (1 mM total). The equilibrium constant was determined by fitting the data according to equation 3. After nonlinear regression, a K_{eq} of 2.05×10^{-2} was obtained (correlation coefficient: 0.998).

then calculated from the Nernst equation (7), where E'_o is the biochemist's standard potential of the DTT/DTT_{ox} couple ($E'_{o\text{ DTT}} = -0.323$ V, at pH 7 and 30°C; Szajewski and Whitesides 1980), R is the gas constant (8.315 J K⁻¹ mol⁻¹), T is the absolute temperature (303.15 K), n is the number of transferred electrons (2), and F is the Faraday constant (9.649 × 10⁴ C mol⁻¹) and found to be -0.272 V.

$$E'_{o\text{ rosGFP2}} = E'_{o\text{ DTT}} - (RT / nF) \times \ln K_{eq} \quad (7)$$

pH-Dependence of Redox Potentials

Redox potentials involving the liberation of H⁺ ions are intrinsically based on pH. The pH-dependence on the redox potential is more apparent when examining the two half-reactions involving rosGFP and DTT (equation 8 and 9).



At equilibrium the concentrations of rosGFP_{ox} and rosGFP_{red} are equal and thus the K_{eq} is equal to the [H⁺]². The standard redox potential of rosGFP2 ($E'_{o\text{ rosGFP2}}$) at pH 0 could then be determined from equation 10.

$$E'_{o\text{ rosGFP2}} = E'_{o\text{ rosGFP2}} - (RT / nF) \times \ln K_{eq} \quad (10)$$

$E'_{o\text{ rosGFP2}}$ was calculated to be 0.149 V. Equation 11 simplifies the expression for the pH-

dependence of redox potentials involving two protons.

$$E_o^{pH} = E_o' - 60.2 \text{ mV} \times (pH - 7) \quad (11)$$

The pH-dependence on the redox potential therefore changes 60.2 mV with each pH unit.

Experimentally $E_{o\text{rosGFP2}}$ varied 65.5 mV per pH unit from pH 6 to 8 (correlation coefficient: 0.9999). Therefore, although a linear correlation between pH and $E_{o\text{rosGFP2}}$ is observed, the pH-dependence of the rosGFP2 standard potential does not directly correspond to this model. The deviation from this model for the pH-dependence of E_o may be due in part to the contributions of charged residues near the introduced disulfide of rosGFP2 as well as potentially different pK_a values for the cysteine residues (Wunderlich and Glockshuber 1993).

BIBLIOGRAPHY

- Baird, G.S., Zacharias, D.A., and Tsien, R.Y. 1999. Circular permutation and receptor insertion within green fluorescent proteins. *Proc. Natl. Acad. Sci. USA* 96: 11241-11246.
- Baird, G.S., Zacharias, D.A., and Tsien, R.Y. 2000. Biochemistry, mutagenesis, and oligomerization of DsRed, a red fluorescent protein from coral. *Proc. Natl. Acad. Sci. USA* 97: 11984-11989.
- Barltrop, J.A. and Coyle, J.D. 1978. *Principles of Biochemistry*. John Wiley & Sons, Inc., New York, NY.
- Bindoli, A., Callegaro, M.T., Barzon, E., Benetti, M., and Rigobello, M.P. 1997. Influence of the redox state of pyridine groups and permeability transition. *Arch. Biochem. Biophys.* 342, 22-28.
- Brejc, K., Sixma, T.K., Kitts, P.A., Kain, S.R., Tsien, R.Y., Ormö, M., and Remington, S.J. 1997. Structural basis for dual excitation and photoisomerization of the *Aequorea victoria* green fluorescent protein. *Proc. Natl. Acad. Sci. USA* 94: 2306-2311.
- Cai, J. and Jones, D.P. 1999. Mitochondrial redox signaling during apoptosis. *J. Bioenerg. Biomemb.* 31: 327-334.
- Calzi, M.L. and Poole, L.B. 1997. Requirement for the two Ahpf cystine disulfide centers in catalysis of peroxide reduction by alkyl hydroperoxide reductase. *Biochemistry* 36, 13357-13364.
- Carothers, D.J., Pons, G., and Patel, M.S. 1989. Dihydrolipoamide dehydrogenase: functional similarities and divergent evolution of the pyridine nucleotide-disulfide oxidoreductases. *Arch. Biochem. Biophys.* 268, 409-425.
- Chalfie, M., Tu, Y., Euskirchen, G., Ward, W.W., and Prasher, D.C. 1994. Green fluorescent protein as a marker for gene expression. *Science* 263: 802-805.
- Chattoraj, M., King, B.A., Bublitz, G.U., and Boxer, S.G. 1996. Ultra-fast excited state dynamics in green fluorescent protein: Multiple states and proton transfer. *Proc. Natl. Acad. Sci. USA* 93: 8362-8367.
- Cody, C.W., Prasher, D.C., Westler, W.M., Prendergast, F.G., and Ward, W.W. 1993. Chemical structure of the hexapeptide chromophore of the *Aequorea* green-fluorescent protein. *Biochemistry* 32, 1212-1218.

- Collaborative Computation Project, Number 4. 1994. *Acta Crystallogr. D.* 50: 760-763.
- Cuozzo, J.W. and Kaiser, C.A. 1999. Competition between glutathione and protein thiols for disulphide-bond formation. *Nat. Cell Biol.* 1: 130- 135.
- Debarbieux, L. and Beckwith, J. 1999. Electron avenue: Pathways of disulfide bond formation and isomerization. *Cell* 99: 117-119.
- Deneke, S.M. 2000. Thiol-based antioxidants. *Curr. Top. Cell. Regul.* 36, 151-180.
- Ehrig, T., O'Kane, D.J., Predergast, F.G. 1995. Green-fluorescent protein mutants with altered fluorescence excitation spectra. *FEBS Lett.* 367: 163-166.
- Ellis, H.R. and Poole, L.B. 1997. Roles for the two cysteine residues of AhpC in catalysis of peroxide reduction by alkyl hydroperoxide reductase from *Salmonella Typhimurium*. *Biochemistry* 36, 13349-13356.
- Elslinger, M.-A., Wachter, R.M., Hanson, G.T., Kallio, K., and Remington, S.J. 1999. Structural and spectral response of green fluorescent protein variants to changes in pH. *Biochemistry* 38: 5296-5301.
- Fasano, J.M., Swanson, S.J., Blancaflor, E.B., Dowd, P.E., Teh-hui, K., and Gilroy, S. 2001. Changes in root cap pH are required for the gravity response of the *Arabidopsis* root. *Plant Cell* 13, 907-921.
- Gill, S.C., and von Hippel, P.H. 1989. Calculation of protein extinction coefficients from amino acid sequence data. *Anal. Biochem.* 182: 319-326.
- Gillies, R.J., Liu, Z., and Bhujwalla, Z. 1994. 31P-MRS measurements of extracellular pH of tumors using 3-aminopropylphosphonate. *Am. J. Physiol.* 267: C195-C203.
- Grynkiewicz, G., Poenie, M., and Tsien, R.Y. 1985. A new generation of Ca^{2+} indicators with greatly improved fluorescence properties. *J. Biol. Chem.* 260: 3440-3448.
- Guilbault, G.G. 1990. General aspects of luminescence spectroscopy. In *Practical fluorescence*, 2nd ed. (ed. G.G. Guilbault), pp.1-41. Marcel Dekker, Inc., New York, NY.
- Hall, A.G. 1999. The role of glutathione in the regulation of apoptosis. *Eur. J. Clin. Invest.* 29: 238-245.
- Hamlin, R. 1985 Multiwire area X-ray diffractometers. *Methods enzymol.* 114: 416-452.
- Haugland, R.P. *Handbook of fluorescent probes and research chemicals*, 6th ed. Molecular Probes, Inc., Eugene, OR.
- Hawkins, H.C., de Nardi, M., and Freedman, R.B. 1991. Redox properties and cross-linking of the dithiol/disulphide active sites of mammalian protein disulphide-isomerase. *Biochem. J.* 275: 341-348.

- Heikal, A.A., Hess, S.T., Baird, G.S., Tsien, R.Y., and Webb, W.W. 2000. Molecular spectroscopy and dynamics of intrinsically fluorescent proteins: Coral red (dsRed) and yellow (Citrine). *Proc. Natl. Acad. Sci. USA* 97: 11996-12001.
- Heim, R., Cubitt, A.B., and Tsien, R.Y. 1995. Improved green fluorescence. *Nature* 373: 663-664.
- Heim, R., Prasher, D.C., and Tsien, R.Y. 1994. Wavelength mutations and posttranslational autoxidation of green fluorescent protein. *Proc. Natl. Acad. Sci. USA* 91: 12501-12504.
- Howard, A.J., Nielsen, C., and Xuong, N.H. 1985. Software for a diffractometer with multiwire area detector. *Methods enzymol.* 114: 452-471.
- Hwang, C., Sinskey, A.J., and Lodish, H.F. 1992. Oxidized redox state of glutathione in the endoplasmic reticulum. *Science* 257: 1496-1502.
- Inouye, S. and Tsuji, F.I. 1994. *Aequorea* green fluorescent protein. Expression of the gene and fluorescence characteristics of the recombinant protein. *FEBS Lett.* 341: 277-280.
- Jayaraman, S., Haggie, P., Wachter, R.M., Remington, S.J., and Verkman, A.S. 2000. Mechanism and cellular applications of a green fluorescent protein-base halide sensor. *J. Biol. Chem.* 275: 6047-6050.
- Johnson, F.H., Shimomura, O., Saiga, Y., Gershman, L.C., Reynolds, G.T., and Waters, J.R. 1962. *J. Cell Comp. Physiol.* 60: 85-103.
- Jones, T.A., Zou, J.-Y., Cowan, S.W., and Kjeldgaard, M. 1991. Improved methods for building protein models in electron density maps and the location of errors in these models. *Acta Cryst. A*. 47: 110.
- Keese, M.A., Saffrich, R., Dandekar, T., Becker, K., Schirmer, R.H. 1999. Microinjected glutathione reductase crystals as indicators of the redox status in living cells. *FEBS Lett.* 447: 135-138.
- Kneen, M., Farinas, J., Li, Y., and Verkman, A.S. 1998. Green fluorescent protein as a noninvasive intracellular pH indicator. *Biophys. J.* 74: 1591-1599.
- Kosower, N.S. and Kosower, E.M. 1976. The glutathione status of cells. *Int. Rev. Cytol.* 54, 109-160.
- Lehninger, A.L., Nelson, D.L., and Cox, M.M. 1993. *Principles of biochemistry*, 2nd ed. Worth Publishers, Inc., New York, NY.
- Lenton, K.J., Therriault, H., and Wagner, J.R. 1999. Analysis of glutathione and glutathione disulfide in whole cells and mitochondria by postcolumn derivatization high-performance liquid chromatography with *ortho*-Phtaldehyde. *Anal. Biochem.* 274, 125-130.

- LêQuôc, D. and LêQuôc, K. 1989. Relationships between the NAD(P) redox state, fatty acid oxidation, and inner membrane permeability in rat liver mitochondria. *Arch. Biochem. Biophys.* 273, 466-478.
- Leslie, A. 1996. In *Crystallographic computing V* (eds. D. Moras, A.D. Podjarny, and J.C. Thierry), pp. 27-38. Oxford University Press, Oxford, UK.
- Llopis, J., McCaffery, M., Miyawaki, A., Farquhar, M.G., and Tsien, R.Y. 1998. Measurement of cytosolic, mitochondrial, and Golgi pH in single living cells with green fluorescent protein. *Proc. Natl. Acad. Sci. USA* 95: 6803-6808.
- Matsumura, M., Becktel, W.J., Levitt, M., and Matthews, B.W. 1989. Stabilization of phage T4 lysozyme by engineered disulfide bonds. *Proc. Natl. Acad. Sci. USA* 86: 6562-6566.
- Matsuyama, S., Llopis, J., Deveraux, Q.L., Tsien, R.Y., and Reed, J.C. 2000. Changes in intramitochondrial and cytosolic pH: early events that modulate caspase activation during apoptosis. *Nat. Cell Biol.* 2: 318-325.
- Matz, M.V., Fradkov, A.F., Labas, Y.A., Savitsky, A.P., Zraiky, A.G., Markelov, M.L., and Lukyanov, S.A. 1999. Fluorescent proteins from nonbioluminescent Anthozoa species. *Nat. Biotech.* 17: 969-973.
- Meister, A. 1995. Glutathione metabolism. *Methods Enzymol.* 251, 3-7.
- Miesenböck, G., De Angelis, D. A., and Rothman, J.E. 1998. Visualizing secretion and synaptic transmission with pH-sensitive green fluorescent proteins. *Nature* 394: 192-195.
- Miyawaki, A., Llopis, J., Heim, R., McCaffery, J.M., Adams, J.A., Ikura, M., and Tsien, R.Y. 1997. Fluorescent indicators for Ca^{2+} based on green fluorescent proteins and calmodulin. *Nature* 388: 882-887.
- Morin, J.G. and Hastings, J.W. 1971. Energy transfer in a bioluminescent system. *J. Cell Physiol.* 77: 313-318.
- Morise, H., Shimomura, O., Johnson, F.H., and Winant, J. 1974. Intermolecular energy transfer in the bioluminescent system of *Aequorea*. *Biochemistry* 13:2656-1662.
- Ormö, M., Cubitt, A.B., Kallio, K., Gross, L.A., Tsien, R.Y., and Remington, S.J. 1996. Crystal structure of the *Aequorea victoria* green fluorescent protein. *Science* 273: 1392-1395.
- Otwinowski, Z. and Minor, W. 1997. Processing of X-ray diffraction data collected in oscillation mode. *Methods Enzymol.* 276: 307-326.
- Palm, G.J., and Wlodawer, A. 1997. The structural basis for spectral variations in green fluorescent protein. *Nat. Struct. Biol.* 4: 361-365.

- Prasher, D.C., Eckenrode, V.K., Ward, W.W., Prendergast, F.G., and Cormier, M.J. 1992. Primary structure of the *Aequorea victoria* green-fluorescent protein. *Gene* 111: 229-233.
- Prendergast, F.G. and Mann, K.G. 1978. Chemical and physical properties of aequorin and the green fluorescent protein isolated from *Aequorea forskåleae*. *Biochemistry* 17: 3448-3453.
- Ramirez, R., Rasschaert, J., Sener, A., and Malaisse, W.J. 1996. The coupling of metabolic to secretory events in pancreatic islets. Glucose-induced changes in mitochondrial redox state. *Biochim. Biophys. Acta* 1273, 263-267.
- Remington, S.J. 2000. In *Bioluminescence and chemiluminescence* (eds. T.O. Baldwin and M.M. Sigler), pp. 195-211. Academic, San Diego, CA.
- Robey, R.B., Ruiz, O., Santos, A.V.P., Ma, J., Kear, F., Wang, L.-J., Li, C.-J., Bernardo, A.A., Arruda, J.A.L. 1998. pH-dependent fluorescence of a heterologously expressed *Aequorea* green fluorescent protein mutant: In situ spectral characteristics and applicability to intracellular pH estimation. *Biochemistry* 37:9894-9901.
- Robinson, B.H. 1996. Use of fibroblast and lymphoblast cultures for detection of respiratory chain defects. *Methods Enzymol.* 264, 454-464.
- Romoser, V.A., Hinkle, P.M., and Persechini, A. 1997. Detection in living cells of Ca²⁺-dependent changes in the fluorescence emission of an indicator composed of two green fluorescent protein variants linked by a calmodulin-binding sequence. *J. Biol. Chem.* 272: 13270-13274.
- Rost, J. and Rapoport, S. 1964. Reduction-potential of glutathione. *Nature* 201: 185.
- Schmidt, W.K. and Moore, H.P. 1995. Ionic milieu controls the compartment-specific activation of pro-opiomelanocortin processing in AtT-20 cells. *Mol. Biol. Cell* 10: 1271-1285.
- Shimomura, O. 1979. *FEBS Lett.* 104: 220-222.
- Shimomura, O., Johnson, F.H., and Saiga, Y. 1962. *J. Cell. Comp. Physiol.* 59: 223-239.
- Siegel, M.S. and Isacoff, E.Y. 1997. A genetically encoded optical probe of membrane voltage. *Neuron* 19: 735-741.
- Sowdhamini, R., Srinivasan, N., Shoichet, B., Santi, D.V., Ramakrishnan, C., and Balaram, P. 1989. Stereochemical modeling of disulfide bridges. Criteria for introduction into proteins by site-directed mutagenesis. *Protein Eng.* 3: 95-103.
- Stewart, R. 1985. In *The Proton: Applications to organic chemistry*, pp.228-234. Academic, Orlando, FL.

- Szajewski, R.P. and Whitesides, G.M. 1980. Rate constants and equilibrium constants for thiol-disulfide interchange reactions involving oxidized glutathione. *J. Am. Chem. Soc.* 102: 2011-2026.
- Taylor, R.W., Chinnery, P.F., Clark, K.M., Lightowers, R.N., and Turnbull, D.M. 1997. Treatment of mitochondrial disease. *J. Bioenerg. Biomembr.* 29: 195-205.
- Terskikh, A., Fradkov, A., Ermakova, G., Zaraisky, A., Tan, P., Kajava, A.V., Zhao, X., Lukyanov, S., Matz, M., Kim, S., Weissman, I., and Siebert, P. 2000. "Fluorescent timer": Protein that changes color with time. *Science* 290:1585-1593.
- Torchinsky, Y.M. 1981. *Sulfur in proteins*. Pergamon Press Ltd., New York, NY.
- Tronrud, D.E., Ten Eyck, L.F., and Matthews, B.W. 1987. An efficient general-purpose least-squares refinement program for macromolecular structures. *Acta Cryst. A*. 43: 489.
- Tsien, R.Y. 1998. The green fluorescent protein. *Annu. Rev. Biochem.* 67: 509-544.
- Tsien, R.Y. 1999. Rosy dawn for fluorescent proteins. *Nat. Biotech.* 17: 956-957.
- Voet, D. and Voet, J.G. 1995. *Biochemistry*, 2nd ed. John Wiley & Sons, Inc., New York, NY.
- Wachter, R.M. and Remington, S.J. 1999. Sensitivity of the yellow variant of green fluorescent protein to halides and nitrate. *Curr. Biol.* 9: R628-R629.
- Wachter, R.M., Elsliger, M.-A., Kallio, K., Hanson, G.T., and Remington, S.J. 1998. Structural basis of spectral shifts in the yellow-emission variants of green fluorescent protein. *Structure* 6:1267-1277.
- Wachter, R.M., King, B.A., Heim, R., Kallio, K., Tsien, R.Y., Boxer, S.G., and Remington, S.J. 1997. Crystal structure and photodynamic behavior of the blue emissiond variant Y66H/Y145F of green fluorescent protein. *Biochemistry* 36: 9759-9765.
- Wachter, R.M., Yarbrough, D., Kallio, K., and Remington, S.J. 2000. Crystallographic and energetic analysis of binding of selected anions to the yellow variants of green fluorescent protein. *J. Mol. Biol.* 301: 157-171.
- Wall, M.A., Socolich, M., and Ranganathan, R. 2000. The structural basis for red fluorescence in the tetrameric GFP homolog DsRed. *Nat.Struct. Biol.* 7: 1133-1138.
- Ward, W.W. and Bokman, S.H. 1982. Reversible denaturation of *Aequorea* green-fluorescent prtoein: Physical separation and characterization of the renatured protein. *Photochem. Photobiol.* 35: 803-808.
- Ward, W.W. and Cormier, M.J. 1979. An energy transfer protein in coelenterate bioluminescence. Characterization of the *Renilla* green-fluorescent protein. *J. Biol. Chem.* 254: 781-788.

- Ward, W.W., Cody, C.W., Hart, R.C., and Cormier, M.J. 1980. Spectrophotometric identity of the energy transfer chromophore in *Renilla* and *Aequorea* green-fluorescent proteins. *Photochem. Photobiol.* 31: 611-615.
- Ward, W.W., Prentice, H.J., Roth, A.F., Cody, C.W., and Reeves, S.C. 1982. Spectral perturbations of the *Aequorea* green-fluorescent protein. *Photochem. Photobiol.* 35: 803-808.
- Whitaker, J.E., Haugland, R.P., and Predergast, F.G. 1991. Spectral and photophysical studies of benzo[c]xanthene dyes: Dual emission pH sensors. *Anal. Biochem.* 194: 330-344.
- Wilson, D.W., Lewis, M.J., and Pelham, H.R. 1993. pH-dependent binding of KDEL to its receptor in vitro. *J. Biol. Chem.* 268: 7465-7468.
- Wunderlich, M. and Glockshuber, R. 1993. Redox properties of protein disulfide isomerase (DsbA) from *Escherichia coli*. *Protein Sci.* 2: 717-726.
- Xu, C., Zipfel, W., Shear, J.B., Williams, R.M., and Webb, W.W. 1996. Multiphoton fluorescence excitation: New spectral windows for biological nonlinear microscopy. *Proc. Natl. Acad. Sci. USA* 93: 10763-10768.
- Yang, F., Moss, L.G., and Phillips, G.N.Jr. 1996. The molecular structure of green fluorescent protein. *Nature Biotech.* 14: 1246- 1251.
- Yarbrough, D., Wachter, R.M., Kallio, K., Matz, M.V., and Remington, S.J. 2001. Refined crystal structure of DsRed, a red fluorescent protein from coral, at 2.0-Å resolution. *Proc. Natl. Acad. Sci. USA* 98: 462-467.